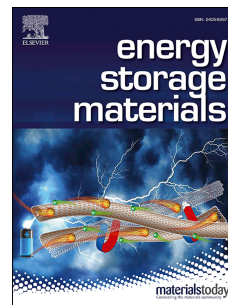


# Accepted Manuscript

Recent Progress on Solid-State Hybrid Electrolytes for Solid-State Lithium Batteries

Jianneng Liang, Jing Luo, Qian Sun, Xiaofei Yang, Ruying Li, Xueliang Sun



PII: S2405-8297(19)30843-8

DOI: <https://doi.org/10.1016/j.ensm.2019.06.021>

Reference: ENSM 810

To appear in: *Energy Storage Materials*

Received Date: 16 March 2019

Revised Date: 30 May 2019

Accepted Date: 14 June 2019

Please cite this article as: J. Liang, J. Luo, Q. Sun, X. Yang, R. Li, X. Sun, Recent Progress on Solid-State Hybrid Electrolytes for Solid-State Lithium Batteries, *Energy Storage Materials*, <https://doi.org/10.1016/j.ensm.2019.06.021>.

This is a PDF file of an unedited manuscript that has been accepted for publication. As a service to our customers we are providing this early version of the manuscript. The manuscript will undergo copyediting, typesetting, and review of the resulting proof before it is published in its final form. Please note that during the production process errors may be discovered which could affect the content, and all legal disclaimers that apply to the journal pertain.

## Recent Progress on Solid-State Hybrid Electrolytes for Solid-State Lithium Batteries

Jianneng Liang<sup>1</sup>, Jing Luo<sup>1</sup>, Qian Sun<sup>1</sup>, Xiaofei Yang<sup>1</sup>, Ruying Li<sup>1</sup>, Xueliang Sun<sup>1,\*</sup>

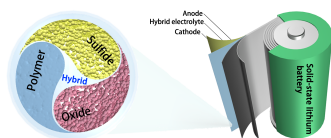
<sup>1</sup>Department of Mechanical and Materials Engineering, University of Western Ontario, London, Ontario, N6A 5B9, Canada

E-mail: xsun@eng.uwo.ca (X.L. Sun)

### Abstract

Lithium batteries are promising energy storage system for applications in electric vehicles. However, conventional liquid electrolytes inherit serious safety hazards including leak, ignition and even explosion upon overheating. Solid-state electrolytes (SSEs) are considered as the ultimate solution to these safety concerns because of their excellent thermal and electrochemical stabilities. Nevertheless, few individual SSE has reached practical application standards due to incomprehensive performance. High ionic conductivity, low interfacial resistance, and high stability towards electrodes are difficult to achieve simultaneously with an individual SSE. Hybrid electrolytes rationally combining two or more SSEs with complementary advantages are promising for building feasible solid-state lithium batteries (SSLBs). Coupling desired soft electrolyte and stiff inorganic SSEs can ensure good electrode wettability, high ionic conductivity, and high mechanical strength to prevent lithium dendrite formation at the same time. In this review, comprehensive perspectives from the broad context of the importance of hybrid electrolytes to subtle design concepts are summarized. This review not only covers the introductory of classifications, synthesis methods, and ionic conductivity mechanism, but also crystallizes the strategies for enhancing the ionic conductivity of hybrid electrolyte, the understandings of the interfacial challenges for the electrolyte/electrolyte and electrolyte/electrode interfaces, and the strategies for building feasible SSLBs with different hybrid electrolyte combinations

**Key words:** Solid-state electrolytes, Solid-state batteries, Hybrid electrolytes, Interface.



ACCEPTED MANUSCRIPT

## 1. Introduction

Lithium-ion batteries (LIBs) are playing a more and more important role in our daily life. LIBs not only power our portable devices (e.g. cellphones, laptops and cameras), but also drive the transportation (e.g. electric vehicles (EVs), hybrid electric vehicles (HEVs)), and even serve as temporary storage system for excess peak energy delivered by renewable energy sources, such as solar, wind, nuclear and hydro power. Since Sony launched the first commercial LIB with an intercalating  $\text{LiCoO}_2$  (LCO) cathode in 1990s [1], LIBs have attracted increasing research attentions in recent 30 years. In order to meet the requirements for large-scale applications in EVs and grid energy storage system, a variety of high-energy-density cathode candidates such as Ni-rich lithium nickel manganese cobalt oxide cathode (NMC) [2, 3], Li-rich NMC [4, 5], lithium nickel cobalt aluminum oxide (NCA) [6, 7], and alternative conversion-type battery systems of Li-sulfur (Li-S) and Li-air [8-12] have been developed and attracted substantial research attentions. However, the usage of liquid electrolytes in the commercial LIBs poses serious safety concerns such as fire and explosion. Most of those liquid electrolyte solvents have very low boiling point (below  $300\text{ }^\circ\text{C}$ ) and flash point (below  $150\text{ }^\circ\text{C}$ ) [13-15]. The thermal instability, volatility and flammability of organic liquid electrolytes are key problems that cause the safety issues of LIBs [13-16]. Li dendrite formation problem due to inhomogeneous charging of the anode is another safety concern that can cause cell short circuit in liquid-based LIBs [17-21].

Replacing liquid electrolytes with solid-state electrolytes (SSEs) provide a promising solution to tackle the safety issues. SSEs are thermally stable and basically nonflammable. The key functional properties of a SSE applied in solid-state lithium batteries (SSLBs) should include (i) high total (bulk and grain boundary)  $\text{Li}^+$  ion conductivity over a wide temperature range, (ii) wide electrochemical window to couple with lithium metal anode and high-voltage cathode, (iii) chemically and mechanically compatible interfaces with anode and cathode, (iv) chemically stable in ambience environment, and (v) low interfacial resistance toward electrodes.

Even though SSEs have many attractive properties, especially in safety, an individual SSE having comprehensive functionalities has not yet been developed. Figure 1 summaries the main drawbacks of each type of electrolytes including liquid electrolyte, solid polymer electrolyte,

oxide-based SSE, sulfide-based SSEs. The oxide- and sulfide-based SSEs are also classified as inorganic SSEs. Different SSEs encounter various challenges that hinder their practical applications. Firstly, most of SSEs including oxide-based SSE and the dry solid polymer electrolyte (SPE) have a relatively low ionic conductivity compared to the liquid-based counterpart at room temperature (RT). For example, PEO-based SPE (e.g. polyethylene oxide complexing with lithium salt) have an ionic conductivity around  $10^{-7}$ - $10^{-5}$  S/cm at RT. Most ceramic SSEs such as NASICON-type SSEs (e.g.  $\text{Li}_{1+x}\text{Al}_x\text{Ti}_{2-x}(\text{PO}_4)_3$  (LATP)) and  $\text{Li}_{1+x}\text{Al}_x\text{Ge}_{2-x}(\text{PO}_4)_3$  (LAGP) [22, 23]. garnet-type SSEs ( $\text{Li}_2\text{La}_3\text{Zr}_2\text{O}_{12}$ , (LLZO) [24] and perovskite-type SSEs ( $\text{Li}_{3x}\text{La}_{(2/3)-x}\text{TiO}_3$ , (LLTO) [25] have an ionic conductivity around  $10^{-5}$ - $10^{-3}$  S/cm. Secondly, besides the low ionic conductivity problem, the high interfacial resistance between the SSEs and electrodes also restricts the practical applications of SSEs. Mismatch between the rigid SSEs and the solid-state electrodes is a common cause for the high interfacial resistance. Another reason for the high interfacial resistance is due to the formation of space charge layer (SCL) between sulfide-based SSEs and  $\text{LiCoO}_2$  cathodes [26], or the formation of interphase materials original from the side reaction between SSEs and electrodes materials.

To build a comprehensive SSE, a new concept of hybrid electrolyte has been developed to rationally combine two or more types of  $\text{Li}^+$  ion conductors. A hybrid electrolyte intends to compensate the advantage and disadvantage of each constituent. The most common hybrid electrolyte is composite electrolyte consisting of a soft polymer electrolyte and a rigid inorganic SSE. While the rigid inorganic SSE maintains relatively high ionic conductivity at RT, the soft and flexible SPE solves the mismatch and wettability problems on the interface with electrodes [27, 28]. Meanwhile, the Li dendrite formation problem due to the mechanically poor SPE can be alleviated by the stiff ceramic SSE fillers [29]. Another types of hybrid electrolytes are multilayer structured hybrid electrolytes where a ceramic SSE layer serves as the major  $\text{Li}^+$  ion conductor and separator with SPE outer layers to tailor the interface against electrodes. Or, instead of SPE, trace amount of liquid electrolyte is spread on the oxide SSE surface to ensure ionic conduction between the rigid oxide SSEs and electrodes. We refer this kind of configuration as liquid-oxide hybrid electrolyte. The design concepts and the advantages of hybrid electrolytes SSLBs are summarized in Figure 2.

As increasing research efforts have been dedicated to developing hybrid electrolytes for

advanced SSLBs, the progresses of hybrid electrolytes for lithium batteries have been reviewed with particular focuses of classifications, ionic conductivities, and applications in solid-state batteries [30, 31]. Differently, this review aims to provide comprehensive perspectives from the broad context of the importance of hybrid electrolytes to subtle design concepts. We not only cover the introductory of classifications, synthesis methods, and ionic conductivity mechanism of the hybrid electrolyte, but also crystallize the strategies for enhancing the ionic conductivity, the understandings of the interfacial challenges for the electrolyte/electrolyte and electrolyte/electrode interfaces, and the strategies for building feasible SSLBs with different hybrid electrolyte combinations.

### **1.1 Solid-state electrolytes and challenges**

Before introducing hybrid electrolytes, different types of SSEs including SPEs, oxide-based SSEs and sulfide-based SSEs will be systematically introduced and compared. In-depth details about ionic conductivities, interface properties, electrochemical/chemical properties, design mechanism and lithium ion transportation mechanism of SPEs, oxide-based SSEs and sulfide-based SSEs have been extensively reviewed [16, 32-63], so the introduction to each individual SSE here mainly focuses on their distinct characteristics and important parameters that are related to hybrid electrolyte designs.

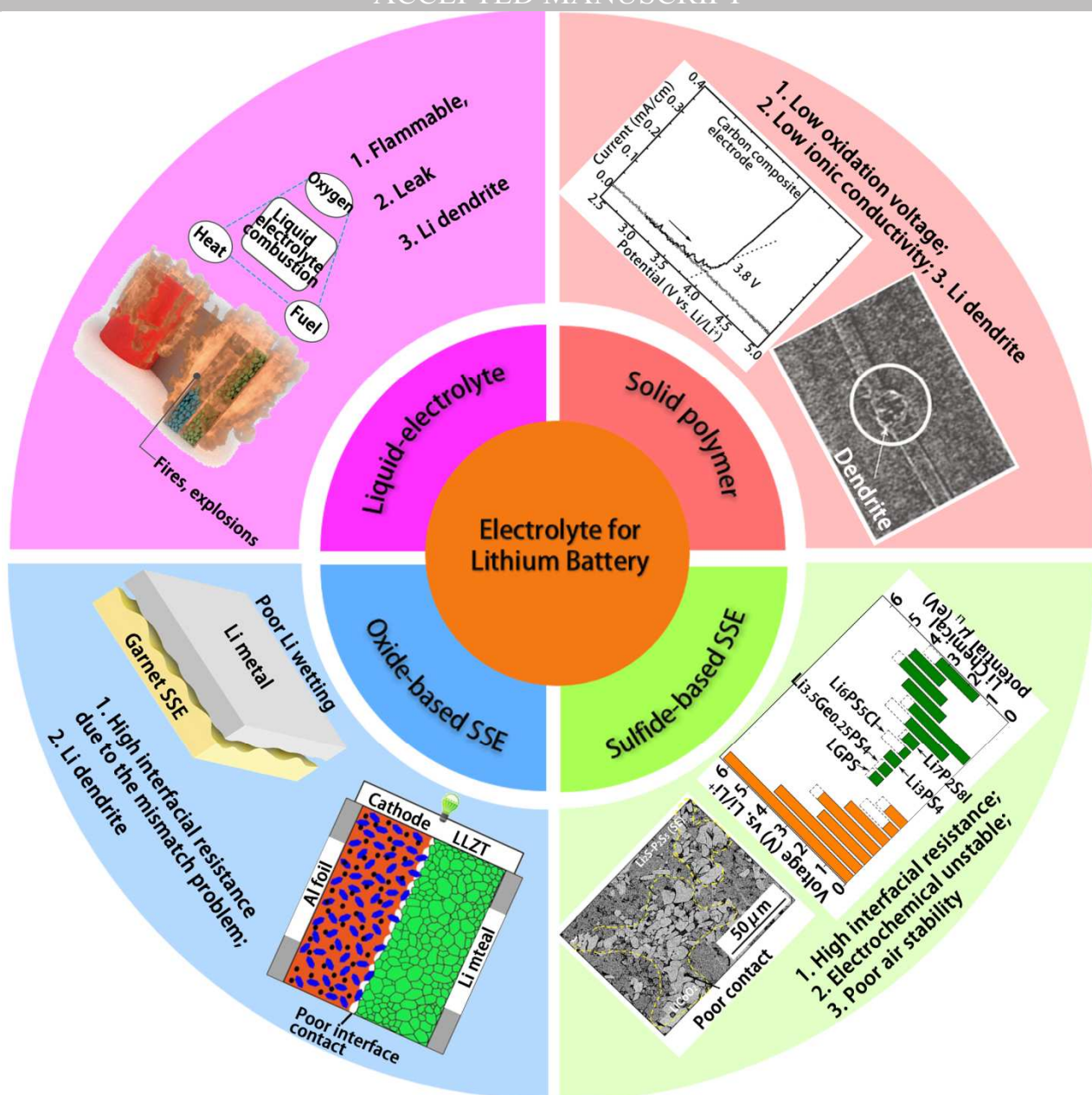


Figure 1. Common electrolytes for lithium batteries and their main drawbacks.[29, 64-70]



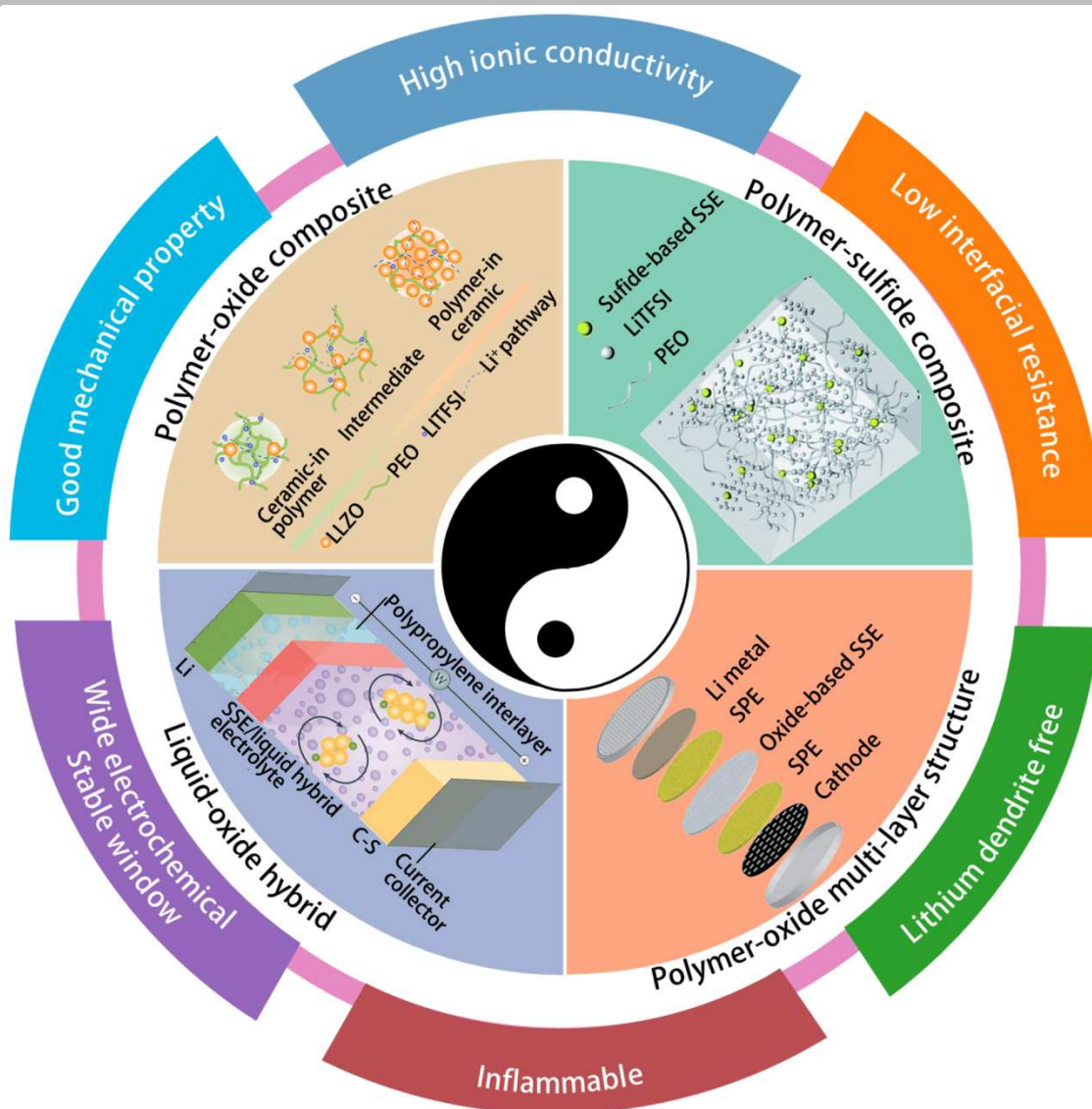


Figure 2. Design concepts and the advantages of hybrid electrolytes for SSLBs.[71-74]

### 1.1.1 Solid polymer electrolytes (SPEs)

In 1973, the discovery of ionic conductive complexes between polyethylene oxide (PEO) and alkali metal salts by Wright et al. [75] opened a new direction for SSE research. Generally speaking, a good SPE usually consists of a high dielectric host polymer complexed with a lithium salt with a low lattice energy (Figure 3a shows the structure of a SPE with PEO complexing with  $\text{LiAsF}_6$ ). Polymers with polar functional groups are chosen to facilitate the dissociation and transport of alkali ions; salts with high ionization ability are selected. Among all SPEs, PEO-based SPEs are most widely studied[76-84] due to their excellent salt-solvating ability and interfacial compatibility with electrodes. Moreover, SSLBs with a  $\text{LiFePO}_4$  cathode, a Li metal anode and a polyether-based



SPE show excellent cycling performance at 70 °C [84]. They have been commercialized in an electric car model, Bolloré Bluecar, to provide 30 KWh electricity with a driving range of 250 km. Other host polymer candidates including polyacrylonitrile (PAN) [85-87], poly(methylmethacrylate) (PMMA) [88, 89], poly(vinylidene fluoride-co-hexafluoropropylene) (PVDF-HFP) [90, 91] and poly(propylene carbonate) (PPC) [92, 93], poly(ethylene carbonate) (PEC) [94] also receive increasing research interest lately for potential application in SSLBs.

However, the ionic conductivity of PEO-based SPEs is in the range of  $10^{-5}$ - $10^{-7}$  S/cm at RT (Figure 3b) [76-78], which falls short to the requirement of SSLBs for operating at a wide temperature range. Moreover, due to the poor mechanical strength of the polymer matrix, SPEs suffer from Li dendrite formation problem [29]. Li dendrite growth at a Li/SPE/Li symmetrical cell had been observed using X-ray tomography technique (Figure 3d-h) [29, 95]. The results show that the defect of Li anode surface plays a key role in the nucleation of Li dendrites. N.S. Schauer et al. investigated the temperature influence on the Li dendrite formation in SPE. At a higher temperature (over 105 °C), significant dendrite growth was observed and caused failure of the cell, while under a lower temperature (lower than 90 °C), Li dendrite growth is prohibited [95]. These results were probably due to the lower mechanical strength of SPE under higher temperature that led to serious Li dendrite formation. Thus, to prevent growth of lithium dendrite, a high shear modulus is required for SPEs. As proposed by Monroe and J. Newman, if the shear modulus of SPE is higher than that of lithium metal, the dendrite growth can be inhibited [96-99].

Another challenge is the instability of SPEs at high voltages, which seriously restrict their applications in high-energy-density LIBs [69]. The instability of SPE under high voltage makes SPE/cathode interface a big challenge in high-energy-density LIBs system. PEO-based SPEs are known to be electrochemically stable under 3.8 V (vs. Li/Li<sup>+</sup>) (Figure 3c), so they are relatively stable towards LiFePO<sub>4</sub> cathode that has a charging plateau at about 3.4 V [84]. However, PEO-based SPEs fail to deliver good performance in SSLBs with a high voltage (> 4 V) cathode such as LiCoO<sub>2</sub> [100]. To improve the stability of SPE at high voltage, engineering the SPE/cathode interface with an artificial solid electrolyte interphase (SEI), such as Al<sub>2</sub>O<sub>3</sub>, Li<sub>3</sub>PO<sub>4</sub> and poly(ethylcyanoacrylate), has been reported with improvement in cycling performance [100-102]. Therefore, the study of SSLBs with SPEs should focus on enhancing the mechanical properties for

preventing Li dendrite formation and increasing electrochemical stability of SPEs for high-energy-density LIBs.

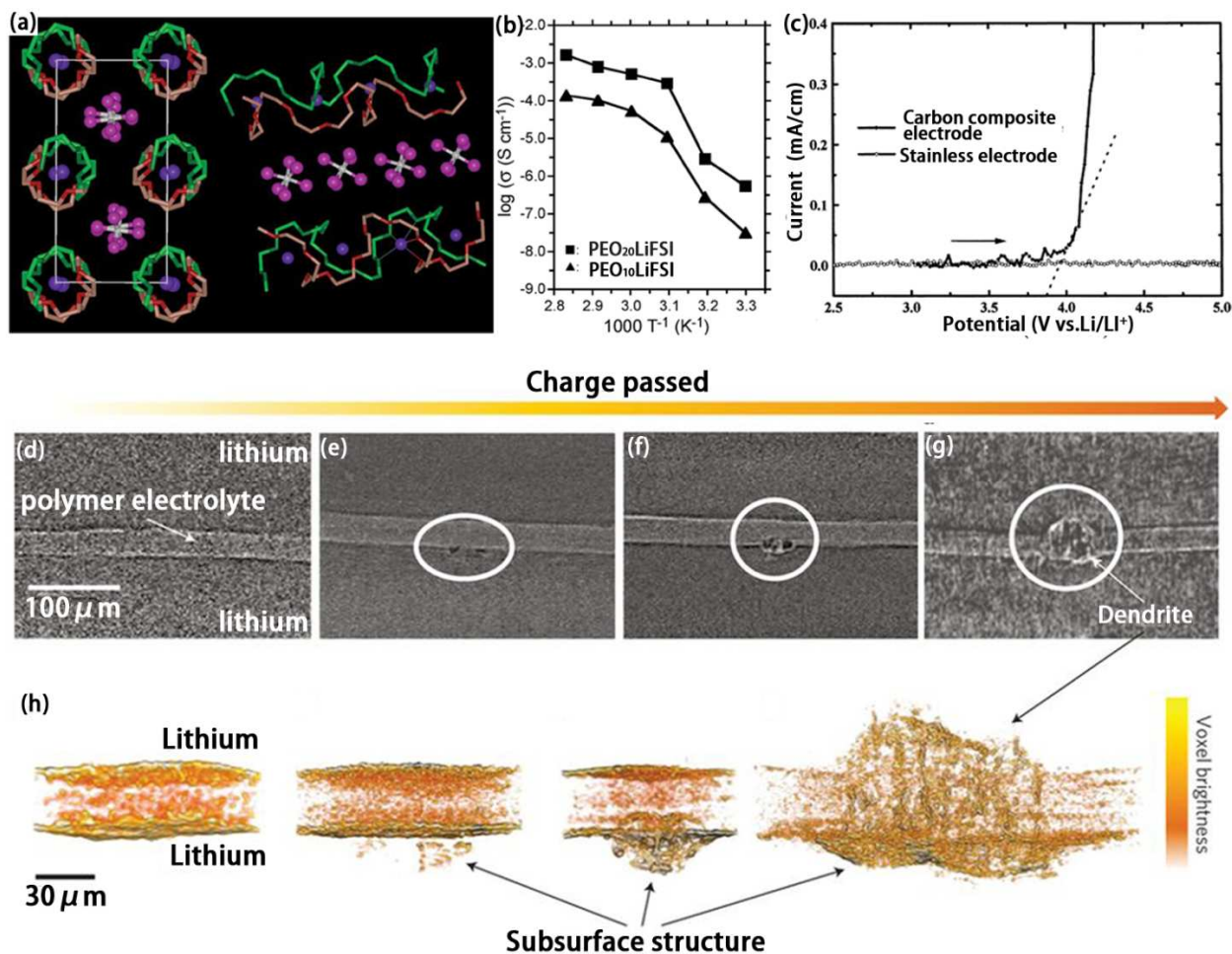


Figure 3. (a) Structure of a crystalline PEO-based SPE consisting of PEO and LiAsF<sub>6</sub>. Left, PEO chain axis is perpendicular to the page. Right, PEO chain axis is parallel to the page. Purple spheres, Li; white spheres, As; pink spheres, F; light green, carbon in PEO chain 1; dark green, oxygen in PEO chain 1. Light red, carbon in PEO chain 2; dark red, oxygen in PEO chain 2. Hydrogens are not shown [103]. (b) Temperature dependent ionic conductivity of PEO-based SPEs [104]. (c) The electrochemical stable window of a PEO-based SPE is only 3.8 V [69]. (d)-(g) X-ray tomography slices show the evolution of Li dendrite formation in SPE and their 3-dimensional (3D) reconstructions diagrams (h) [29].

### 1.1.2 Oxide-based SSEs

NASICON-type, perovskite-type, and garnet-type SSEs are the most popular oxide-based SSEs and have demonstrated feasibilities in hybrid electrolytes for SSLBs. Their intrinsic advantages

such high ionic conductivity and air stable properties make them attractable in the applications of hybrid electrolyte. Categorized by different structures, the oxide-based SSEs exhibit different ionic conductivities and chemical properties and face different challenges in the application of SSLBs. Representative examples will be discussed in this section.

NASICON-type SSEs, the name was first given to a sodium superionic conductor  $\text{NaM}_2(\text{PO}_4)_3$  ( $M = \text{Ge}, \text{Ti}, \text{Zr}$ ), having the crystalline NASICON framework consists of corner sharing  $\text{PO}_4$  tetrahedra and  $\text{MO}_6$  ( $M = \text{Ge}, \text{Ti}, \text{Zr}$ ) octahedra forming a 3D network structure [105].  $\text{Na}^+$  ions are located on interstitial sites and transported along the  $c$  axis.[106] By replacing  $\text{Na}^+$  with  $\text{Li}^+$ , NASICON-type SSEs become  $\text{Li}^+$  ion conductors without the change of NASICON crystal structure (Figure 4a). The currently most popular NASICON-type SSEs are  $\text{Li}_{1+x}\text{Al}_x\text{Ti}_{2-x}(\text{PO}_4)_3$  (LATP) and  $\text{Li}_{1+x}\text{Al}_x\text{Ge}_{2-x}(\text{PO}_4)_3$  (LAGP), which are obtained by partial Al substitution of Ti or Ge in  $\text{LiTi}_2(\text{PO}_4)_3$  and  $\text{LiGe}_2(\text{PO}_4)_3$ , respectively. The highest ionic conductivity of NASICON-type SSEs reported to date at RT is in the range of  $10^{-3}$  to  $10^{-2}$  S/cm [106], which is almost comparable to that of liquid-based electrolytes. However, the rigid nature of NASICON-type SSEs makes them challenging to achieve good interface with electrodes. Another challenge is that the Ti-containing LATP can react with reductants such as lithium metal (Figure 4j) and polysulfides, seriously restricting its application in high-energy-density SSLBs.

Garnet-type SSEs have a general chemical formula of  $\text{A}_3\text{B}_2(\text{XO}_4)_3$  ( $A = \text{Ca}, \text{Mg}, \text{Y}, \text{La}$  et al.  $B = \text{Al}, \text{Fe}, \text{Ga}, \text{Ge}, \text{Mn}, \text{Ni}$  or  $\text{V}$ ;  $X = \text{Si}, \text{Ge}, \text{Al}$ ) where A, B, and X have eight, six, and four oxygen coordinated cation sites in a crystalline face-center-cubic structure.[107] The crystalline structure of cubic phase garnet-type SSE is showed in Figure 4b. The studies of garnet-type SSEs cover  $\text{Li}_3$ -type  $\text{Li}_3\text{Ln}_3\text{Te}_2\text{O}_{12}$  ( $\text{Ln} = \text{Y}, \text{Pr}, \text{Nd}, \text{Sm-Lu}$ ) [108],  $\text{Li}_5$ -type  $\text{Li}_5\text{La}_3\text{M}_2\text{O}_{12}$  ( $M = \text{Nb}, \text{Ta}$ ) [109],  $\text{Li}_6$ -type  $\text{Li}_6\text{Ala}_2\text{M}_2\text{O}_{12}$  ( $A = \text{Mg}, \text{Ca}, \text{Sr}, \text{Ba}$ ) [110], and  $\text{Li}_7$ -type  $\text{Li}_7\text{La}_3\text{X}_2\text{O}_{12}$  ( $X = \text{Zr}, \text{Sn}, \text{Ta}$ ) [24]. The first three garnet SSEs have relatively low RT ionic conductivity ( $\sim 10^{-5}$  S/cm), while  $\text{Li}_7\text{La}_3\text{Zr}_2\text{O}_{12}$  (LLZO) possesses relatively high ionic conductivity ( $10^{-4} \sim 10^{-3}$  S/cm). Therefore, research interests are mostly dedicated in LLZO and its derivatives with different elemental doping [111-113]. Garnet-type SSEs are also attractive for their wide electrochemical window and stability towards lithium metal anodes [67]. LLZO has two different phases, a lower ionic conductive tetragonal phase and a higher ionic conductive cubic phase. Cubic phase LLZO is more desirable for practical

applications, but it usually requires very high sintering temperatures to obtain the cubic phase [24]. The  $\text{Li}^+/\text{H}^+$  exchange [114] upon exposure to moisture can cause  $\text{Li}_2\text{CO}_3$  formation on the LLZO surface leading to additional problems such as poor lithium wettability and poor ionic conductivity. Even though LLZO is known to be high ionic conductivity and stable towards lithium metal anodes, Li dendrite problem [115, 116] and interfacial mismatch issue due to the rigid properties remain challenging for garnet-type SSEs.

Perovskite-type SSEs with a structure of  $\text{ABO}_3$  ( $\text{A} = \text{Ca}, \text{Sr}, \text{La}$ ;  $\text{B} = \text{Al}, \text{Ti}$ ) were first reported as an oxygen ion conductor [117]. After aliovalent substitution of both metal ions in A-sites with a formula of  $\text{Li}_{3x}\text{La}_{2/3-x}\text{TiO}_3$ , a  $\text{Li}^+$  ion conductor is obtained with a high bulk ionic conductivity over  $10^{-3}$  S/cm at RT [118]. Unfortunately, the high grain boundary resistance, high interfacial resistance, and poor compatibility of  $\text{Ti}^{4+}$  with lithium metal anode restrict their wide applications.

Overall, oxide-based SSEs have relatively high ionic conductivity and chemical stability at ambient environment. Oxide-based SSEs have the highest Young's modulus among all types of SSEs. The Young's moduli for LATP, garnet-type SSE LLZO, and perovskite-type SSE are 115 GPa [119], 150 GPa for [120], and 203 GPa [121], respectively. This rigid property could be beneficial for suppressing lithium dendrite if engineered properly but resulting in the mismatch problem towards electrodes. Figure 4i shows the mismatch problem between NASICON SSE and electrodes where a big gap is present at the interface. More details about mechanical properties of the SSEs will be discussed and summarized in following content.

In terms of oxide-based SSE/electrode interface, several strategies have been reported to improve the interfacial contact and lower the interfacial resistance and they are summarized in Figure 5. For example, melting lithium metal onto the oxide-based SSE surface instead of simply pressing a lithium metal foil to the SSE can achieve a matching interface. Molten lithium metal has high fluidity which can fill the gaps of the uneven SSE surface and enable intimate interfacial contact. However, garnet-type SSEs may have poor wettability to molten lithium, namely "lithiophobic" (Figure 5a left). Thus, coatings including  $\text{Al}_2\text{O}_3$ , ZnO, Ge, etc. on SSEs can enable good lithium wettability, namely "lithiophilic" coatings (Figure 5a right) [122-124]. For example, L. Hu's group [123] dramatically reduced the contact angle between molten lithium and a garnet-type SSE and reduced the RT interfacial resistance of from  $1710 \text{ } \Omega/\text{cm}^2$  to  $1 \text{ } \Omega/\text{cm}^2$  via a thin layer of  $\text{Al}_2\text{O}_3$  coating on the

garnet-type SSE by atomic layer deposition (ALD) (Figure 5b). The lithium symmetric cell with  $\text{Al}_2\text{O}_3$  coated garnet SSE presented excellent plating/stripping performance over 90 h with negligible increase of overpotential at a current density of  $0.2 \text{ mA/cm}^2$ .

However, this melting strategy is not suitable for engineering the cathode interface because of the high melting points of SSEs and cathode materials. Moreover, cathode is heterogeneous structure containing nano-size or micro-size active material particles, nano-size conductive carbon and polymer binder. The stiff and rough morphology of cathodes even make the mismatch problem more prominent. Alternatively, a feasible method is co-sintering oxide-based SSE and cathode materials together with a low-melting-point SSE as a sintering additive to promote the sintering process at a relatively low temperature (Figure 5c). Ohta et al. developed a solid-state  $\text{LiCoO}_2$  batteries with LLZO as the SSE and  $\text{LiBO}_3$  as the sintering additive to lower the co-sintering temperature to  $700 \text{ }^\circ\text{C}$ . This  $\text{LiCoO}_2$  SSB delivered a discharge capacity of  $85 \text{ mAh/g}$  in a voltage window of  $3.0 - 4.05 \text{ V}$  (vs.  $\text{Li/Li}^+$ ) [125]. A similar study by C. Wang's group used  $\text{Li}_{2.3}\text{C}_{0.7}\text{B}_{0.3}\text{O}_3$  as the sintering additive to construct an all ceramic SSLB with excellent cycling performance (Figure 5d) [126]. Creating porous structure SSE to enlarge the contact area between SSE and electrode materials is another strategy to realize SSLB with oxide-based SSE (Figure 5e-g) [127].

Even though SSE/cathode interfacial mismatch problem can be partially addressed by the co-sintering method [125, 128-130] or creating porous structure SSE to enlarge the contact area between SSE and electrode materials [127, 131], the volume change of electrode materials during charge/discharge will still lead to loss of contact between SSEs and electrode materials due to the stiffness nature of SSEs [132-134].

The interphase problem due to side reactions or elemental diffusion at the interface between oxide-based SSE and cathode have been reported [129, 135]. At the  $\text{LiCoO}_2/\text{LLZO}$  interface, Co undergoes mutual diffusion with Zr and La (Figure 4d-h) forming an interphase with low ionic conductivity (i.e. high interfacial resistance). Another common problem is the incompatibility between Li anode and Ti-containing oxide-based SSEs.  $\text{Ti}^{4+}$  in LATP or LLTO can be easily reduced by the lithium metal anode (Figure 4j) resulting in a phase change of the SSE which decreases ionic conductivity but increases electronic conductivity. This kind of highly electronic conductive interphase is particularly prone to exacerbate Li dendrite growth [136, 137]. Our group has



demonstrated a thin layer of  $\text{Al}_2\text{O}_3$  coating on the LATP surface to prevent  $\text{Ti}^{4+}$  reduction in LATP, significantly enhancing the stability of LATP towards lithium metal anode (Figure 5h, i)[138].

In summary, interfacial mismatch and side reactions between the oxide-based SSE and electrodes are the key challenges to the application of oxide-based SSEs and more research efforts are required. The strategies for these interfacial problems include (i) solidifying melting state lithium on SSE to ensure intimate contact, (ii) co-sintering active materials and SSE with a sintering additive, (iii) creating a porous structure SSE to increase the contact area between electrode materials and SSE, and (iv) using coating layer to prevent side reaction. It is believed that engineering the interface with a soft and high ionic conductive layer between SSE and electrodes may be a good strategy to tackle the challenges for SSLBs with oxide-based SSE.

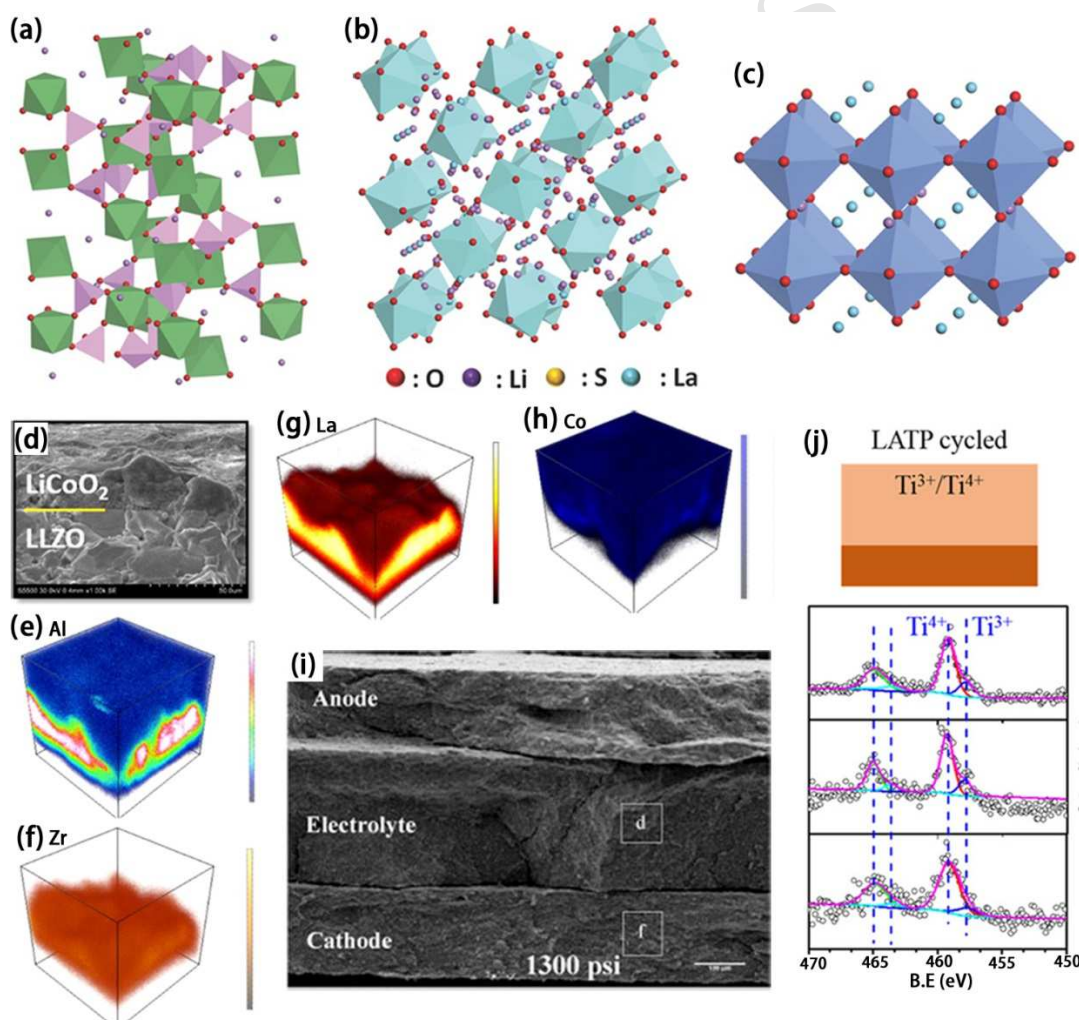


Figure 4. The crystalline structures of (a) NASICON, (b) Garnet, and (c) Perovskite SSEs [139]. Time-of-flight secondary ion mass spectroscopy (TOF-SIMS) study of  $\text{LiCoO}_2/\text{LLZO}$  interface: (d) SEM image of a  $\text{LiCoO}_2/\text{LLZO}$  interface and elemental distributions of (e)  $\text{Al}^+$ , (f)  $\text{Zr}^+$ , (g)  $\text{La}^+$ , and



(h)  $\text{Co}^{+}$ ; color scales show the concentrations of each ion where the upper color represent higher concentrations [129]. (i) Scanning electron microscopy (SEM) image showing the poor contact between NASICON SSE and  $\text{Li}_2\text{MnO}_4$  [140]. (j) X-ray photoelectron spectroscopy (XPS) study on the reduction of  $\text{Ti}^{4+}$  in LATP by lithium metal anode [138].

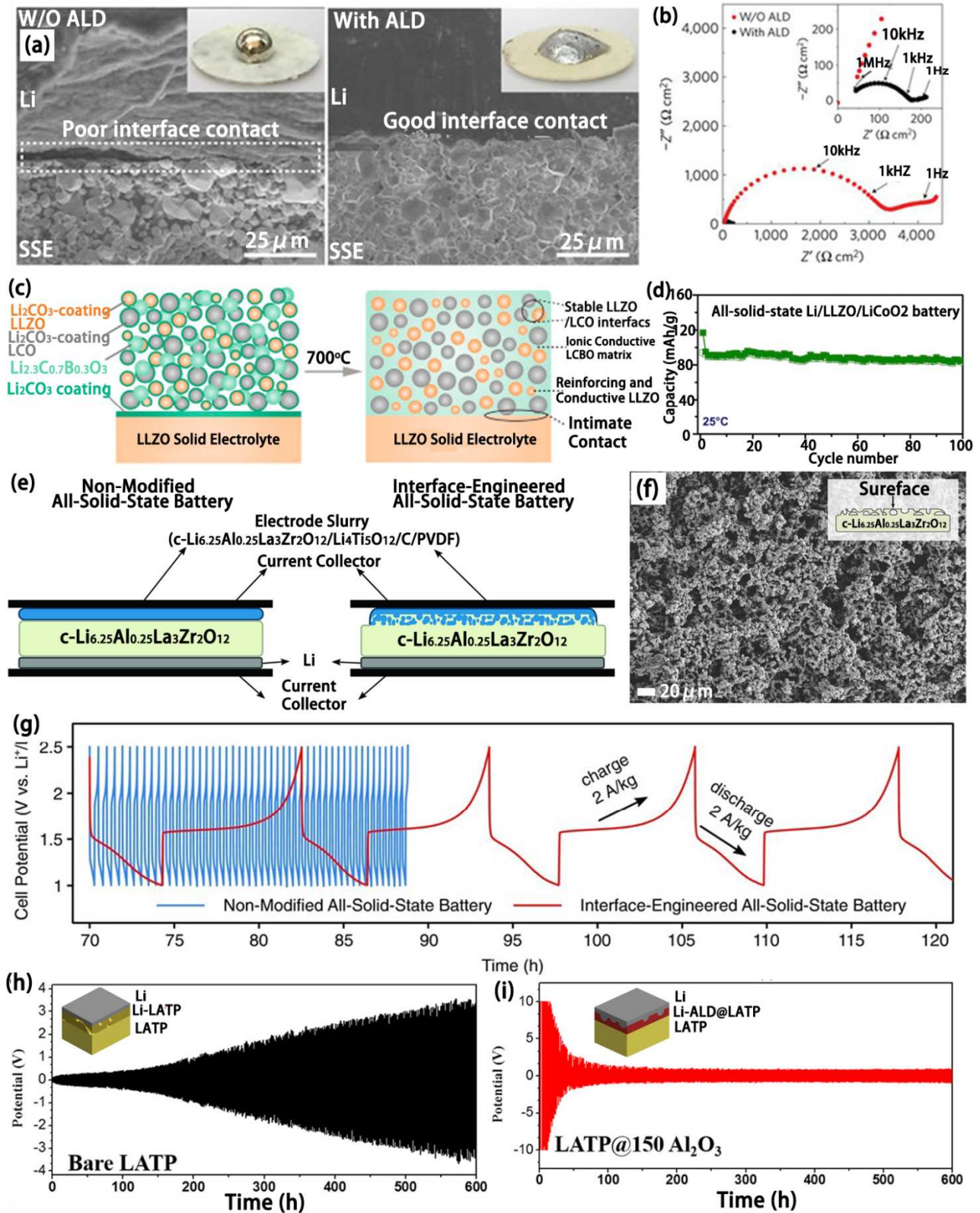


Figure 5. Summary of strategies for building SSLBs with oxide-based SSEs. (a) SEM images of the garnet SSE/lithium metal interface without ALD  $\text{Al}_2\text{O}_3$  coating (left) and with ALD  $\text{Al}_2\text{O}_3$  coating (right). The insets are photos of melted lithium metal on top of the garnet SSE surfaces. An intimate contact between lithium metal and SSE was achieved with ALD  $\text{Al}_2\text{O}_3$  coating. (b) Comparison of the impedances of symmetrical lithium cells with garnet SSEs with/without ALD  $\text{Al}_2\text{O}_3$  coating. The inset is the enlarged EIS curve of ALD  $\text{Al}_2\text{O}_3$  coating garnet SSE symmetrical cell where a very small impedance is presented [123]. (c) Schematic diagram shows the process of co-sintering to make a SSLB with oxide-based SSE. Left, mixture of LLZO particles, LCO particle,  $\text{Li}_{2.3}\text{C}_{0.7}\text{B}_{0.3}\text{O}_3$  sintering additive on the top of LLZO SSE pellet. Right, co-sintering this pellet at  $700\text{ }^\circ\text{C}$  to obtain an intimate SSE/cathode interface. (d) Cycling performance at RT of the SSLB obtained from (c), lithium metal was used as anode [126]. (e) Schematic diagrams show the structure of SSLBs with dense SSE (left) and porous structure SSE (right). (f) Surface SEM image of porous structure SSE pellet. (g) Comparison of SSLBs performances with dense SSE and porous structure SSE [127]. (h) Cycling performance of bare LATP/lithium symmetric cell at a current density of  $0.01\text{ mA/cm}^2$ . A significant increase of overpotential is observed. (i) Cycling performance of ALD  $\text{Al}_2\text{O}_3$  coating LATP/lithium symmetric cell at a current density of  $0.01\text{ mA/cm}^2$ ; The potential profile is quite stable with ALD coating [138].

### 1.1.3 Sulfide-based SSEs

Sulfide-based SSEs can be categorized by amorphous, crystalline, and glass-ceramic sulfide SSEs. The representative amorphous sulfide-based SSEs are  $x\text{Li}_2\text{S}\cdot(1-x)\text{P}_2\text{S}_5$  and  $x\text{Li}_2\text{S}\cdot(1-x)\text{SiS}_2$  systems. Both systems present a RT ionic conductivity over  $10^{-4}\text{ S/cm}$  [141, 142]. Crystalline sulfide-based SSE  $\text{Li}_3\text{PS}_4$  was first reported by Tachez et al [143]. Later, Kanno's group reported a thio-LISICON type SSE produced by replacing  $\text{O}^{2-}$  of LISICON [ $\text{Li}_{14}\text{Zn}(\text{GeO}_4)_4$ ] family with  $\text{S}^{2-}$  [144]. The replacement leads to a higher ionic conductivity at RT because  $\text{S}^{2-}$  has larger ionic radius, higher polarizability, and lower electronegativity than  $\text{O}^{2-}$ . The replacement of  $\text{O}^{2-}$  by  $\text{S}^{2-}$  lowers the binding of  $\text{Li}^+$  in the crystal framework and enlarges the ion transport channel thus enhance the ionic conductivity [145]. Most of the reported crystalline sulfide-based SSEs have an ionic conductivity over  $10^{-4}\text{ S/cm}$  at RT (Figure 6f) [145-148]. Glass-ceramic SSEs are prepared by

crystallization of glass-state SSEs. Glass-ceramic SSE based on  $x\text{Li}_2\text{S}-(1-x)\text{P}_2\text{S}_5$  have received tremendous research attentions especially after the discovery of  $\text{Li}_{10}\text{GeP}_2\text{S}_{12}$  (LGPS) (Figure 6a-c) families and their derivations such as  $\text{Li}_{9.54}\text{Si}_{1.74}\text{P}_{1.44}\text{S}_{11.7}\text{Cl}_{0.3}$  (Figure 6d,e) [146, 149, 150], which both exhibit ionic conductivities over  $10^{-2}$  S/cm at RT.

The high RT ionic conductivity and relatively soft mechanical properties of sulfide-based SSEs make them promising candidates for the applications in SSLBs. SSLBs with a sulfide-based SSE can be fabricated by simply cold pressing without high temperature co-sintering. However, sulfide-based SSEs suffer from serious instability issues towards lithium metal anodes and the conventional cathode materials, which significantly hinder their practical applications in SSLBs. The side reaction behaviors between electrodes and sulfide-based SSEs have received many research attentions [67, 70, 151-154]. The electrochemical stability window of different types of sulfide-based SSEs were evaluated by theoretical calculations (Figure 6g for LGPS) and experimental results [67, 70, 154, 155], where they showed the sulfide-based SSEs have a narrow electrochemical stable window. In-situ XPS was performed to clarify the interfacial chemistry between sulfide-based SSE and lithium metal, which confirmed the decomposition products of  $\text{Li}_3\text{P}$ ,  $\text{Li}_2\text{S}$ , and Li-Ge alloy at the interface [153]. The decomposed products have low ionic conductivities and thus introduce high interfacial resistance. To address this problem, alternative anodes like indium are commonly used in SSLBs [156]. An alternative strategy is interfacial engineering the lithium/SSE interface to stabilize the interface and lower the interfacial resistance [151, 157-159]. C. Wang's Group applied LiF, LiI as a protecting layer on lithium metal anode in to stabilize lithium/sulfide-based SSE interface [158, 159]. Our group first reported a molecule layer deposition (MLD) engineered lithium metal anode for stable contact with a sulfide-based SSE [151].

Considering the interface between sulfide-based SSEs and cathodes, the electrochemical instability problem and the formation of space-charge layer (SCL) seriously hinder the application of sulfide-based SSEs. The instability between sulfide-based SSEs and cathode materials such as  $\text{LiCoO}_2$  were studied by the theoretical calculation and transmission electron microscopy (TEM) confirming the side-reaction products of  $\text{Li}_2\text{S}$ ,  $\text{CoS}_3$  and  $\text{Co}(\text{PO}_3)_2$  at the interface that cause high interfacial resistance [152, 160]. SCL is typically formed at the interface between sulfide-based

SSEs and  $\text{LiCoO}_2$  due to the chemical potential difference between them (Figure 6h-j) [26]. The high resistance of SCL significantly lowers the capacity and rate performance of SSLBs. Interfacial engineering by an oxide material coating layer such as  $\text{Al}_2\text{O}_3$ ,  $\text{Li}_4\text{Ti}_5\text{O}_{12}$ , and  $\text{LiNbO}_3$ , has been demonstrated as an effective way to inhibit the side-reactions and SCL formation [26, 161, 162].

Even though sulfide-based SSEs are relatively soft compared to oxide-based SSEs, sulfide-based SSEs still experience the mismatch problem. Their poor flexibility makes it difficult to buffer the volume change of the electrode materials during charge and discharge; the loss of intimate contact between SSE and cathode particles eventually deteriorates the performance of the SSLBs (Figure 6k) [163]. Therefore, understanding the mechanical properties of SSEs and controlling the mechanical properties of SSEs to ensure good contact between SSEs and active materials are as important as preventing the SSE/electrode interfacial side-reaction for building a high performance SSLB.



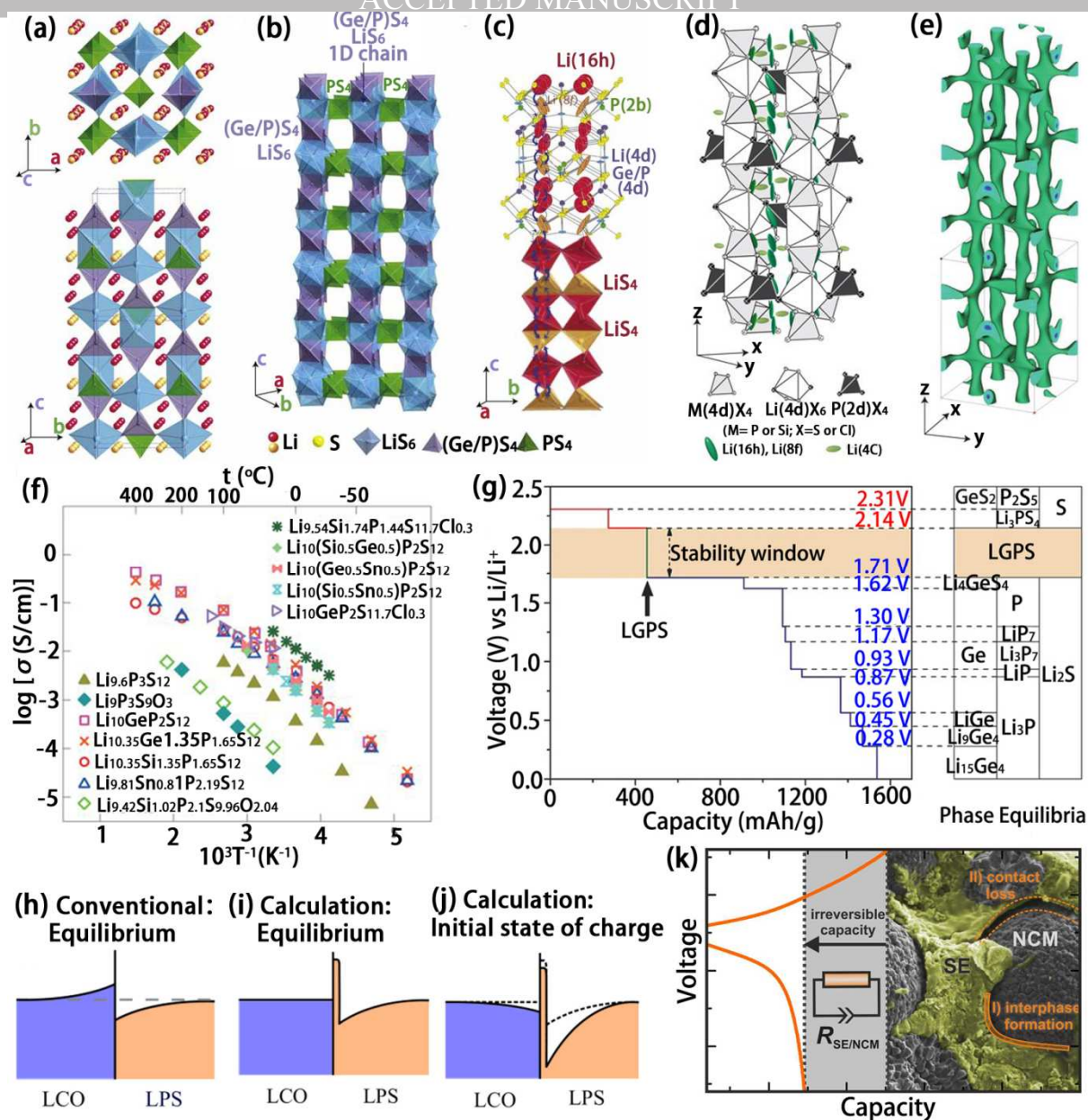


Figure 6. (a) Crystal structure of LGPS sulfide-based SSE; (b) one dimensional view of LGPS framework; (c) Li<sup>+</sup> ion conduction pathways in LGPS; zigzag conduction pathways along the c-axis are indicated [146]. (d) Crystal structure of  $\text{Li}_{9.54}\text{Si}_{1.74}\text{P}_{1.44}\text{S}_{11.7}\text{Cl}_{0.3}$ ; (e) nuclear distributions of Li atoms in  $\text{Li}_{9.54}\text{Si}_{1.74}\text{P}_{1.44}\text{S}_{11.7}\text{Cl}_{0.3}$  at 25 °C [149]. (f) Comparison on ionic conductivities of the LGPS family,  $\text{Li}_{9.6}\text{P}_3\text{S}_{12}$  and  $\text{Li}_{9.54}\text{Si}_{1.74}\text{P}_{1.44}\text{S}_{11.7}\text{Cl}_{0.3}$  [149]. (g) The first principles calculation for the phase equilibria of LGPS during lithiation and delithiation process, where it shows the stable window of LGPS is 1.71 – 2.14 V [67]. The equilibrium Li concentrations predicted by the conventional model (h) and the calculation model (i). (j) The equilibrium Li concentrations predicted by calculation model at the initial stage of charging for the LCO/LPS interface [26]. (k) Capacity lose at the initial

charge/discharge cycle and the lose of interfacial contact between cathode particles and a sulfide-based SSE [163].

#### 1.1.4 The mechanical properties of SSEs

Different from the liquid electrolytes which have the fluidity to fill in pores and gaps to ensure intimate contacts with electrodes, the solid nature of SSEs could be a drawback in terms of physical compatibility with electrode materials under operating conditions. Especially, the volumetric evolutions of most active materials during charging and discharging cast extra difficulties in maintaining intimate contacts between the SSEs and the active materials. Commercial active materials such as  $\text{LiCoO}_2$ ,  $\text{LiFePO}_4$ ,  $\text{LiMn}_2\text{O}_4$ , and graphite usually experience big volumetric changes during charging and discharging, while next-generation active materials such as sulfur and silicon have even more significant volumetric changes of 80% and 400% respectively. Therefore, practical SSEs must be able to accommodate the resulting strain/stress without the mechanical degradation such as cracking or pulverizing. Understanding and Improvements in SSE mechanical properties are progressing for SSLB applications [164-168]. Table 1 and 2 summarize the general mechanical properties of inorganic SSEs (oxide- and sulfide-based SSEs) and polymer involved hybrid electrolytes, respectively. Interestingly, the mechanical properties of inorganic SSEs are highly related to their phase structures. Particularly, the relative Young's moduli are in an descending order from perovskite, garnet, NASICON, phosphaste, to thiophosphate structured inorganic SSEs, with the magnitude from 200 GPa to 20 GPa [164]. However, the Young's moduli of polymer-based electrolytes are lower by about 3 orders of magnitude compared to that of inorganic SSEs. Young's moduli is a parameter to describe the stiffness of a solid material. It defines the relation between the stress (force per unit area) and strain (proportional deformation) of the solid material which undergo a uniaxial deformation in the linear elasticity region. The higher the Young's moduli, the stiffer the material, the harder to be deformed.

Mechanical related interfacial properties are an important topic in SSLBs. C. Monroe and J. Newman suggested that the shear modulus of SSEs should be at least twice higher than that of lithium metal to prevent lithium dendrite formation [99]. The shear modulus of lithium metal is 4.25 GPa, which means that SSEs with a shear modulus over 8.5 GPa can suppress lithium dendrite



formation. Regarding mechanical suppression on lithium dendrites, most inorganic SSEs (oxide- and sulfide-based SSEs) are strong enough, but the polymer-based electrolytes and composite electrolytes cannot satisfy this parameter (Table 1 and 2). Even though the shear modulus of polymer electrolytes are not given directly in Table 2, we can estimate them from the Young's modulus according to the following relationship:[120]

$$G = E \frac{1}{2(1+\nu)} \quad \text{Eq. (1)}$$

where E is Young's modulus; G is shear's modulus; and  $\nu$  is Poisson's ratio. For most homogeneous materials,  $\nu$  is between 0 and 0.5, giving a smaller value of G than E. Thus, the shear modulus of polymer electrolytes is at the MPa level or below, which is 1000 times smaller than that of lithium metal.

However, in practice, the high-shear-modulus inorganic SSEs such as LLZO and  $\text{Li}_3\text{PS}_4$  still suffer from lithium dendrite formation problem [123, 136, 137]. Possibly, the reason is that lithium dendrite grows around the grain boundary of inorganic SSEs where shear modulus is lower than that of the bulk materials (0.2 – 0.6 times of grain's shear modulus). If it is true, C. Monroe and J. Newman's proposal is still valid. However, lithium dendrite penetrating single crystal LLZO reported by T. Swamy et al. may overthrow this theory [169]. On the other hand, SPEs and hybrid electrolytes have low shear moduli actually demonstrated better compatibility with lithium anodes than the stiff inorganic SSEs because of the intimate contact with lithium anodes and uniform  $\text{Li}^+$  ion flux across the interface. Therefore, not only the mechanical properties but also the interfacial  $\text{Li}^+$  ion distributions are critical for inhibiting the lithium dendrite formation [73, 123].

Maintaining good solid-solid contacts can become even more challenging when incorporating particle shaped active materials in SSLBs. Active material particles such as graphite, silicon,  $\text{LiCoO}_2$ ,  $\text{LiFePO}_4$ , and sulfur experience volume changes of 13%, 400%, 2.6%, 7%, and 80% respectively. If the SSEs were to accommodate volumetric changes of active materials without mechanical degradation, SSEs should have low Young' modulus and low fracture toughness values. A detailed study between the battery performance and Young's modulus of sulfide-based SSEs was reported by M. Tatsumisago's group [170]. They found that lowering the Young's modulus of sulfide-based SSEs can enhance the performance of batteries. G. Bucci et al. suggested that a

volumetric change over 7.5 % (corresponding to 2.5 % increase in the radius) for active particles will trigger the delamination between SSEs and active materials. If the elastic modulus of the SSE is lower than 25 GPa, the onset of delamination can be increase to 25 % volumetric change of active particles, which is sufficient for accommodating LiCoO<sub>2</sub>, LiFePO<sub>4</sub>, and graphite [166, 167]. In other words, sulfide-based SSEs and SPEs with Young's moduli below 25 GPa are suitable for SSLBs using commercial electrode materials such as LiCoO<sub>2</sub>, LiFePO<sub>4</sub>, and graphite etc. For the active materials with larger volumetric expansion such as sulfur and silicon, SPEs and hybrid electrolytes with an even lower Young's modulus are favorable.

Table 1 The mechanical parameters of inorganic SSEs

Inorganic SSEs	Phase	Grain size ( $\mu\text{m}$ )	Relative density (%)	Young's modulus (GPa)	Shear modulus (GPa)	Hardness (GPa)	Fracture toughness (MPa m <sup>1/2</sup> )	Refs.
Li <sub>3</sub> Ti <sub>2</sub> (PO <sub>4</sub> ) <sub>3</sub> (calculated)	NASICON			143.7	57.6			[164]
Li <sub>1.3</sub> Al <sub>0.3</sub> Ti <sub>1.7</sub> (PO <sub>4</sub> ) <sub>3</sub>	NASICON	1.7 ± 0.7	96	115			1.1 ± 0.30	[119]
Li <sub>3</sub> PO <sub>4</sub> (calculated)	phosphate			103.4	40.9			[164]
Li <sub>7</sub> La <sub>3</sub> Zr <sub>2</sub> O <sub>12</sub> (calculated)	garnet			175.1	68.9			[164]
Li <sub>5</sub> La <sub>3</sub> Nb <sub>2</sub> O <sub>12</sub> (calculated)	garnet			141.1	54.8			[164]
Li <sub>5</sub> La <sub>3</sub> Ta <sub>2</sub> O <sub>12</sub> (calculated)	garnet			144.2	56.1			[164]
Li <sub>6.24</sub> La <sub>3</sub> Zr <sub>2</sub> Al <sub>0.24</sub> O <sub>11.98</sub>	garnet	4.5 - 5	97	149.8 ± 0.4		6.3 ± 0.3		[171]
Li <sub>6.24</sub> La <sub>3</sub> Zr <sub>2</sub> Al <sub>0.24</sub> O <sub>11.98</sub>	garnet	4.5 - 5	94	132.6 ± 0.2		5.2 ± 0.4		[171]
Li <sub>6.19</sub> La <sub>3</sub> Zr <sub>2</sub> Al <sub>0.27</sub> O <sub>12</sub>	garnet	3.7 ± 1.8	98	140		9.1	0.97 ± 0.1	[172]
Li <sub>6.19</sub> La <sub>3</sub> Zr <sub>2</sub> Al <sub>0.27</sub> O <sub>12</sub>	garnet	2.7 ± 1.7	85	135		9.1	2.37 ± 0.1	[172]
Li <sub>6.17</sub> La <sub>3</sub> Zr <sub>2</sub> Al <sub>0.28</sub> O <sub>12</sub>	garnet	5 - 50	99	150.3 ± 2.2	59.8 ± 0.9			[120]
Li <sub>6.28</sub> La <sub>3</sub> Zr <sub>2</sub> Al <sub>0.24</sub> O <sub>12</sub>	garnet	2 - 30					0.86 - 1.63	[173]
Li <sub>6.5</sub> La <sub>3</sub> Ta <sub>0.5</sub> Zr <sub>2</sub> O <sub>12</sub>	garnet	1 - 10	99	153.8 ± 2.7	61.2 ± 1.1			[120]
Li <sub>0.5</sub> Ta <sub>0.5</sub> TiO <sub>3</sub> (calculated)	perovskite			262.5	104.0			[164]
Li <sub>0.13</sub> Ta <sub>0.63</sub> TiO <sub>3</sub> (calculated)	perovskite			233.9	91.2			[164]
Li <sub>0.33</sub> La <sub>0.57</sub> TiO <sub>3</sub>	perovskite	0.8 ± 0.3	97	200 ± 3		9.2 ± 0.2	~ 1	[174]
Li <sub>0.33</sub> La <sub>0.55</sub> TiO <sub>3</sub>	perovskite	2.42	99	222.6		7.18		[175]
Li <sub>0.33</sub> La <sub>0.567</sub> TiO <sub>3</sub>	perovskite	13.0 ± 4.39	99	203		8.4 ± 0.48	1.24 ± 0.12	[121]
Li <sub>0.33</sub> La <sub>0.567</sub> TiO <sub>3</sub> - 2.5 % La	perovskite	4.08 ± 1.16	99	198		9.3 ± 1.1	1.08 ± 0.20	[121]
Li <sub>0.33</sub> La <sub>0.567</sub> TiO <sub>3</sub> + 2.5 % La	perovskite	1.41 ± 4.76	99	191		8.1 ± 0.75	1.22 ± 0.25	[121]
xLi <sub>2</sub> S•(100-x)P <sub>2</sub> S <sub>5</sub> (hot press)				18 - 25				[176]
xLi <sub>2</sub> S•(100-x)P <sub>2</sub> S <sub>5</sub> (cold press)				14 - 17				[176]

70Li <sub>2</sub> S•30P <sub>2</sub> S <sub>5</sub>		18.5 ± 0.9	1.9 ± 0.2	0.23 ± 0.04	[177]
(100-y)(75Li <sub>2</sub> S•25P <sub>2</sub> S <sub>5</sub> )•yLiI		19 - 23	7.1 - 8.7		[170]
70(50Li <sub>2</sub> S•50P <sub>2</sub> S <sub>5</sub> )•30LiI		17	6.3		[170]
Li <sub>10</sub> GeP <sub>2</sub> S <sub>12</sub> (calculated)	thiophosphate	37.19	14.35		[178]
Li <sub>10</sub> GeP <sub>2</sub> S <sub>12</sub> (calculated)	thiophosphate	21.7	7.9		
Li <sub>10</sub> SiP <sub>2</sub> S <sub>12</sub> (calculated)	thiophosphate	24.8	9.2		
Li <sub>10</sub> SnP <sub>2</sub> S <sub>12</sub> (calculated)	thiophosphate	29.1	11.2		
Li <sub>7</sub> P <sub>5</sub> S <sub>11</sub>	thiophosphate	21.9	8.1		[164]
Li <sub>6</sub> PS <sub>5</sub> Cl	thiophosphate	22.1	8.1		
Li <sub>6</sub> PS <sub>5</sub> Br	thiophosphate	25.3	9.3		
Li <sub>6</sub> PS <sub>5</sub> I	thiophosphate	30	11.3		
LIPON	thiophosphate	77		3.9 - 4.1	[179]
Li		5	4.25	10 <sup>-3</sup>	[120, 177]

Table 2 Mechanical properties of polymer and hybrid electrolytes

Polymer electrolyte	Inorganic fillers size and percentage	Plasticizer and percentage	Temperature (°C)	Young's modulus (GPa)	Shear modulus (GPa)	Tensile strength (GPa)	Refs.
PEO			RT	84.5 ± 10.3 × 10 <sup>-3</sup>			[180]
PEO-LiClO <sub>4</sub>			RT	14.5 ± 6.4 × 10 <sup>-3</sup>			[180]
PEO/(PEO-b-PE)-LiClO <sub>4</sub>			RT	114.2 ± 9.3 × 10 <sup>-3</sup>			[180]
PEO-LITFSI			RT			1.7 × 10 <sup>-3</sup>	[181]
PEO-LITFSI			85	~10 <sup>-6</sup>			[182]
PMMA-PVC-LiC F <sub>3</sub> SO <sub>3</sub>		dibutyl phthalate		1.18 × 10 <sup>-6</sup>			[183]
PVDF-HFP		1M LIPF6 in EC/DMC (425%)		9.2 × 10 <sup>-3</sup>		6.5 × 10 <sup>-3</sup>	[184]
PVDF-HFP	Al <sub>2</sub> O <sub>3</sub> 30-50 nm (6%)	1M LIPF6 in EC/DMC (459%)		18.5 × 10 <sup>-3</sup>		9.2 × 10 <sup>-3</sup>	[184]
PVDF-HFP	SiO <sub>2</sub> 30-50 nm (6%)	1M LIPF6 in EC/DMC (459%)		16.9 × 10 <sup>-3</sup>		10.3 × 10 <sup>-3</sup>	[184]
PVDF-HFP	BaTiO <sub>3</sub> 30-50 nm (6%)	1M LIPF6 in EC/DMC (462%)		17.3 × 10 <sup>-3</sup>		12.5 × 10 <sup>-3</sup>	[184]
PVDF(80)-PEO(20)	LTAP (6%)			14.8 × 10 <sup>-3</sup>		9.3 × 10 <sup>-3</sup>	[185]
PFPE-LITFSI	75Li <sub>2</sub> S•25P <sub>2</sub> S <sub>5</sub> (7%)				2.6 × 10 <sup>-3</sup>		[186]

Table 3 Summaries of the challenges and solutions for SSE/electrode interfaces

SSEs	Interface issues	Solutions for SSE/Li interface	Interface issues toward	Solutions for SSE/cathode
------	------------------	--------------------------------	-------------------------	---------------------------

	toward Li anode		cathode	interface
PEO SPE	1. Li dendrite formation [29];	1. inorganic fillers for enhancing mechanical strength and interface stability [187]; 2. rigid support for enhancing the mechanical strength [188, 189]; 3. cross-linked polymer for enhancing the mechanical strength [190];	1. electrochemical oxidation of PEO at low voltage (<3.8V) [69];	1. interface modification with metal oxide and polymer materials [100, 101]; 2. SPE modification with a high voltage stable polymer electrolyte [191];
LLZO	1. poor wettability [123]; 2. high interfacial resistance;	1. interface engineering to achieve a lithiophilic LLZO/Li interface [123]; 2. Li <sub>2</sub> CO <sub>3</sub> free LLZO surface for good lithium wettability [192];	1. poor interface contact [66]; 2. high interfacial resistance; 3. side reaction [135]; 4. volumatic expansion induced mechanical degradation [193];	1. co-sintering with low melting point SSE [129]; 2. interface coating to avoid side reaction [126]; 3. enlarging the SSE/electrode materials contact by porous SSE [127];
LATP	1. reduction of Ti <sup>4+</sup> [138];	1. interface engineering LATP/Li to prevent the directly contact [138];	1. poor interface contact [140];	
Sulfide-based SSEs	1. side reaction [153]; 2. Li dendrite formation [136];	1. indium anode; [156] 2. interface modification to avoid side reaction [158];	1. poor contact [68]; 2. space charge layer (SCL) [26]; 2. side reaction [160]; 3. volumatic expansion induced mechanical degradation [163];	1. metal oxide coating to prevent SCL and side reaction [26, 160]; 3. cycling battery at high pressure [132];

Other SSEs such as nitride-based SSEs Li<sub>3</sub>N, LiPON and LiBH<sub>4</sub> [194] are also received some research interests in SSLBs due to their intrinsic advantages. For example, Li<sub>3</sub>N has an ionic conductivity over 10<sup>-4</sup> S/cm at RT [195]. LiPON is widely used in thin film battery even though its ionic conductivity is only around 10<sup>-6</sup> S/cm [196]. However, a detail discussion about these SSEs will not be covered in here because few of these SSEs are reported as a component of hybrid electrolytes.

The challenges and solutions for SSE/electrode interface is summarized in Table 3. There is no simple solution to address all the aforementioned issues in an individual SSE. Thus, hybrid electrolytes are proposed to combine the merits of two or more types of SSEs and show promising

applications in SSLBs. According to the components and structure difference, the hybrid electrolytes can be classified into four types: polymer-oxide composite, polymer-sulfide composite, liquid-oxide, and polymer-oxide multilayer hybrid electrolytes (Figure 2b). These hybrid electrolytes will be systematically discussed in the following sections.

## 2. Composite electrolytes

### 2.1 Synthesis of composite electrolytes

A hybrid electrolyte with inorganic fillers in SPE (ceramic in polymer) or SPE filled inorganic SSE (polymer in ceramic) is named composite electrolyte. When designing a composite electrolyte, the execution and fabrication method is very important. Before introducing the properties of the hybrid electrolytes and their application in SSLBs, we will start with their common synthesis methods. Figure 7 schematically describes four common methods including solution casting, mechanochemical (hot press), infusion methods and 3D printing. Each method will be discussed in detail in the following sections.

#### 2.1.1 Solution casting method

Among of the preparation methods, solution casting is one of the most popular method and scalable for practical application. Solution casting is a solidification process by evaporating the solvent of a SPE slurry in an inert mold of a desired shape or by doctor blade casting as thin film. This method is commonly used for preparing SPE, gel polymer electrolyte, and inorganic SSE fillers-containing composite electrolytes. The casting procedures of a composite electrolyte include three steps: (i) disperse designated polymer, salt and fillers in a solvent; (ii) cast the mixture into a mold or doctor blade on a substrate followed by evaporation of the solvent to solidify the electrolyte; (iii) detach the solidified electrolyte film from the mold or substrate. The solution casting method is facile, easily tunable for film thickness, low cost, and scalable.

Solvents used in the casting process must be carefully chosen. Desired solvents should be volatile and chemically inert to materials being dispersed. For casting a composite electrolyte with a PEO matrix, acetonitrile is the most common solvent because of its good solubility with PEO and low boiling point. More importantly, most ceramic SSEs are stable against acetonitrile solvent. Thus,

acetonitrile is most commonly used to cast PEO-inorganic SSE composite electrolytes with good electrochemical performance. Water can be another good solvent in some cases, serving an essential role in the in-situ hydrolysis of titanium ethoxide or tetraethyl orthosilicate in PEO solution to make a composite electrolyte with in-situ formation of ultra-tiny  $\text{TiO}_2$  or  $\text{SiO}_2$  particles fillers to effectively enhance the ionic conductivity [197, 198]. However, oxide-based SSEs such as LLZO can undergo  $\text{Li}^+/\text{H}^+$  exchange in an moisture environment [199] and sulfide-based SSE is not stable against water, either [200]. Thus, the instability of oxide-based and sulfide-based SSEs in water limits its usage as a universal solvent.

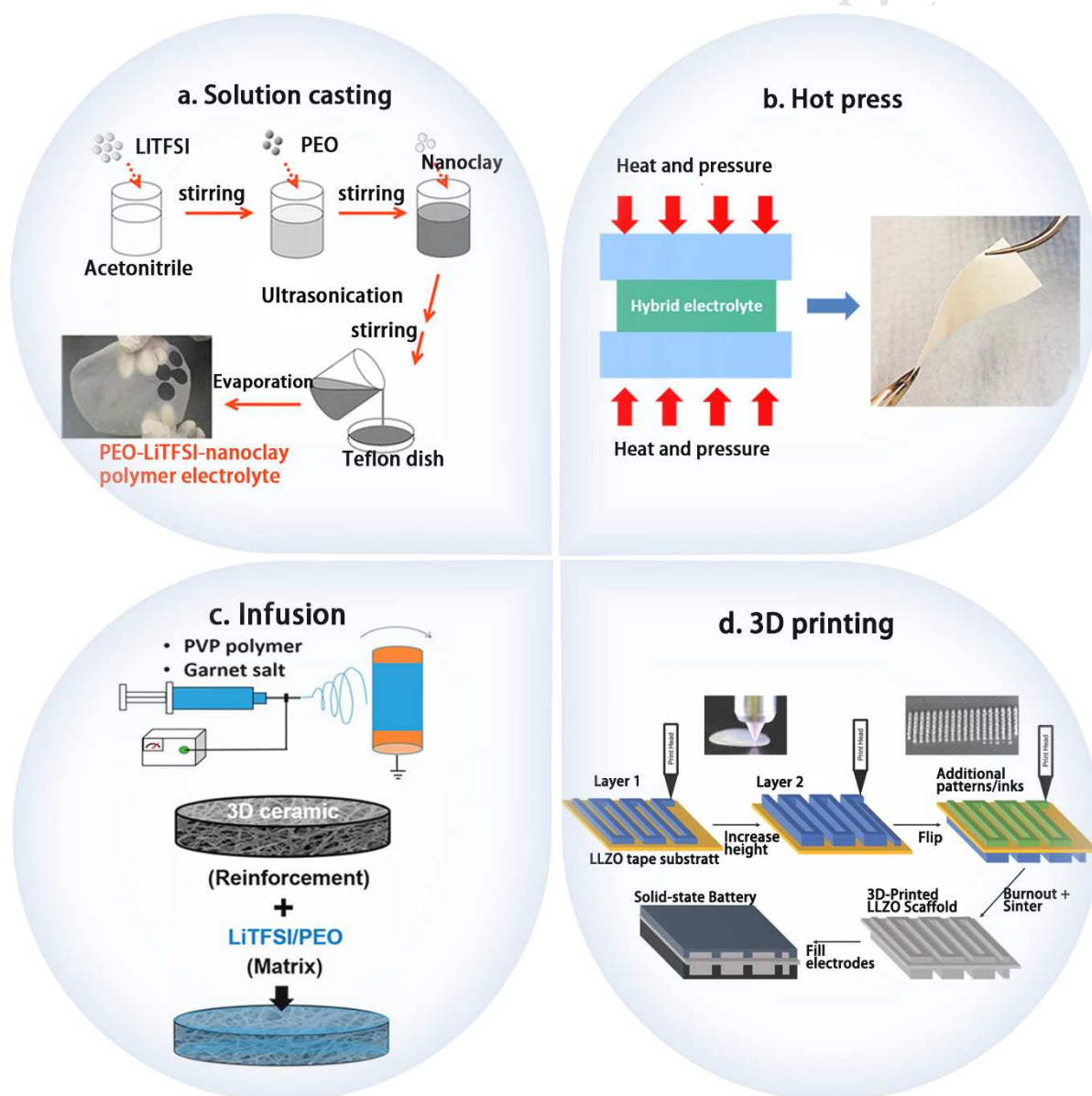


Figure 7. Fabrication methods of composite hybrid electrolytes. (a) solution casting method, (b) hot press method (mechanochemical method), (c) infusion method and (d) 3D printing method [28,



201-203].

### 2.1.2 Mechanochemical method

Composites of polymers and inorganic SSEs powders can be prepared mechanochemically, coupling mechanical and chemical processes. Ball milling is a typical example, in which locally high pressure and high temperature is created to facilitate the complex between polymers and inorganic fillers. Mechanochemical methods can eliminate the use of solvents and corresponding drawbacks such as possible side reactions caused by solvents. Such a preparation method is particularly favorable to hybrid electrolytes involving solvent-sensitive components, such as sulfide-based SSEs. Ball milling in Ar atmosphere for preparation of PFPE(hydroxy-terminated perfluoropolyether polymer, with molecule structure of  $\text{HO-CH}_2\text{-CF}_2\text{O-(CF}_2\text{CF}_2\text{O)}_x\text{-(CF}_2\text{O)}_y\text{-CF}_2\text{-CH}_2\text{-OH}$ )-75Li<sub>2</sub>S•25P<sub>2</sub>S<sub>5</sub>-lithium bis(trifluoromethanesulfonyl)imide (LITFSI), PEG(polyethylene glycol)-70Li<sub>2</sub>S•30P<sub>2</sub>S<sub>5</sub> and PEO-LLZO-LITFSI hybrid electrolytes have been studied [186, 202, 204]. Also, mechanochemical method is a powerful way to prepare hybrid electrolytes with components that are insoluble in any solvents. C. Liang's group reported a LLZO-βLi<sub>3</sub>PS<sub>4</sub>(LPS) hybrid electrolyte by ball milling LPS and LLZO followed by a pressing process to reduce grain boundary resistance and reshape the hybrid electrolyte. The highest ionic conductivity of the LLZO-LPS hybrid electrolyte can reach over 10<sup>-4</sup> S/cm at RT [205]. After ball milling, hot pressing is common subsequent step for a mechanochemical process to ensure uniform thickness of a composite electrolyte film. The hot pressing process is involved in most of the preparation processes in the SPE-oxide composite electrolyte [202] and the fabrication of cathode-polymer composites electrode to reduce interfacial resistance between SSE and cathode electrode [206].

### 2.1.3 Infusion method

Hybrid electrolytes prepared by solution casting or a mechanochemical method often consist of a continuous SPE matrix with low ionic conductivity and dispersed inorganic SSEs particles with high ionic conductivity. The high ionic conductivity of inorganic SSEs cannot be fully utilized at a discrete condition. The preferential Li<sup>+</sup> ion conduction through the SPE rather than the inorganic SSEs significantly limits the RT ionic conductivity and feasibility of hybrid electrolyte.

Alternatively, taking the advantage of the fluidity of a polymer solution, a composite electrolyte can be prepared by infusing a polymer solution into a porous inorganic SSEs framework and subsequent evaporation of solvent. In this case, the inorganic SSE component is continuous and accessible for fast  $\text{Li}^+$  ion transport.

L. Hu's group fabricated a PEO-LLZO-LiTFSI hybrid electrolyte by repeated drop-casting (infusing) PEO/LiTFSI solution into an electrospun 3D LLZO nanofiber membrane [28]. Similarly, Y. Yang's group synthesized a PEO-LATP- $\text{LiClO}_4$  membrane by employing a vertically aligned interconnected template of LATP SSE filled with a PEO- $\text{LiClO}_4$ -acetonitrile solution [207]. G. Yu and his co-workers developed a 3D nanostructured hydrogel-derived LLTO framework, which was used as a scaffold for fabricating PEO-LLTO-LiTFSI hybrid electrolyte [208]. Beneficial for the high ionic conductivity of continuous inorganic SSEs phase, these composite electrolytes delivered a high ionic conductivity of close and even over  $10^{-4}$  S/cm at RT.

#### 2.1.4 3D printing

Additive manufacturing (AM) alias 3D printing is emerging as a versatile technology for designing and fabricating complex electronic devices. For lithium batteries, many research efforts are dedicated to realize the 3D printing technique for creating electrodes of unique shapes [209-211], and preparing electrolytes to couple with unique shapes of electrodes [203, 212-216]. Different from the casting method and hot press method where the electrolytes are produced as flat thin films, 3D printing derived electrolytes could be easily designed with novel structures such as porous, discrete lines, grid-like, vertical columns and others [203, 213]. For example, using 3D printing method, D. W. McOwen et al. synthesized a novel structure of LLZO garnet type SSE. They created a stacked array LLZO SSE for implanting lithium anode. The as-prepared lithium symmetric cell with 3D printed LLZO SSE showed small LLZO/Li interface resistance and it can be cycled at a current density of  $0.33 \text{ mA/cm}^2$  with the potential of 7.2 mV [203]. The high performance LLZO/Li symmetrical cell is possibly originated from the 3D lithium metal anode created by infusing melting Li into the 3D printed LLZO SSE frameworks, which can minimize the local current densities for stable lithium plating and stripping. Moreover, the 3D printed ceramic-polymer composite electrolyte reported by Aaron J. Blake et al. demonstrated better thermal stability compared to

commercial Celgard separator and excellent LIB performance [212]. It is expected that 3D printing would perform important role in SSEs and SSLBs fabrications.

Although significant achievements have been obtained in 3D printing lithium batteries materials, there are still many challenges and difficulties that need to be overcome. Firstly, the most common used 3D printing method in electrode/electrolyte fabrication is the extrusion method. The extrusion type 3D printing is yet hard to achieved high resolution due to the limitation of extrusion head [214]. The large extrusion diameters make it hard to precisely control the microstructure of electrodes. Secondly, the ink/paste/slurry for the 3D printing must meet unique viscoelastic properties (high viscosity and shear-thinning behavior) to facilitate 3D printing [209], posing difficulty to prepare 3D printing ink/paste/slurry with SSEs and/or active materials. Thirdly, even though hybrid electrolyte combining SPE and inorganic SSE composite can be printable by 3D printing technique, the composite has low ionic conductivity at RT without plasticizer. To enhance its ionic conductivity, the elevated temperature over the glass transition temperature or plasticizer have to be applied. However, in these ways, the polymer will become gel state and the 3D printed hybrid electrolyte is hard to maintain its 3D structure. Therefore, applying high resolution and advanced 3D printing techniques in hybrid electrolyte fabrication and developing high ionic conductivity 3D printed hybrid electrolytes will be expected for 3D printed SSLBs.

## 2.2 Configurations of composite electrolytes

### 2.2.1 Insulating fillers in SPEs

Before wide development of the hybrid electrolyte concept, composite electrolytes with insulating fillers and a SPE matrix had received many research attentions. The insulating fillers in the composite electrolytes can improve the ionic conductivity to some extent. In early 1980s,  $\alpha$ -Al<sub>2</sub>O<sub>3</sub> was introduced to a SPE for the first time. The insulating fillers are shown to be able to improve the ionic conductivity by almost two orders of magnitude to 10<sup>-5</sup> S/cm level at RT [217, 218]. Thereafter, other different metal oxides such as TiO<sub>2</sub> [218-220], ZrO<sub>2</sub> [221, 222], and SiO<sub>2</sub> [221, 223, 224] have been widely studied in the composite electrolytes. Besides metal oxides fillers, metal organic framework (MOF) with a coordination network composed of central metal ions and organic ligands, exhibiting properties of both inorganic and organic materials, are proposed as unique

fillers. In comparison with the traditional inorganic fillers, MOFs not only possess some similar properties to metal oxide fillers such as high thermal stability, large surface area, and abundant Lewis-acid sites, but also have easily modified organic functional groups for improving the ionic conductivity and interfacial compatibility as well [187, 225]. Based on the above advantages, C. Yuan et al, dispersed the MOF-5 nanoparticles into a PEO electrolyte. As a result, improved interfacial stability and a ionic conductivity of  $3.16 \times 10^{-5} \text{ S cm}^{-1}$  at 25 °C were obtained [226]. Following up, several different kinds of MOFs such as Al(BTC) and MIL-53(Al) with similar roles were proposed to improve ionic conductivity [227, 228]. In order to compensate the decreased ionic conductivity resulted from the aggregation of high surface energy of MOFs fillers, Z. Wang et al, linked the MOF nanoparticles to the flexible polymer chains by one-pot UV photopolymerization method. Beneficial for the uniformly dispersed MOF fillers via chemical bonding, a ionic conductivity of  $4.31 \times 10^{-5} \text{ S cm}^{-1}$  at 30 °C was achieved [225]. Despite the improved ionic conductivity, mechanical properties and interfacial compatibility by adding these insulating fillers, the relative low ionic conductivity of  $10^{-5} \text{ S cm}^{-1}$  level at RT still cannot meet the practical demands for SSLBs.

### 2.2.2 Polymer-oxide SSE composite electrolyte

Considering aforementioned inorganic fillers are ionic insulator, which significantly limits further improvements of the ionic conductivity. A composite electrolyte with oxide-based SSEs mixing with SPE is discussed in this part. Combination of a SPE and an oxide-based SSE can possibly ensure mechanical flexibility, high ionic conductivity, good wettability to electrodes, good mechanical properties, dendrite free, and enhanced electrochemical stable window at the same time. The composite electrolyte can be classified as ‘ceramic in polymer’ and ‘polymer in ceramic’ according to the contents of the ceramic fillers (Figure 8a, b).

Many recent studies focus on enhancing the ionic conductivity of SPEs by adding oxide-based SSE fillers. NASICON SSEs, including LATP and LAGP, have been widely studied as fillers [207, 229-232]. The inorganic SSE fillers can not only reduce the crystalline of polymer matrix but also possibly provide extra ion transporting pathway. Y. Wang et al. systematically studied the effect of the incorporation of LATP fillers in a PEO-LATP hybrid electrolyte. They found that increasing the LATP content can decrease the melting temperature ( $T_m$ ) of the PEO complex. Scanning electron microscopy (SEM) analysis showed decreased size of the PEO spherulites after addition of LATP

fillers. An ionic conductivity of  $1.167 \times 10^{-3}$  S/cm at  $60^\circ\text{C}$  was achieved with 15 wt.% LATP fillers at a  $\text{EO}/\text{Li}^+$  ratio of 8 [230].

Since LATP suffers from  $\text{Ti}^{4+}$  reduction problem in contact with lithium metal anode, LAGP of the same structure but without  $\text{Ti}^{4+}$  also received many research attentions in composite electrolytes. Y. Zhao et al. had studied the influence of size and concentration of LAGP on the ionic conductivity of the PEO-LAGP-LiTFSI hybrid electrolyte. With different sizes of LAGP fillers, the hybrid electrolyte achieved optimal ionic conductivities with 15 - 20 wt.% of LAGP. For example, the ionic conductivity of PEO-LAGP-LiTFSI was optimized to  $6.76 \times 10^{-4}$  S/cm at  $60^\circ\text{C}$  with 20 wt.% nano-sized LAGP [233].

Enhanced ionic conductivity with perovskite-type SSE fillers in SPE matrix was also observed [234]. Y. Cui's group synthesized a nanowire shape of LLTO and incorporate it into PAN-LiClO<sub>4</sub> SPE and they found that with 15 wt.% nanowire LLTO fillers, the hybrid electrolyte PAN-LLTO-LiClO<sub>4</sub> exhibited a RT ionic conductivity of  $2.4 \times 10^{-4}$  S/cm.

Similar to other oxide-based SSEs, the garnet-type SSE LLZO has high ionic conductivity at RT, good electrochemical chemical and thermal stability. Unlike the LATP containing an unstable  $\text{Ti}^{4+}$  constituent, LLZO possesses superior electrochemical stability towards lithium metal anode [154, 235]. Consequently, LLZO fillers are expected to not only improve the ionic conductivity but also further improve the stability of hybrid electrolyte at the interface with lithium metal anode [236]. The reported data shows that SPE-LLZO hybrid electrolytes with different polymer-to-filler ratio had a wide range of ionic conductivities from  $10^{-6}$  to  $10^{-4}$  S/cm at RT. While a RT ionic conductivity of  $10^{-6}$  S/cm order of PEO-LiTFSI SPE filled in LLZO (70 wt.%) was reported by M. Keller et al. [202], a RT ionic conductivity of  $10^{-4}$  S/cm of PEO-LLZO hybrid electrolyte had been prepared by L. Hu' group [28] and J. Zhang et al. [237]. In the latter two cases, the reasons for the higher ionic conductivities are probably because of the usage of the 3D LLZO framework and ultra-small (~40 nm) size LLZO as the fillers.

In addition to the wide application of PEO-based SPEs in composite electrolytes, polymer electrolytes based on other polymers such as polyvinylidene fluoride (PVDF), PVDF-HFP, and polyethylene carbonate (PEC) also received many research attentions for constructing composite electrolytes due to their unique properties such as high mechanical strength and high lithium

transference number [93, 238-242]. However, additional solvent, liquid electrolyte, or combination with other SSEs are required to achieve feasible battery performance in these systems. The PVDF-LLZO hybrid electrolyte reported by X. Zhang et al. exhibited a high ionic conductivity of  $5 \times 10^{-4}$  S/cm at 25 °C, but residual DMF solvent remaining from the preparation process was found in the hybrid electrolyte according to their thermogravimetric analysis (TGA) results. The DMF content could have played an important role in the high ionic conductivity and battery performance. LiCoO<sub>2</sub> batteries with this PVDF-LLZO hybrid electrolyte exhibited excellent cycling performance and rate performance, delivering a discharge capacity of 130 mAh/g at 4C rate, which is comparable to that of liquid electrolyte system [239]. C. Sun's group reported a PVDF-HFP-LLZO hybrid electrolyte with RT ionic conductivity of  $1.23 \times 10^{-6}$  S/cm, which was increased to  $1.1 \times 10^{-4}$  S/cm with the addition of 20  $\mu$ L liquid electrolyte [242]. The LiFePO<sub>4</sub> battery with the PVDF-HFP-LLZO-liquid hybrid electrolyte presented excellent electrochemical performance at RT. L. Fan's group reported a PEC-LLZO hybrid electrolyte prepared by solution casting method, which had an ionic conductivity of  $5.24 \times 10^{-5}$  S/cm at 55 °C. This PEC-LLZO hybrid electrolyte presented much better thermal stability compared to commercial Celgard separator, and rendered a stable flexible SSLB at elevated temperature [238].

'Polymer in ceramic' composite electrolyte has high mechanical strength which is good at dendrite suppression. However, poor interfacial contact with electrode results in high interfacial resistance. 'Ceramic in polymer' composite electrolyte has better interfacial contact with electrodes, but its strength is not enough for dendrite suppression. The design using 'polymer in ceramic' composite electrolyte as the main ionic conductor and separator, 'ceramic in polymer' composite electrolyte as the interface to ensure intimate contact with lithium anode can render a long cycling performance, dendrite free SSLB (Figure 8c-e) [243].



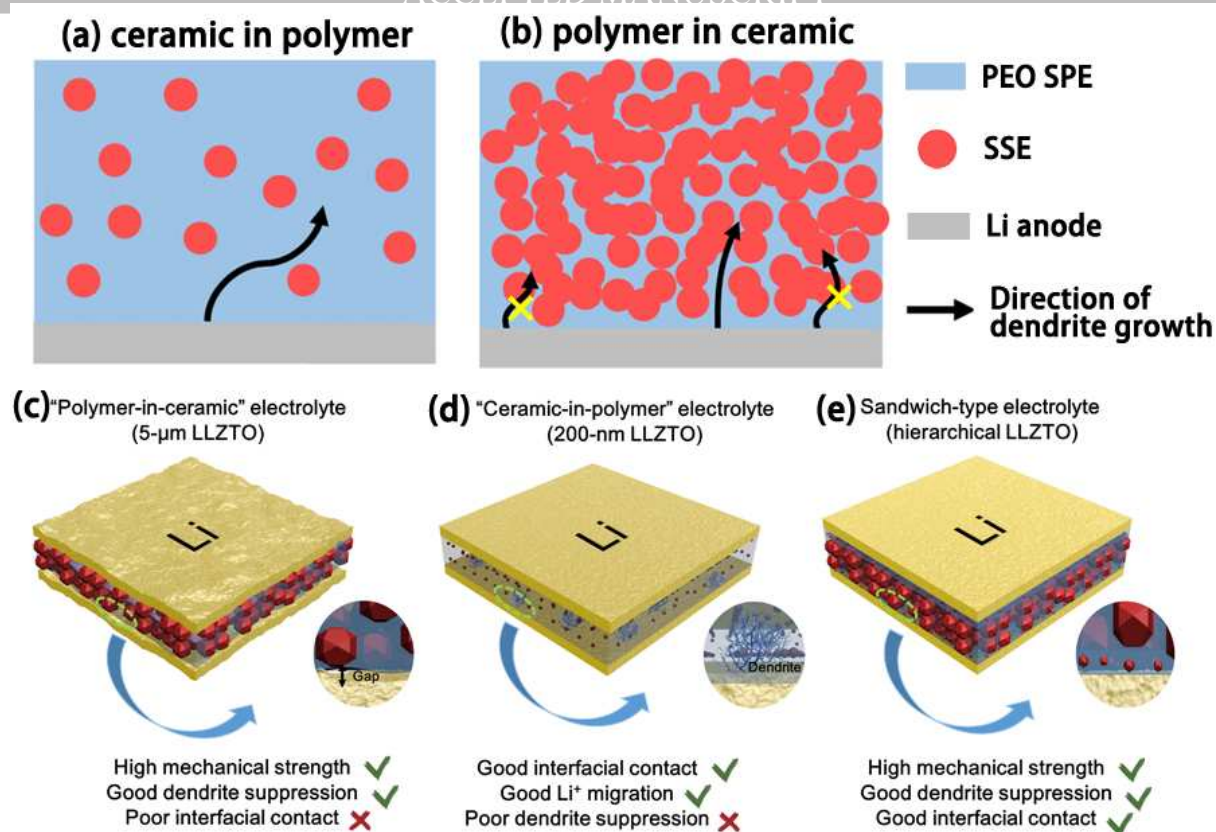


Figure 8. The composite electrolytes of (a) ceramic in polymer and (b) polymer in ceramic. Lithium dendrite growth mechanism of (c) ‘polymer in ceramic’ with SPE filled in 5  $\mu\text{m}$  size of LLZTO garnet SSE, (d) ‘ceramic in polymer’ with 200 nm size of LLZTO garnet SSE filled in SPE and (e) sandwich type composite electrolyte with ‘ceramic in polymer’ composite electrolyte at the Li/‘polymer in ceramic’ composite electrolyte interface [243].

### 2.2.3 Polymer-sulfide composite electrolytes

Sulfide-based SSEs have much higher ionic conductivities at RT than oxide-based SSEs, some of which are even comparable to liquid electrolytes [146]. Therefore, it is attractive to combine sulfide-based SSEs with SPEs to achieve a decent ionic conductivity and mechanical property. X. Xu’s group reported an improved ionic conductivity, enlarged electrochemical window, and stabilized electrolyte/Li interface hybrid electrolyte consisting of LGPS and PEO-LITFSI SPE [244]. In addition, the succinonitrile doping further increased the RT ionic conductivity of this hybrid electrolyte [244]. Another type of sulfide-based SSE containing  $\text{Li}_2\text{S}$ ,  $\text{P}_2\text{S}_5$  and  $\text{P}_2\text{O}_5$ ,  $\text{Li}_3\text{PS}_4$  have also been reported to complex with PEO-based SPE [72, 245]. Similar to the insulating fillers and oxide-based SSE filler, the enhancement in the ionic conductivity and interfacial stability

toward lithium metal anode was also achieved after adding sulfide-based SSEs into SPE.

To address the instability of sulfide-based SSEs in air and to enhance its flexibility, integrating SPEs into a sulfide-based SSE matrix is a strategy ('polymer in ceramic'). Sulfide-based SSEs have a Young's modulus in the range of 14-37 GPa (Table 1). Although the values are lower than that of oxide-based SSEs (~150 GPa) [176, 246], the sulfide-based SSEs are still rigid and brittle resulting in high grain boundary resistance and high interfacial resistance towards electrodes. The rigid property cannot accommodate the volume change of electrodes during charge/discharge process. To address these problems, a SPE, whose elastic modulus is around 20 MPa,  $10^3$  order lower than that of sulfide-based SSE [247], is introduced to improve flexibility and enhance the ambient stability of the sulfide-based SSE. However, the incorporation of a low ionic conductive SPE into a sulfide-based SSE matrix will sacrifice the high ionic conductivity. For example, incorporation of 1 wt.% - 5 wt.% comb shaped SPE (poly(oxyethylene)s with tri(oxyethylene)s as side chains complexing with  $\text{LiClO}_4$ . This polymer has the molecule structure of  $-(\text{CH}_2\text{CH}_2\text{O})_l-(\text{CH}_2\text{CHO}-(\text{CH}_2\text{O}(\text{CH}_2\text{CH}_2\text{O})_3\text{CH}_3))_m)_p-$ ,  $l = 81$ ,  $m = 19$ .) into 95(0.6 $\text{Li}_2\text{S}$ ·0.4 $\text{SiS}_2$ )·5 $\text{Li}_4\text{SiO}_4$  (mol%) sulfide-based SSE resulted in an ionic conductivity of  $\sim 10^{-5}$  S/cm at 60 °C, which is almost 10 times lower than that of the bulk sulfide-based SSE despite enhancing the flexibility of the SSE [248]. Thus, SPEs with a higher ionic conductivity are preferred. PFPE random copolymers-based SPE with an ionic conductivity over  $10^{-4}$  S/cm at RT is favorable [249]. I. Villaluenga et al. integrated 23 wt.% of PFPE-LITFSI SPE into a sulfide-based SSE, 75 $\text{Li}_2\text{S}$ ·25 $\text{P}_2\text{S}_5$ , matrix to fill up the gaps in the sulfide-based SSE pellets obtained from the cold press process. Significantly faster ion transport was achieved in this hybrid electrolyte by the compact packing and low grain boundary resistance. They also developed a method to calculate the ionic conductivity  $\sigma_{calc}$  of the hybrid electrolyte by the following equation (Eq.2) (ignoring any tortuosity):

$$\sigma_{calc} = \varphi_{sulfide} * \sigma_{sulfide} + \varphi_{PFPE} * \sigma_{PFPE} \quad \text{Eq. (2)}$$

where  $\varphi_{sulfide}$  and  $\varphi_{PFPE}$  are the volume fractions of the sulfide-based SSE and PFPE-LITFSI SPE;  $\sigma_{sulfide}$  and  $\sigma_{PFPE}$  are the corresponding ionic conductivities. The calculated values were in good consistence with the experimental values. The as-prepared hybrid electrolyte achieved an ionic conductivity over  $10^{-4}$  S/cm at 30 °C [186].

In a short summary of the as-mentioned SSEs, SPE-oxide and SPE-sulfide composite hybrid electrolytes, the ionic conductivities of each individual SSE and composite hybrid electrolytes are compared in Figure 9 below. From the chart, it is clear that the reported hybrid electrolytes have comparable ionic conductivities to the individual SSEs, not to mention other comprehensive advantages.

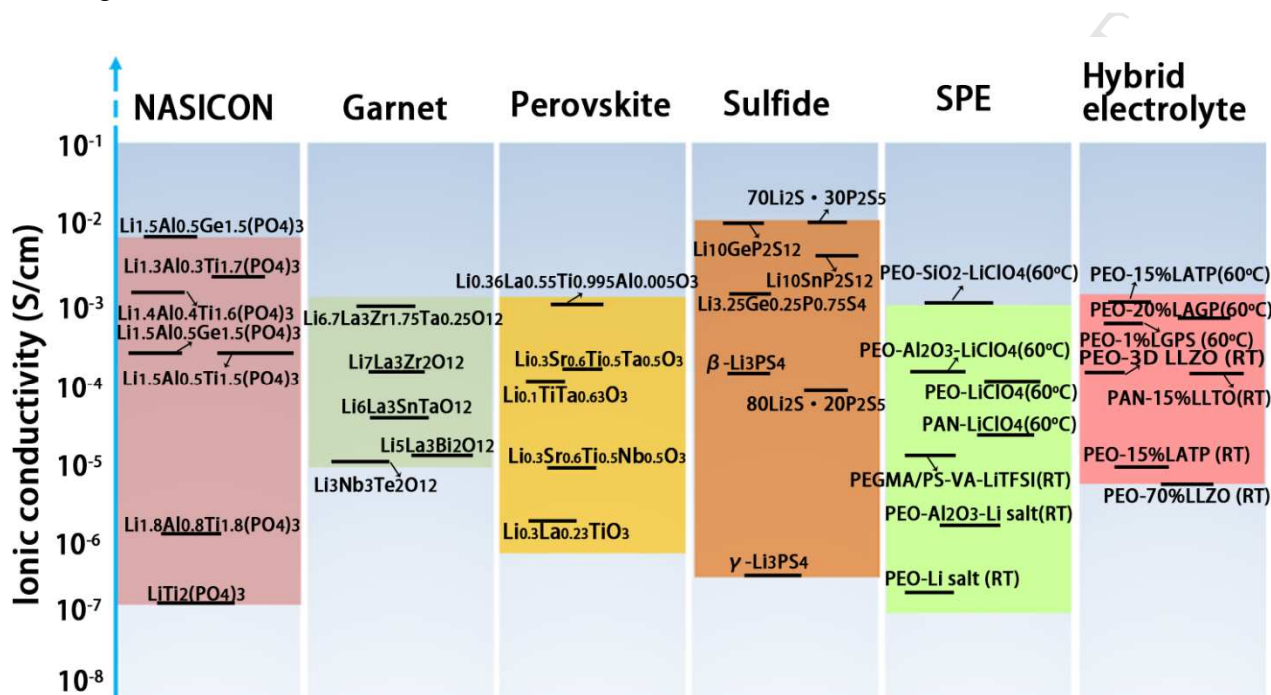


Figure 9. Comparison on ionic conductivities of different types of SSEs including NASICON-type [106, 230, 250-256], garnet-type [24, 108, 257-260], perovskite-type [261-266], sulfide-based SSEs [36, 143, 145, 146, 267-271], SPE [75, 83, 234, 272, 273], and hybrid electrolytes with composite structure [28, 202, 206, 207, 230, 232, 233, 236, 274, 275]. Hybrid electrolytes show comparable ionic conductivities to other individual SSEs.

### 2.3 Strategies to improve ionic conductivity of hybrid electrolytes

In the past two decades, many efforts have been dedicated to study the mechanism of insulating fillers (e.g.  $\text{Al}_2\text{O}_3$ ,  $\text{TiO}_2$ ,  $\text{SiO}_2$ ) in improving the ionic conductivity of the composite electrolytes. The improvements due to insulating ceramic fillers were proposed by following mechanisms: (i) the fillers physically interrupt and suppress the crystalline of polymer; (ii) Lewis acid-base type surface interactions between the filler surface and polymer chains kinetically inhibit the crystallization of

polymer chains; (iii) Lewis acid-base interactions at the interface between fillers surface and SPE provide preferential pathways for  $\text{Li}^+$  ion conduction; (iv) Lewis acid-base type surface interactions with the lithium salt facilitate the dissociation of the salt [147, 276-280].

In addition to the above mentioned filler effects, the inorganic SSE filler bulk can also serve as extra  $\text{Li}^+$  ion conduction channels, showing advantages over the insulating fillers [202, 281]. Therefore, SSEs fillers are preferred when designing a high ionic conductive hybrid electrolyte. In this chapter, focusing on the ionic conductivity enhancement for hybrid electrolytes, effects of size, concentration, and shape of the SSE fillers as well as plasticizer effects will be discussed.

### 2.3.1 Size and concentration of fillers

For insulating fillers such as  $\text{TiO}_2$ ,  $\text{Al}_2\text{O}_3$  and  $\text{SiO}_2$ , smaller size is preferred. Especially, nano-sized fillers have a high specific surface area are able to provide strong interaction with the polymer chains and lithium salts. Ceramic fillers interrupt the long-range order of polymer chains and thus increase the percentage of amorphous phase. The effect is more significant when the size of fillers is close to the chain length of the polymer [282]. M. Dissanayake et al. had systematically studied the effects of  $\text{Al}_2\text{O}_3$  filler size and concentration on conductivities in a PEO- $\text{LiCF}_3\text{SO}_3$  (LiTf) SPE [276]. They found that the smaller size of the fillers led to a higher ionic conductivity. The optimal ionic conductivity achieved with 5.8-nm size  $\text{Al}_2\text{O}_3$  fillers was one order of magnitude higher than that with 10- $\mu\text{m}$  size fillers. They believed that the smaller sized  $\text{Al}_2\text{O}_3$  fillers have higher surface area which is beneficial to the favorable surface interactions.

The effects of size and concentration of LLZO SSE fillers in a PEO polymer matrix was systematically studied by J. Zhang et al [237]. In the study, PEO-LLZO hybrid electrolytes were prepared without any lithium salts. They believed that  $\text{Li}^+$  near the LLZO particle surface can be influenced by the PEO polymer. In consequence, lithium vacancies on LLZO grain surface are created. The surface Li vacancies of LLZO provide sites for  $\text{Li}^+$  transfer. As a result, both high ionic conductivity of LLZO particle and the surface vacancies contributed to the overall conductivity enhancement of the hybrid electrolyte. The percolation effect was considered to play an important role in improving ionic conductivity. Figure 10a shows the ionic conductivities of PEO-LLZO hybrid electrolytes with different sizes of LLZO fillers and different concentrations. With the size of 40 nm, 400 nm and 10  $\mu\text{m}$  LLZO fillers, the conductivities were optimized at 12.7, 15.1, and 21.1

vol.%, respectively. The highest ionic conductivity of PEO-LLZO composite electrolyte at 30 °C can be over  $10^{-4}$  S/cm with 12.7 vol.% 40 nm LLZO fillers. Y. Zhao et al. also studied the effects of LAGP fillers size and concentration effect on ionic conductivity for PEO-LAGP-LITFSI composite electrolyte [233]. With different sizes of LAGP fillers, the conductivities were optimized with 15 - 20 wt.% LAGP fillers. For example, with 20 wt.% nano-size LAGP fillers, the hybrid electrolytes exhibited the highest ionic conductivity of  $6.76 \times 10^{-4}$  S/cm at 60 °C.

### 2.3.2 Shape of fillers

Depending on the  $\text{Li}^+$  ion conduction mechanism, the shape of SSE fillers can be an important factor effecting the ionic conductivity of composite electrolytes. For insulating ceramic fillers, the conductivity improvement mainly relies on the interactions of their surface groups with the surrounding polymer chains and lithium salts. As long as the insulating fillers have high surface area allowing effective surface interactions, a particular shape of insulating fillers is not of importance. Particle shape of insulating fillers are most commonly used in this case due to the variety of metal oxides such as nano-size  $\text{Al}_2\text{O}_3$ ,  $\text{SiO}_2$ , and  $\text{TiO}_2$  particles with different surface groups are commercially available [76, 197, 273, 283, 284]. Differently, besides surface interactions between fillers and polymer and lithium salts, ionic conducting SSE fillers can provide additional  $\text{Li}^+$  ion pathways within the fillers, hence particular interconnecting structures can be designed to maximize ionic conductivity and minimize the grain boundary. In addition to commercial and home-made nano-size SSEs particles [233], novel shapes of nanowire (random or vertical aligned) and 3D network structures have been rationally designed and synthesized for hybrid electrolyte [28, 207, 234].

One dimensional LLTO nanowire fillers can be prepared by electrospinning polyvinylpyrrolidone polymer fiber that contains Li, La, and Ti salts and subsequent calcination at 600 ~ 900°C in air for 2 h [234]. This nanowire fillers were applied in PAN- $\text{LiClO}_4$  based hybrid electrolyte in comparison with LLTO nanoparticle fillers. As schematically shown in Figure 10b, the interconnecting nanowires provide a network for express  $\text{Li}^+$  ion conduction, while the  $\text{Li}^+$  ion pathway is intermittent through the discrete particles. The nanowire LLTO fillers enabled significantly higher ionic conductivity than nanoparticle LLTO fillers of the same concentration. With 15 wt.% LLTO nanowire fillers, an ionic conductivity over  $10^{-4}$  S/cm was achieved at 20 °C.



Simply mixing the inorganic SSE particles and SPE, where the SPE is a continuous phase and the inorganic SSE is a dispersed phase, is the most common method to prepare composite electrolyte. However, the  $\text{Li}^+$  ion can only transfer within SPE rather than from high conductive inorganic SSE particle to another, which significantly decreased the capability of SSE fillers. In this consideration, 3D continuous inorganic conductive frameworks were developed for shortening the  $\text{Li}^+$  ion transport pathway and further enhance the ionic conductivity. A vertically aligned LATP fabricated via an ice-template method filling with PEO-based SPE had been reported by Y. Yang's group (Figure 10c). The vertical structure of LATP is expected to provide a fast-ionic conductive channel in the composite electrolyte, thus, the result showed that a high ionic conductivity of  $5.2 \times 10^{-5}$  S/cm at RT was achieved [207]. L. Hu's group developed a 3D  $\text{Li}^+$  ion conducting network with garnet-type SSE LLZO to provide continuous channels for  $\text{Li}^+$  ion conduction in a PEO matrix (Figure 10d) [28, 285]. The RT ionic conductivity of this composite electrolyte was up to  $2.5 \times 10^{-4}$  S/cm, which was among the highest reported ionic conductivity for polymer-oxide hybrid electrolyte [28]. As a proof of concept, a continuous  $\text{Li}^+$  ion conducting network can effectively improve the RT ionic conductivity of polymer-oxide hybrid electrolytes.

### 2.3.3 Adding plasticizers

Besides tuning the design and properties of fillers, composite electrolytes can be tailored for higher ionic conductivity by adding plasticizers. Plasticizers can be low-molar-mass organics, organic solvents or ionic liquids (ILs). The working principle of plasticizers is to increase the content of amorphous phase of the SPE and improve segmental motion; at the same time, plasticizers promote the dissociation of lithium salt and thus increase the number of effective charge carriers [286-288]. Succinonitrile (SN) is a good example of a plasticizer which remains a plastic crystal under RT. Importantly, composites of SN and lithium salts have very high RT ionic conductivity (in the order of  $10^{-4}$  S/cm) [289]. Study shows that incorporating just a small amount of SN (9 wt.%) into a PEO-LAGP- $\text{LiClO}_4$  hybrid electrolyte can significantly improve the RT ionic conductivity from  $3.0 \times 10^{-5}$  to  $1.1 \times 10^{-4}$  S/cm. Using this hybrid electrolyte, SSLB with a  $\text{LiFePO}_4$  cathode delivered satisfying discharge capacity at 0.2 C and 0.5 C under 25 °C [232].

Using liquid electrolytes as plasticizers is also a very popular method to enhance the ionic conductivity and ensure complete wetting of electrodes for RT SSLBs functionality [231]. Hybrid

electrolytes of P(VdF-co-HFP)-LAGP-carbonate liquid electrolyte and P(VdF-co-HFP)-LLTO-carbonate liquid electrolyte had been reported by Seul-Ki Kim et al. and Hang T. T. Le et al. respectively. Both hybrid electrolytes presented good electrochemical performance in RT SSLBs [231, 290].

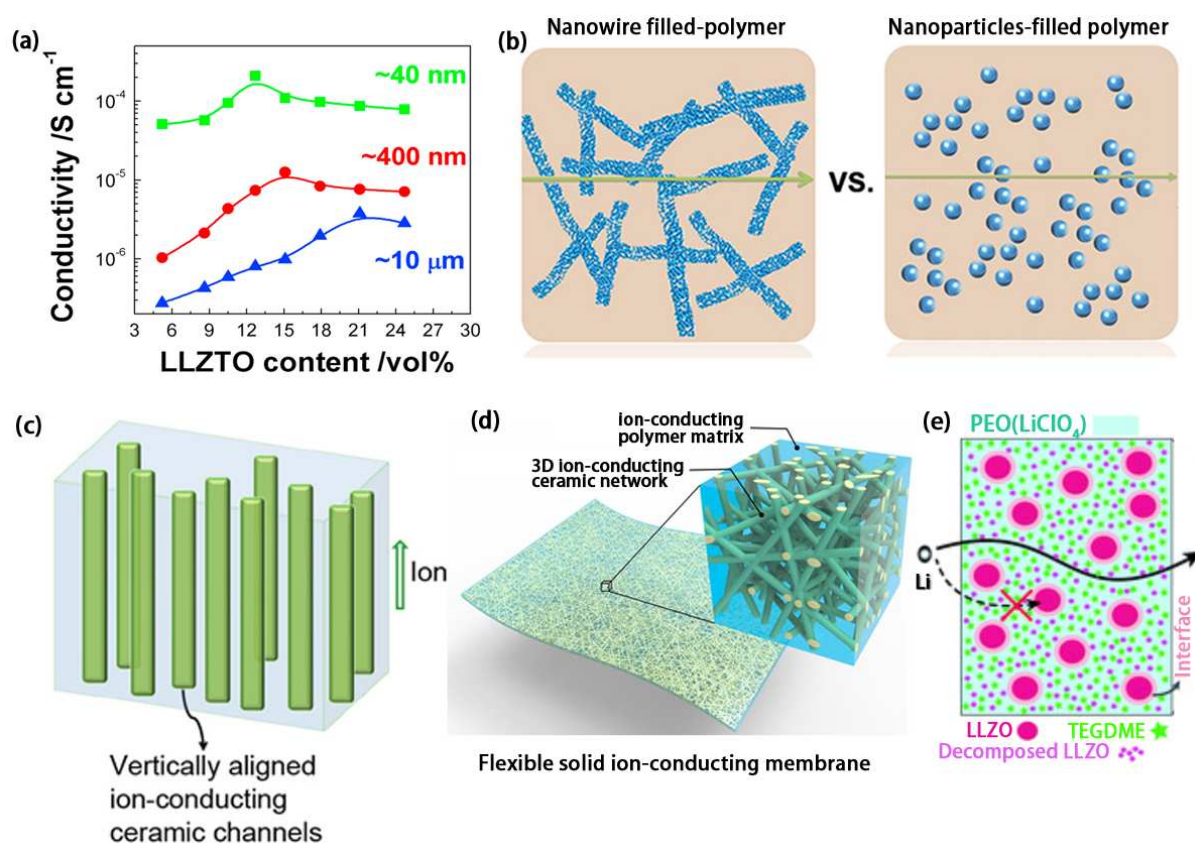


Figure 10. Strategies for designing a high ionic conductivity hybrid electrolyte. (a) Size and concentration effects on the ionic conductivity of PEO-LLZO hybrid electrolytes [237]. (b) Comparison of the Li<sup>+</sup> ion transport pathways in hybrid electrolytes with nanowire or particle LLTO fillers [234]. (c) Vertically aligned Li<sup>+</sup> ion transporting channels to enhance the ionic conductivity [207]. (d) Creating a 3D ionic conducting ceramic network for enhancing the ionic conductivity of a hybrid electrolyte [28]. (e) Plasticizer additives to increase the RT ionic conductivity of a hybrid electrolyte [291].

In summary, the influences of the size, concentration, and the shape of the SSEs fillers in composite hybrid electrolyte are critical for the enhancement of the ionic conductivity of hybrid electrolytes. Small size and interconnected shape of SSEs fillers are favorable. The present of plasticizers in composite electrolytes can also enhance the ionic conductivity because it can lower

the crystalline of SPE and promote the dissociation of lithium salt.

## 2.4 Li<sup>+</sup> ion conduction in hybrid electrolytes

Understanding the Li<sup>+</sup> ion transporting pathways or conduction mechanisms within hybrid electrolytes is very important for the development of hybrid electrolytes. In the past several decades, many efforts have been dedicated to study the Li<sup>+</sup> ion conduction mechanism in SPE, oxide-based SSEs and sulfide-based SSEs [76, 103, 113, 278, 292-294]. Understanding the Li<sup>+</sup> ion conduction mechanism can provide researchers the guidelines for designing a high ionic conductivity SSE.

While liquid electrolytes dissolve lithium salts in solvents and the diffusion of solvated ions provide the ionic conductivity, SPE complex designated salts in a polymer matrix and the diffusion of ions does not play the key role in the ionic conductivity of SPE. To facilitate the dissociation of Li<sup>+</sup> ions, the lithium salts used in SPEs usually have low lattice energy. The dielectric constant of the host polymer should be relatively high to avoid conduction of electrons [32]. The Li<sup>+</sup> ions from salts are coordinated with the function groups on the polymer chains (e.g. -O- in PEO, -CN in polyacrylonitrilide, -NR in polyamide, etc.). The polymer chains undergo continuous local segmental motions and create free volumes. Li<sup>+</sup> ions migrate from one coordination site to another or hop from one chain to another via the free volumes by the segmental motions [32]. Under such Li<sup>+</sup> ion transfer mechanism, the segmental motions of polymer chains and the number of mobile Li<sup>+</sup> ions in the polymer matrix are the critical factors determining the ionic conductivity of a SPE. The polymer segmental motions significantly depend on temperature, so does the ionic conductivity. The temperature dependent ionic conductivity can be described by the Vogel-Tamman-Fulcher (VTF) relation and the Arrhenius-type relation.

VTF-type relation is expressed as:

$$\sigma = \sigma_0 T^{\frac{1}{2}} \exp\left(-\frac{B}{T-T_0}\right) \quad \text{Eq. (3)}$$

where  $\sigma_0$  is the pre-exponential factor;  $B$  is the pseudo-activation energy for the conductivity; and  $T_0$  is the equilibrium glass transition temperature ( $T_g$ ) ( $T_0 \approx T_g - 50K$ ). For SPEs, a nonlinear relationship between ionic conductivity  $\sigma$  and  $1/T$  typically means that the Li<sup>+</sup> ion hopping motion is coupled with relaxation/breathing and/or segmental motion of polymer chains [32, 295].

Arrhenius-type relation is expressed as:

$$\sigma = \sigma_o \exp\left(-\frac{E_a}{KT}\right) \quad \text{Eq.(4)}$$

where  $E_a$  is the activation energy which can be extracted from the gradient of  $\log \sigma$  versus  $1/T$  plot. Arrhenius-type behavior describes the ion hopping decoupled from long-range motions of the matrix (e.g. amorphous phase and glass phases polymer below the glass transition temperature, inorganic ceramic SSEs, etc) [295].

Oxide-based or sulfide-based SSEs as fillers in a composite electrolyte is expected to deliver higher ionic conductivity than insulating fillers, because not only the polymer matrix but also the fillers have the ability to conduct  $\text{Li}^+$  ions. Even though many composite electrolytes such as PEO-LLZO, PEO-LATP, PAN-LLTO etc [28, 71, 207, 234, 296]. had been reported with improved ionic conductivity compared to that of bare SPE, the underlining  $\text{Li}^+$  ion conduction mechanism in hybrid electrolytes was less discussed. Lack of direct characterization techniques on  $\text{Li}^+$  ion behaviors makes it particularly challenging for mechanism studies. Characterization techniques, such as Infrared (IR) and Raman spectroscopies, have been used to measure the change of salt anions to obtain hints of  $\text{Li}^+$  ions dissociation. For example, the lithium salt,  $\text{LiClO}_4$ , exhibits multiple IR characteristic peaks (624, 635 and  $664 \text{ cm}^{-1}$ ) depending on the status of the salt. IR spectra of PAN- $\text{Al}_2\text{O}_3$ - $\text{LiClO}_4$  composite electrolytes with difference concentration of  $\text{Al}_2\text{O}_3$  fillers was studied by Z. Wang et al. They found that  $\text{Al}_2\text{O}_3$  fillers interacted with the  $\text{ClO}_4^-$  anions and correspondingly increased the effective number of free  $\text{Li}^+$  ions, thus enhanced the ionic conductivity of the SPE [278]. However, IR and Raman characterization cannot give direct information about  $\text{Li}^+$  ions within the SSE.

Development of direct probing techniques to characterize  $\text{Li}^+$  ions pathway in SSEs is particular important for understanding the  $\text{Li}^+$  ion conduction mechanism. Recently, nuclear magnetic resonance spectroscopy (NMR) was proposed as a powerful tool to study the  $\text{Li}^+$  ion transfer mechanism in SSEs [113, 281, 291]. Y. Hu's group first reported the combination of selective isotope labeling and solid-state Li NMR to precisely identify the lithium sites and probe the  $\text{Li}^+$  ion pathway within a PEO-LLZO- $\text{LiClO}_4$  hybrid electrolyte [281]. Figure 11a schematically shows the possible Li environments within a PEO-LLZO- $\text{LiClO}_4$  hybrid electrolyte, including the Li in PEO- $\text{LiClO}_4$  polymer matrix, the LLZO grain, and the PEO/LLZO interface. Corresponding

high-resolution  ${}^6\text{Li}$  NMR spectrum of PEO- $\text{LiClO}_4$  SPE, pure phase LLZO, and PEO-LLZO- $\text{LiClO}_4$  hybrid electrolyte are presented in Figure 11b. On the spectrum of the hybrid electrolyte, the shoulder at 1.4 ppm indicates the Li at the PEO/LLZO interface. The  $\text{Li}^+$  ion pathways were probed in a lithium symmetric cell with  ${}^6\text{Li}$  metal as electrodes (Figure 11c). Upon cycling,  ${}^6\text{Li}$  from one electrode moved across the hybrid electrolyte to the other electrode, replacing  ${}^7\text{Li}$  in the hybrid electrolyte, depicting a diffusion pathway of the  ${}^6\text{Li}^+$  ions. By comparing the  ${}^6\text{Li}$  amount in the different parts of the hybrid electrolyte before and after cycling, the  $\text{Li}^+$  ions pathway can be disclosed. The results showed that there was a significantly increase in the peak of LLZO grains (increased by 39%), slight increase in the peak of PEO/LLZO interface (6%), and unchanged peak of PEO- $\text{LiClO}_4$  SPE (Figure 11d), which suggested a preferred  $\text{Li}^+$  ions pathway through the LLZO phase rather than the SPE. Furthermore, the  $\text{Li}^+$  ions conduction mechanism in the PEO-LLZO- $\text{LiClO}_4$  hybrid system with addition of a plasticizer, tetraethylene glycol dimethyl ether (TEGDME) was also studied (Figure 11e). Li environments in the PEO-TEGDME-LLZO- $\text{LiClO}_4$  hybrid are similar to those in PEO-LLZO- $\text{LiClO}_4$  hybrid electrolyte. However, with the TEGDME additive, LLZO is partially decomposed and dissolved into TEGDME. Then, a completely different  $\text{Li}^+$  ion pathway was found.  $\text{Li}^+$  ion transport favored the liquid TEGDME-associated phases over the LLZO or the PEO/LLZO interface (Figure 11g) [291].

In PEO-LLZO- $\text{LiClO}_4$  hybrid electrolyte without TEGDME,  $\text{Li}^+$  ions prefer the path through the LLZO phase which has a RT ionic conductivity of  $10^{-4}$  S/cm, 3 orders higher than PEO- $\text{LiClO}_4$  SPE ( $\sim 10^{-7}$  S/cm). However, in the presence of TEGDME,  $\text{Li}^+$  ions prefer pathways via the liquid TEGDME-associated phase which possesses an even higher ionic conductivity than the LLZO phase and PEO- $\text{LiClO}_4$  SPE. From these two studies, a conclusion is that  $\text{Li}^+$  ions would choose a low resistant pathway within a hybrid electrolyte. Therefore, a composite electrolyte with high ionic conductive components are critical for improving of the total ionic conductivity.



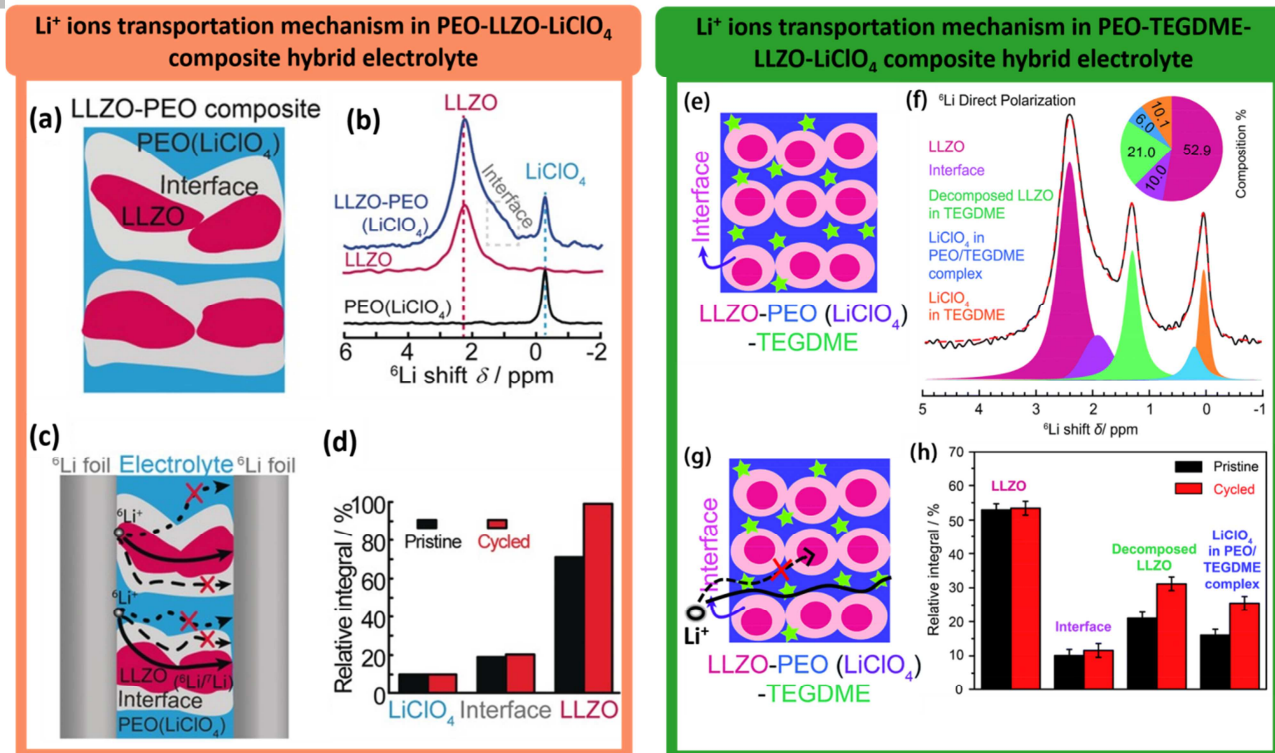


Figure 11. (a) Schematic diagram of Li environment within the PEO-LLZO-LiClO<sub>4</sub> composite electrolyte including PEO-LiClO<sub>4</sub> SPE matrix, LLZO, and PEO/LLZO interface; (b) high-resolution <sup>6</sup>Li NMR spectra of PEO-LiClO<sub>4</sub>, LLZO and PEO-LLZO-LiClO<sub>4</sub> hybrid electrolyte; (c) schematic diagram of <sup>6</sup>Li pathways in a symmetric cell with PEO-LLZO-LiClO<sub>4</sub> hybrid electrolyte; (d) quantitative analysis of <sup>6</sup>Li amount in PEO-LiClO<sub>4</sub>, PEO/LLZO interface, and LLZO in the PEO-LLZO-LiClO<sub>4</sub> composite electrolyte before and after cycling [281]. (e) Schematic diagram of Li environment within the PEO-TEGDME-LLZO-LiClO<sub>4</sub> composite electrolyte. (f) High-resolution <sup>6</sup>Li NMR spectra of PEO-TEGDME-LLZO-LiClO<sub>4</sub> and the concentration of Li in each component; (g) proposed Li<sup>+</sup> ion transport pathway within the composite electrolyte; (h) quantitative analysis of <sup>6</sup>Li amount in LLZO, interface, decomposed LLZO and PEO-TEGDME-LiClO<sub>4</sub> in the PEO-TEGDME-LLZO-LiClO<sub>4</sub> composite electrolyte before and after cycling [291].

In Summary, NMR is a powerful tool to study the Li<sup>+</sup> ion transport mechanism in hybrid electrolytes. A preferential pathway of Li<sup>+</sup> ion through the component of highest ionic conductivity (e.g. the oxide-based SSE phase in SPE-oxide composite electrolyte and the liquid-associated phases in the presence of a plasticizer) is revealed. This should be the reason why SPE-oxide composite electrolytes using SSE nanowire fillers or 3D SSE network fillers showed higher ionic

conductivities than that of discrete nano-particles fillers. With continue  $\text{Li}^+$  ion pathway in the SSE nanowires or 3D SSE network fillers, the  $\text{Li}^+$  ion can transport across fewer boundaries than that with discrete nano-particles fillers. Since  $\text{Li}^+$  ion transportation is favorable in the high ionic conductivity phase, creating a 3D ionic network by a very high ionic conductivity SSE such as sulfide-based SSE as the framework to make SPE-inorganic hybrid electrolyte is expected to have an even higher ionic conductivity at RT.

### 3. Addressing the interfacial issues by hybrid electrolytes

The biggest challenge in building a high-performance SSLB is the high interfacial resistance between SSEs and electrodes. The stiff nature of ceramic SSEs causes poor contact with electrodes and hence high interfacial resistance. Efforts to reduce interfacial resistance by interface engineering have received increasing attentions in recent years. The SSE/anode and SSE/cathode interfaces emphasize different interfacial problems that require differently tailored solutions, which have been discussed in previous chapter. Herein, hybrid electrolyte, as another solution to address the interfacial issues, configured with a stiff inorganic SSE and a rationally engineered interfacial with SPE or liquid electrolyte, will be discussed in detail.

#### 3.1 Solid-state batteries with composite cathode and composite electrolyte

SSLBs created by all composite method have been widely studied and reported to be able to avoid the mismatch problem. All composite methods utilize a certain amount of SPE to fabricate composite electrodes and composite electrolytes by hot pressing method to achieve an intimate SSE/electrode interface. R. Chen et al. demonstrated this kind of all composite SSLB consisting of a composite electrolyte with 40 wt.% PEO-LITFSI SPE filled in 60 wt.% LLZO, a composite  $\text{LiFePO}_4$  cathode with different contents of SPE (10 - 30 wt.%), and a lithium metal as the anode. Prepared by hot press method, the hybrid electrolyte/cathode interface was seamless and free of pores. The cell with 15 wt.% SPE composite cathode delivered the highest discharge capacity of 152 mAh/g with an overall resistance of 1300  $\Omega$  at 60 °C (Figure 12b, c) [206]. Similar work by Y. He's group used a LLZO nanowire fillers filled SPE to construct a composite electrolyte that has an ionic conductivity of  $2.39 \times 10^{-4}$  S/cm at RT and  $1.53 \times 10^{-3}$  S/cm at 60 °C (Figure 12d). By

integrating SPE with  $\text{LiFePO}_4$ , the composite cathode shows an intimate contact to the hybrid electrolyte. the SSLB can deliver a discharge capacity of 158.8 mAh/g at 0.5 C at 60 °C and 158.7 mAh/g at 0.1C at 45 °C (Figure 12e) [297]. Another work done by H. Wang's group who demonstrated a tape casting method to infuse PEO SPE into the porous cathode to ensure intimate contact with the SSE. The resulting  $\text{LiFePO}_4$  SSLB showed improved electrochemical performance compared to the conventional  $\text{LiFePO}_4$  SSLB (Figure 12a) [298].

The lithium dendrite formation problem is detrimental to SPE. It is proposed that a SPE with the higher shear modulus than that of lithium metal can suppress dendrite growth [96, 190]. Thus, the lithium dendrite formation problem can be reasonably addressed by integrating a rigid oxide-based SSE into the SPE matrix, forming composite electrolyte with enhanced mechanical strength. Therefore, lithium symmetrical cells with composite electrolyte presents excellent lithium plating/stripping cycling performance without lithium dendrite formation compared to the bare SPE (Figure 12f) [28, 73, 237, 297].

Another challenge of SPE is the low oxidation window. The inorganic SSEs fillers in the SPE matrix shows an obviously enlarged electrochemical stable window. The higher the filler concentration, the wider the electrochemical window has been observed [236, 237, 274]. This can be explained why the NMC622 SSLB with a PEO-LLZO- $\text{LiClO}_4$  composite electrolyte can deliver a higher capacity than that with a pure PEO- $\text{LiClO}_4$  SPE [236].

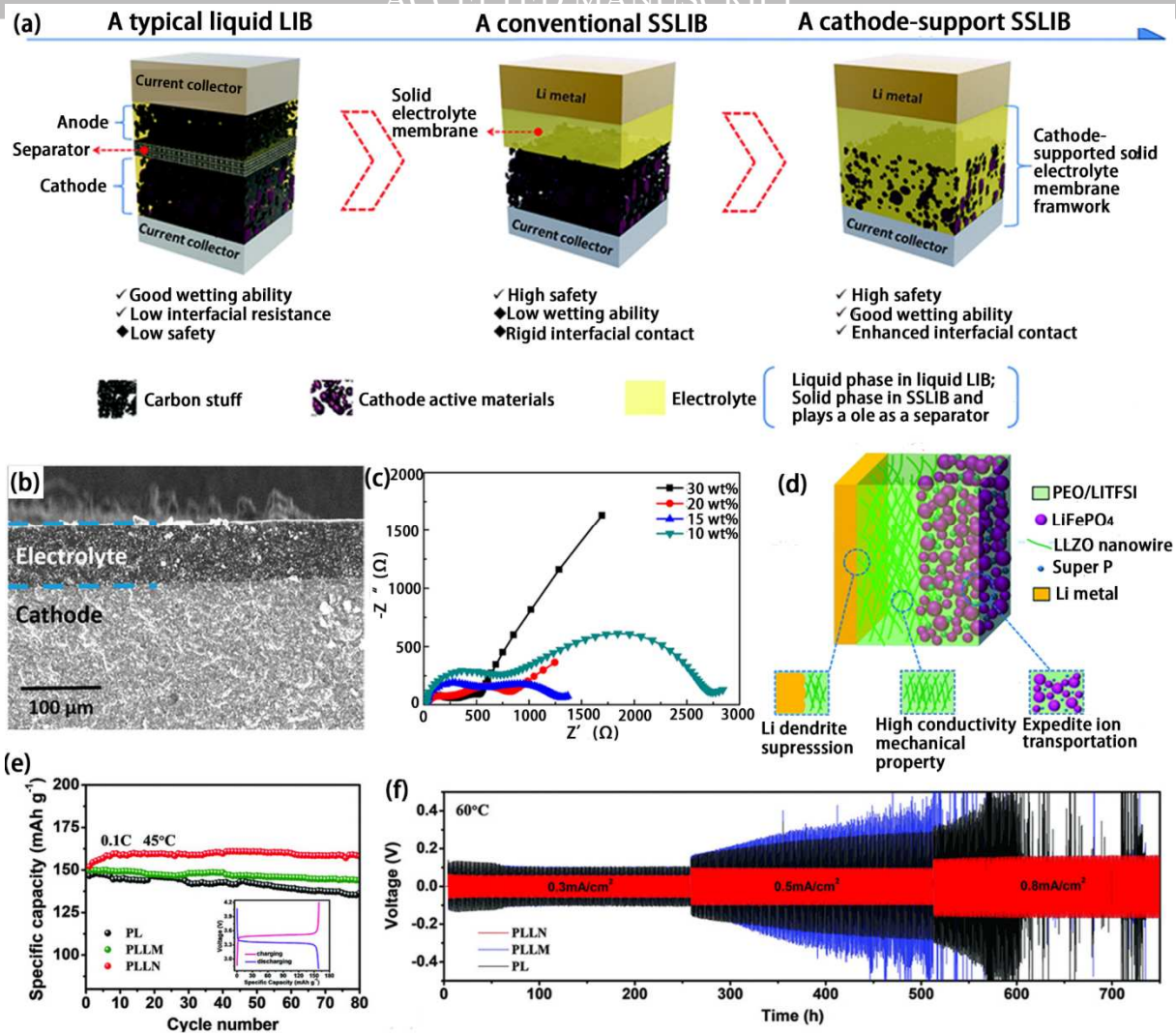


Figure 12. (a) Comparison of the liquid electrolyte-based LIB, solid-state LIB with conventional cathode and solid-state LIB with composite cathode [298]. (b) Cross-section SEM composite cathode/composite electrolyte interface; (c) EIS of the all composite SSLBs with different contents of SPE in the composite cathode [206]. (d) A schematic diagram of the all composite solid-state LIB with nano-wire LLZO fillers in the SPE and SPE-LiFePO<sub>4</sub> composite cathode. The nano-wire LLZO filled SPE can help to prevent dendrite formation, while the SPE in cathode address the mismatch problem and Li<sup>+</sup> ion conduction in cathode; (e) the cycling performance of SSLBs with different composite electrolytes; (f) voltage-time profiles of lithium symmetric cells with bare-SPE (PL), composite electrolyte with LLZO nanoparticles fillers (PLLM) and composite electrolyte with LLZO nano-wire fillers (PLLN) [297].

### 3.2 Liquid-oxide multilayer hybrid electrolyte

To address the high interfacial resistance problem in oxide-based SSE, different strategies have been developed to tailor the interface between oxide-based SSEs and electrodes. Significant progresses have been achieved in reducing the interfacial resistance between lithium anode and oxide-based SSE by solidifying molten lithium on oxide-based SSE surface. A negligible Li/SSE interface resistance can be achieved by this method [122-124].

However, unlike lithium metal with a low melting point of 180 °C, cathodes with a high melting point above 1000 °C are difficult to adopt the melting method for cathode/SSE interface building. Moreover, cathodes are usually in forms of micron-sized or nano-sized particles with pores and gaps [299, 300]. The complicated surface morphology introduces extra challenges for a matching interface. Thus, using liquid electrolytes to compensate the gaps between the oxide-based SSE and the cathode as well as the gaps between the cathode particles is still a common practice to enable SSLBs work effectively [2, 301, 302].

Our group comprehensively studied the amount of liquid electrolyte in addressing the cathode and LATP SSE interface (Figure 13a-c) [303]. The results showed that adding as little as 2  $\mu\text{L}$  of liquid electrolyte at the  $\text{LiFePO}_4$  cathode/LATP interface can enable the battery operation at RT with a discharge capacity of 125 mAh/g at 1 C and 98 mAh/g at 4 C. Interestingly, excess liquid electrolyte showed no further contribution to the electrochemical performance enhancement. Such small amount of liquid electrolyte will be completely absorbed by the electrode and free of leakage concerns.

Liquid-oxide hybrid electrolytes are also widely studied in Li-S batteries. Oxide-based SSEs in this kind of Li-S battery not only can inhibit the polysulfide shuttle due to the dense structure but are also able to suppress the lithium dendrite growth. Even though many previous works focus on achieving all-solid-state Li-S battery (ASSLSB) and avoid using liquid solvent, the reported performance ASSLSBs are far away from satisfaction [304-308]. The reasons behind are probably due to the poor ionic and electronic conductivity of sulfur cathode, the high interfacial resistance, and slow solid-solid reactions. Employing a small amount of liquid electrolyte (i.e. liquid-oxide hybrid electrolyte) to modify the SSE/cathode interface could be critical for Li-S batteries. The presence of desirable solvents can enable the formation of polysulfides, significantly improving the



electrochemical kinetics via solid-liquid transfer reactions. Y. Xia's group applied a liquid-LATP hybrid electrolyte in a Li-S battery and showed greatly enhanced cycle life without sacrificing capacity or inducing polysulfide shuttling (Figure 13d-f) [301]. Similar studies using liquid-oxide hybrid electrolytes in Li-S batteries are also reported by other groups [302, 309-312]. In Li-S batteries with a liquid-oxide hybrid electrolyte, the inorganic oxide-based SSE not only functions as a separator to prevent the short-circuit of the battery but also services as a shield to inhibit the migration of polysulfide, so the self-discharge problem is eliminated. Excellent cycling performance and a Coulombic efficiency of around 100% could be achieved. The liquid electrolyte in the cathode can not only provide a medium for the sulfur-polysulfide-sulfide redox reactions within the cathode, but also reduce the SSE/electrode interfacial  $\text{Li}^+$  ion transport resistance.

Solid-state Li-air batteries are also benefited from the usage of liquid-oxide hybrid electrolytes. Due to the existence of oxide ceramic SSE in the between, the liquid electrolyte in anode side (anolyte) and cathode side (catholyte) can be different in one single cell, which means a hybrid electrolyte with three different electrolytes can be realized in a single cell. Organic electrolytes are not favorable as catholyte in Li-air battery because they are neither stable to air nor soluble for the discharge products. Blockage of the cathode will occur once the insoluble discharge products are produced. Nevertheless, these problems can be addressed by using aqueous-based catholyte. On the other hand, aqueous-based electrolyte is not suitable as anolyte due to the aggressive reaction between lithium metal and water, while organic electrolyte is a good candidate for anolyte. The application of liquid-oxide hybrid electrolyte makes it possible to fabricate a Li-air battery with organic-based anolyte and aqueous-based catholyte with a separator of oxide-based SSEs in between. H. Zhou et al. demonstrated this concept in Li-air battery by using 1M  $\text{LiClO}_4$  in ethylene carbonate/dimethyl carbonate as anolyte and 1M  $\text{KOH} + 1\text{M LiNO}_3$  alkaline solution as the catholyte and NASICON based SSE as the ceramic separator. Stable charge/discharge voltage for 10 cycles is demonstrated (Figure 13g-i) [313].

The liquid electrolyte and oxide-based SSE interface properties have been studied by J. Janek et al.[314]. Liquid electrolyte and LAGP interfacial properties were studied by impedance analysis and XPS. In the lithium battery with a liquid-oxide hybrid electrolyte,  $\text{Li}^+$  ions need to cross 3 types of boundaries including electrode/liquid electrolyte boundary, liquid electrolyte/SSE boundary ( $R_{\text{is}}$ ),

grain boundary within SSE (Figure 14a). The study showed that the  $R_{is}$  plays a determining role in the energy density loss of the lithium battery when the SSE thickness down to 100  $\mu\text{m}$  (Figure 14b). The formation of liquid electrolyte/SSE interface undergoes 3 stages, wetting, formation, and stabilization. At the wetting stage, the magnitude of  $R_{is}$  decreases because the liquid electrolyte fills the surface cavities of the SSE, which implies an increase in contact area and thus a reduction of the cell resistance. Subsequently, the liquid electrolyte/SSE interface was formed and stabilized. Notably, they found that the water contamination in the liquid electrolyte significantly influenced the value of  $R_{is}$ . Higher water concentration in the liquid electrolyte led to a higher interfacial resistance (Figure 14c). XPS studies revealed that the decomposition of lithium salt or SSE contributed to the formation of LAGP-liquid electrolyte interphase (Figure 14d-k). Similar XPS results were reported in LATP-liquid electrolyte interface by our group [303].

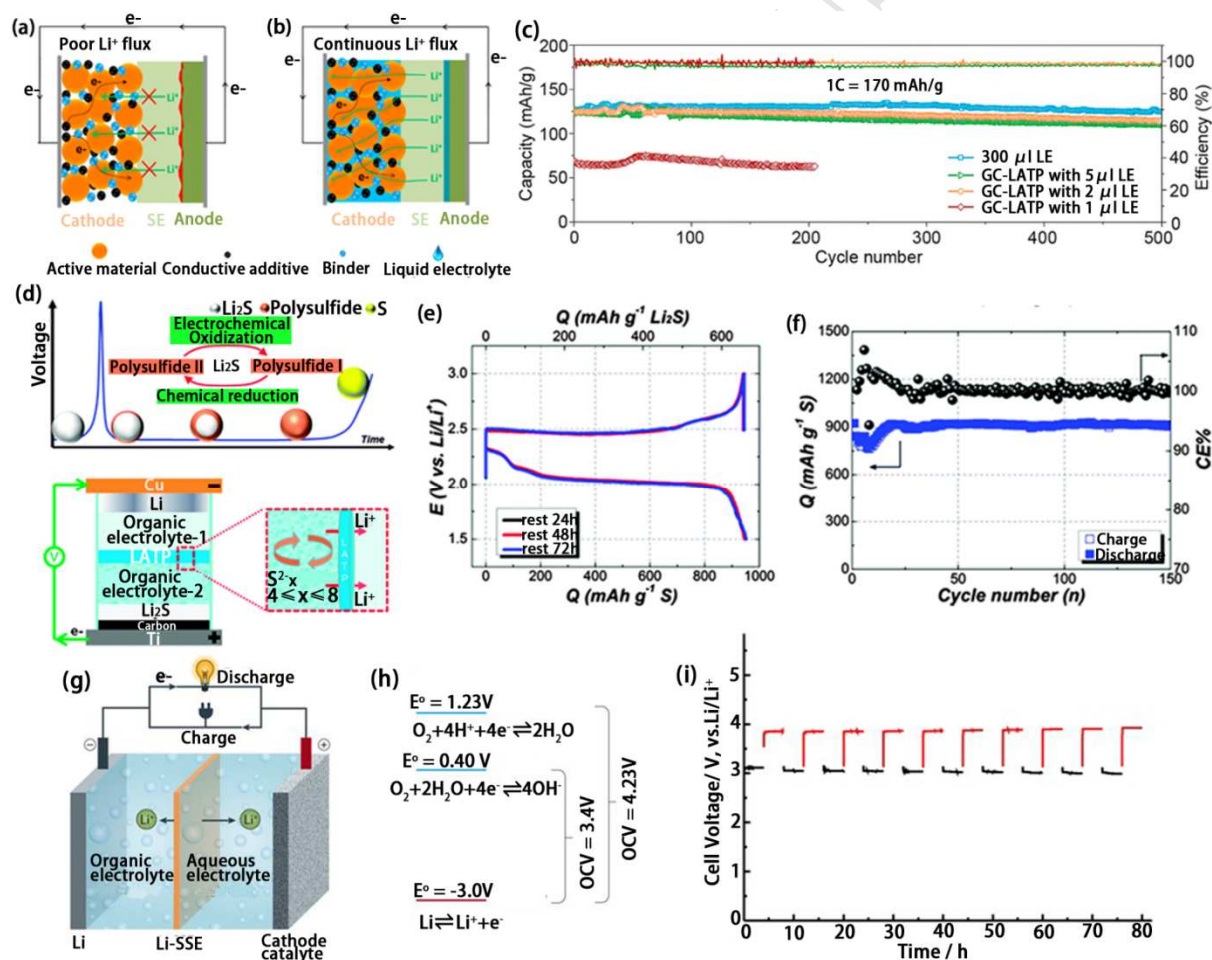


Figure 13. (a) Configurations showing the poor contact between oxide-based SSE and cathode, anode electrodes. (b) After adding small amount of liquid electrolyte, the interface is well wetted, and an unformal lithium flux is realized. (c) Comparisons of the  $\text{LiFePO}_4$  LIBs performances with

different amount of liquid-based electrolyte in LATP/electrode between [303]. (d) Schematic illustration of the activation process of the  $\text{Li}_2\text{S}$  cathode over initial charge and the configuration of Li-S battery with liquid-LATP hybrid electrolyte; polysulfide shuttle effects are prevented by the LATP. Corresponding charge/discharge profiles of Li-S battery after resting at different time are showed in (e). (f) The cycling performance of Li-S battery with liquid-LATP hybrid electrolyte [301]. (g) Configuration of a Li-air battery with organic anolyte, aqueous catholyte, and an oxide-based SSE interlayer. (h) The anodic and cathodic reactions in Li-air battery with the liquid-oxide hybrid electrolyte, as well as the open-circuit voltages (OCVs) of the cell [74]. (i) The performance of a Li-air battery with the liquid-oxide hybrid electrolyte [313].

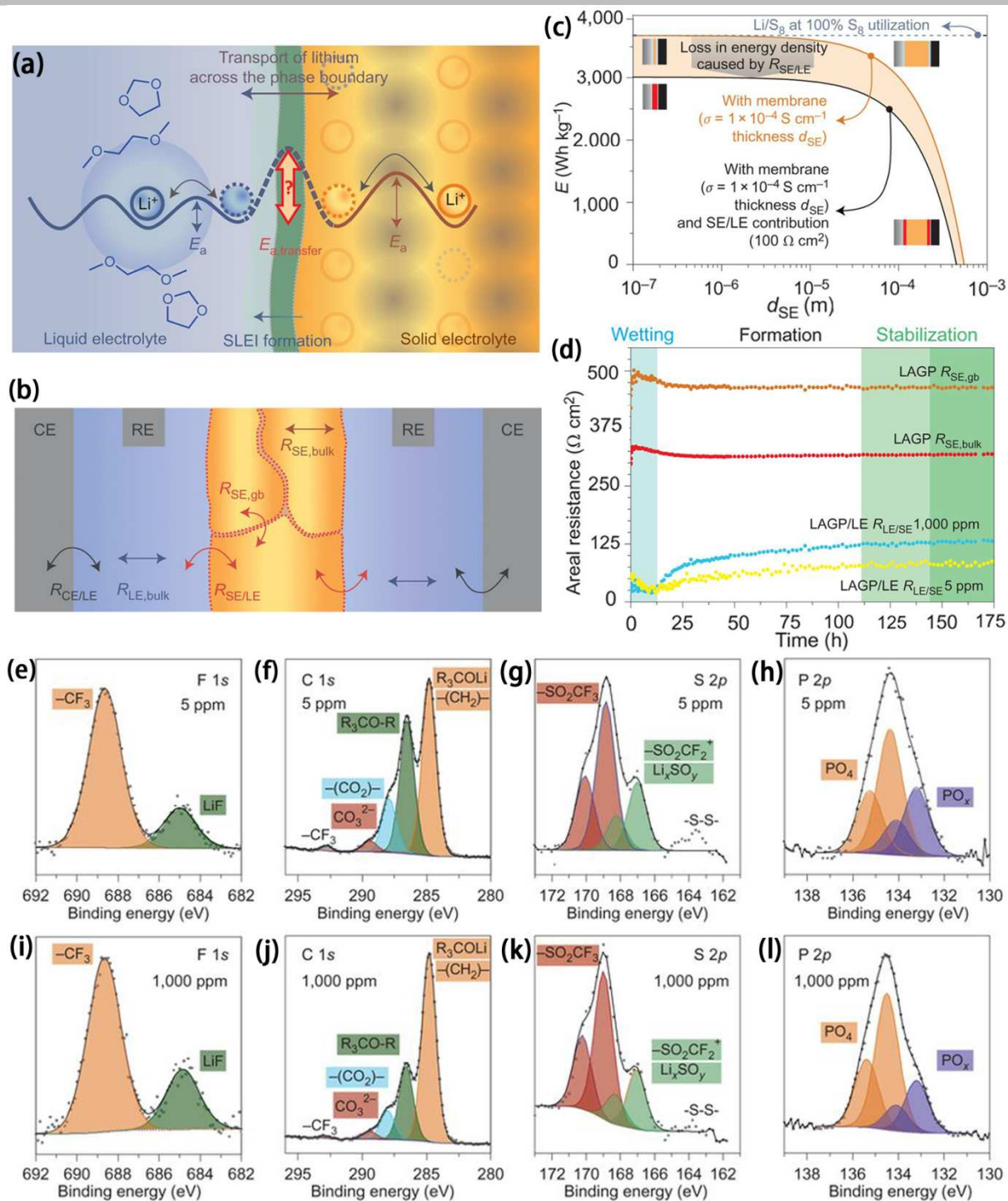


Figure 14. (a), (b) Schematic diagram showing the interfaces within a lithium battery with liquid-oxide hybrid electrolyte. (c) Energy density loss of a lithium battery with liquid-oxide hybrid electrolyte due to the overpotentials from oxide-based SSE resistance and liquid/SSE interfacial resistance. (d) Evolutions of interfacial resistance in lithium battery with liquid-oxide hybrid electrolyte. (e-l) XPS studies of liquid/SSE interphase after time-dependent EIS experiments with water contents of 5 ppm (upper row) and of 1,000 ppm (lower row) [314].

In summary, liquid-oxide hybrid electrolytes can not only address the interface challenge in SSLBs with oxide-based SSEs, but also work as a barrier to prevent shuttles of unfavorable redox species between electrodes. Therefore, liquid-oxide hybrid electrolytes are highly desirable for Li-S and Li-air battery systems. However, the stability between oxide-based SSEs and liquid electrolytes should still be taken into consideration during SSLBs designs.

### 3.3 SPE-oxide multilayer hybrid electrolyte

The existent of liquid electrolyte still poses potential of safety issues such leakage and fire. To totally avoid the usage of liquid electrolytes, flexible SPEs can be another solution to tailor the ceramic SSE/electrode interface. The general configuration of a SPE-oxide multilayer hybrid electrolyte is laminated as SPE/oxide or SPE/oxide/SPE sandwich structures (Figure 15a) [73, 315-319]. Considering the total cell resistance and volumetric energy density, the thickness of multilayer electrolyte should be as thin as possible.

J. B. Goodenough et al. have studied the electrochemical properties of SPE-oxide sandwich hybrid electrolytes. Figure 15b, c proposes the electric potential profiles across a sandwich hybrid electrolyte and a single SPE in a  $\text{LiFePO}_4$  cell. Due to redistribution of charge carriers in different conductors (including anode, SPE, oxide-based SSE, and cathode), an electric double layer was created at the interface between two conductors, causing an electric field (i.e. potential difference) at the interface. In a single SPE cell, a strong electric field generated at the anode/SPE interface can reduce the lowest unoccupied molecular orbital energy of the SPE related to the Fermi energy of lithium, and thus facilitates the decomposition of the SPE [73]. In contrast, the overall electric field across the sandwich electrolyte is interrupted by the oxide-based SSE interlayer (Figure 15b). The oxide-based SSE can block the passage of the salt anions and increased the  $\text{Li}^+$  ion transference number,  $t_{\text{Li}^+}$ . Reduced electric field at the anode/SPE interface helps to stabilize the SPE. The intimate contact between lithium anode and SPE also provides an unformal  $\text{Li}^+$  ion flux that mitigates lithium dendrite formation. As a result, all solid-state  $\text{LiFePO}_4$  batteries with a SPE/LATP/SPE hybrid electrolyte showed significantly improved cycling performance compared to the single layer SPE-based  $\text{LiFePO}_4$  batteries (Figure 15d) [73].

Sandwich hybrid electrolyte can be also used for tackling the interface incompatibility between



electrodes and SSEs by avoiding the directly contact. By placing a layer of plastic crystal electrolyte (PCE) between lithium metal anode and LGPS sulfide-based SSE, the capacity of  $\text{LiFePO}_4$  battery is significantly enhanced (Figure 15e, f). P K-edge and S K-edge X-ray absorption spectroscopy (XAS) results indicate that the reduction of phosphorus by lithium was happened in unprotected Li/LGPS interface while the reduction is prevented in PCE protected Li/LGPS interface (Figure 15g, h) [320].

Additionally, blocking ions or molecules by a ceramic SSE interlayer can tackle the crossover problem in various lithium battery systems. In solid-state Li-S battery with SPE, SPE have the ability to complex with lithium polysulfide so the polysulfide crossover problem still exist [82]. This problem is absent in the Li-S battery with SPE-oxide sandwich hybrid electrolyte due to the blocking effect of the oxide-based SSE interlayer. Sandwich hybrid electrolytes with a LATP or LAGP interlayer have been widely studied for preventing the polysulfide shuttling effects in all solid-state Li-S batteries (ASSLSBs) [317, 318, 321]. However, LATP is actually not stable towards polysulfide species. Our group applied the atomic layer deposition (ALD) technique to protect LATP SSE from being reduced by the polysulfide in the ASSLSBs with SPE-LATP sandwich hybrid electrolyte. Results showed that as thinner as 10 cycles of ALD  $\text{Al}_2\text{O}_3$  coating can significantly enhance the performance of ASSLSBs because the reduction of LATP was inhibited (Figure 15i, j) [318].

However, in SPE-oxide sandwich-type hybrid electrolyte system, although unfavorable interphase formation between SPEs and oxide-based SSEs have not yet been reported, the  $\text{Li}^+$  ion transport still need to cross a SPE/oxide interface. Studies show that different types of oxide-based SSE showed different interfacial properties towards SPE. Takeshi Abe et al. first studied the PEO/LLTO interface and reported a significant larger resistance of the PEO/LLTO interface than that of the bulk LLTO or PEO-based SPE. The PEO/LLTO interfacial resistance was at the  $10^3 \Omega$  level, almost 10 times higher than that of bulk LLTO and 100 times higher than that of bulk PEO SPE [322]. However, in terms of a NASICON-type SSE, W. E. Tenhaeff et al. demonstrated a relatively small resistance between PEO-based SPE and NASICON-type glass ceramic electrolyte interface compared to the overall resistance of this multi-layer hybrid electrolyte. The resistance value was stable upon temperature variations [323]. Regarding the interface between a gel polymer



electrolyte (GPE) and a garnet-type SSE, the results from L. Hu' group showed that the GPE/garnet interface resistance was  $10^2 \Omega/\text{cm}^2$ , which was higher than that of garnet SSE bulk resistance and thus it cannot be negligible in SSLBs [316]. So far, there are still few reports about the chemistry at the SPE/oxide SSE interface. Nevertheless, the SPE/oxide SSE interfacial resistance is still too significant to be neglected in SSLBs.

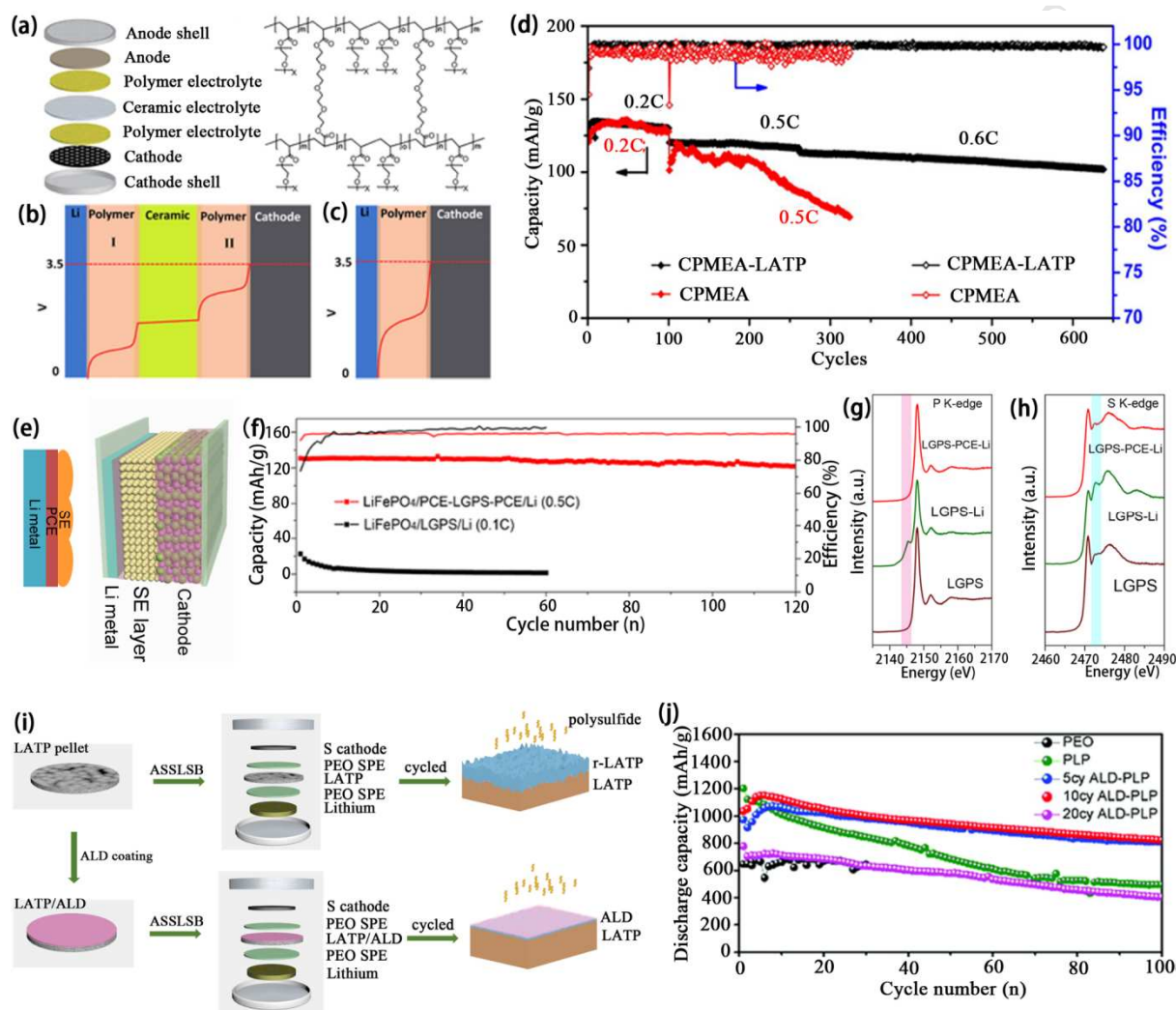


Figure 15. (a) The configuration of a SSLB with a SPE-oxide sandwich hybrid electrolyte and the molecule structure of the SPE. Electric potential profile across (b) a SPE-oxide sandwich electrolyte and (c) a single SPE; (d) Comparison of the performances of the SSLBs with single layer SPE and SPE-oxide sandwich electrolyte at 0.2 C, 0.5 C and 0.6 C [73]. (e) Configuration of a Li-LiFePO<sub>4</sub> battery with LGPS SSE and plastic crystal electrolyte (PCE) in the Li/LGPS interface and its corresponding long cycling performance at 0.5 C (f). Comparison of P K-edge (g) S K-edge (h) of pristine LGPS (wine), LGPS after cycling (green) and LGPS with PCE protecting after cycling (red) [320]. (i) Configuration of ASSLSBs with SPE-oxide sandwich hybrid electrolyte with or without

ALD protection; (j) Corresponding long cycling performance of ASSLSBs with different thicknesses of ALD protection [318].

In conclusion, many efforts have been dedicated to developing SSLBs with oxide-based SSEs, especially interfacial engineering for the SSE/electrode interface using a small amount of liquid electrolyte or SPE interfacial layers. Achievements are promising. However, the multilayer structured hybrid electrolytes still require  $\text{Li}^+$  ion transport across different electrolyte phases that involve different  $\text{Li}^+$  ion transport mechanisms and cause extra interface resistance. The interfacial resistance may pose drawbacks to the overall SSLB performance in terms of rate performance and energy density. Research efforts on interphase formation mechanism and reducing the thickness of the hybrid electrolytes are urgent in this field.

#### 4. Conclusions and perspectives

SSEs are essential to the development of SSLBs, serving as both separator and ionic conductor. SPEs, oxide-based SSEs, and sulfide-based SSEs are typical categories of common SSEs for SSLBs, inheriting different pros and cons. SPEs usually have good flexibility and softness that enable low interfacial resistance towards electrodes, but the low ionic conductivity at RT and relatively narrow electrochemical stability window limit their practical applications. Oxide-based and sulfide-based SSEs exhibit relatively high ionic conductivities at RT compared to SPEs, but the rigid and brittle property cause difficulties in maintaining sufficient contact with electrodes. Rational combinations of liquid electrolyte, SPE, and inorganic SSEs is a promising strategy to maximize the advantages and compensate the disadvantages of each constituent. Studies have shown that inorganic SSE fillers in SPEs can increase the ionic conductivity up to  $10^{-4}$  S/cm at RT, which is higher than that of regular SPEs by several orders of magnitude. Additionally, the size, concentration, and shape of SSE fillers have great influences on the performance of hybrid electrolytes. Nano-size fillers and interconnected  $\text{Li}^+$  ion conducting networks can significantly increase the ionic conductivity of hybrid electrolytes.

Studies on  $\text{Li}^+$  ion conduction mechanism in hybrid electrolytes are important for hybrid electrolyte designs. IR and Raman spectroscopies are often used to study the effects of ceramic fillers in composite electrolytes by characterizing the evolution of salt anions. NMR is another

powerful tool to track  $\text{Li}^+$  ion pathways in SSEs. Using NMR, the higher ionic conductivity phase in hybrid electrolytes is identified as a preferential  $\text{Li}^+$  ion conduction pathway over the lower ionic conductivity phase. However,  $\text{Li}^+$  ion transportation across two electrolyte interface and electrolyte/electrode interface are remained unclear.

In addition to the bulk ionic conductivity, interfacial problems between SSEs and electrodes are not yet fully addressed by an individual SSE. Mismatch, instability, SCL, and lithium dendrite formation are common problems. Composite electrolytes are promising solutions for addressing mismatch in SSLBs. A soft electrolyte component can ensure good electrode wettability, while rigid SSE components enhance the mechanical strength and electrochemical window. In liquid-oxide and SPE-oxide multilayer hybrid electrolytes, the liquid/SPE layers serve as flexible interfaces towards electrodes, enabling low interfacial resistance and dendrite-free lithium anodes; the inorganic SSE interlayer can block anions and redox matters from migrating across the electrolyte. However, one challenge for multilayer electrolytes is the extra interfacial resistance caused by extra electrolyte/electrolyte interfaces. More importantly, the introduction of SPEs often lowers the RT ionic conductivity of hybrid electrolytes, which limits the working temperature range of the SSLBs.

Although significant progress has been achieved using hybrid electrolytes in SSLBs, there are still challenges to be overcome for the development of practical SSLBs. Deeper understandings of different SSEs in terms of ionic conduction mechanisms, origin of chemical and electrochemical instabilities, and possible interface modifications need to be obtained in the future. For practical SSLBs applied in EVs, the energy density and working temperature are the major concerns. Potential research efforts and solutions are proposed as follows:

(1) Understanding the  $\text{Li}^+$  ion transport mechanisms in hybrid electrolytes and SSEs is important for the development of advanced SSEs. Advanced characterization techniques such as NMR, STXM (synchrotron scanning transmission X-ray microscopy) [324] and neutron diffraction [325] are powerful tools for the  $\text{Li}^+$  ion transport mechanisms studies. In particularly, in-situ analyses on  $\text{Li}^+$  ion transport across inorganic SSEs and SPE interface are vital for understanding the ionic conduction mechanisms in hybrid electrolytes, more studies are expected to be done in this field.

(2) In order to achieve high-energy-density for practical SSLBs, it is necessary to minimize the weight percentage of SSEs and maximize the active materials content. Theoretical calculations

pointed out that the thickness of SPEs must be below 90  $\mu\text{m}$  to achieve a comparable energy density to liquid-based lithium battery [326]. The inorganic SSEs, for example LLZO, need to be 4 times thinner for a comparable energy density due to their higher mass density [30]. Therefore, more research efforts should focus on advanced fabrication techniques such as sputtering [327], tape casting [328] and 3D printing [203, 211] to prepare thin-film SSEs. Meanwhile, high active materials loading for high-energy-density could lead to poor electronic and ionic conduction problems, which are more serious in solid-state batteries. Novel electrode designs with high electronic and ionic conductivity are crucial for practical SSLBs.

(3) In order to boost the energy density of SSLBs for EVs applications, implementation of high-voltage and high-capacity cathodes are necessary. However, most of the SSEs such as PEO-based SPEs and sulfide-based SSEs are not stable at high voltage ( $> 3.8$  V). There is an urgent need for developing high-voltage stable SSEs for high-energy-density SSLBs. Composite electrolytes with an enhanced electrochemical stable window compared to bare SPEs can be a superior SSE candidate for high-energy-density SSLBs. On the other hand, engineering the SSE/active materials interface with an artificial solid electrolyte interphase can enhance the interfacial stability, which have been extensively studied in SPE and sulfide-based SSLBs [100-102, 161, 329]. However, the performance is still far away from practical applications. More investigations on interfacial engineering using advanced coating techniques are desired for further enhancing the performance of SSLBs. Atomic layer deposition (ALD) and molecule layer deposition (MLD), the powerful techniques for fabricating conformal coatings with controlled thickness, are perfect tools [318, 330, 331]. Another ultimate approach for high-voltage SSLBs is the pursuit of high voltage stable SSEs. PEO-based SPE and sulfide-based SSEs are reported to have low electrochemical oxidation window, while NASICON-type SSEs (LATP, LAGP) possess a high electrochemical oxidation voltage limit (up to 4.3 V). Implementing NASICON-type SSEs or searching for other high voltage stable SSEs are an important direction for practical and high-energy-density SSLBs.

(4) Implementing sulfur cathodes is another approach for obtaining high-energy-density SSLBs, based on the high theoretical specific capacity of 1672 mAh/g for sulfur. However, there still many challenges need to be overcome, including the incompatibility between sulfur cathode and SSEs,

polysulfide shuttling effects, the volumetric expansion, and the poor ionic/electronic conductivities of sulfur and discharge products. Mechanism studies and the innovative sulfur cathode designs are urgent for developing high-performance solid-state Li-S batteries.

(5) The mechanical properties of the SSEs have great influence on the SSLB performance. To achieve a practical SSLB, a SSE with suitable mechanical properties to accommodate the volumetric expansion of active materials and maintain intimate SSE/active materials contact is critical. Up to date, most of the research works were dedicated to understanding the basic mechanical properties of available SSEs. In the future, inspiring studies on controlling the mechanical properties of the SSEs or developing new SSEs with suitable mechanical properties should receive more attentions. Hybrid electrolytes with polymer-inorganic composite is a favorable strategy to tune the mechanical properties of SSEs. Hybrid electrolytes shall play an important role in practical SSLBs

(6) The working temperature range of SSEs is important for SSLBs. Although the thermal properties of SSEs are much better than conventional liquid electrolytes, most SSEs have not yet achieved practical performance for SSLBs at low temperature. The development of SSEs with a high ionic conductivity and a low activation energy as well as designs of novel electrode structures for good electronic/ionic conductivities are highlighted directions.

(7) SSE/active materials interface is the most important topic in SSLBs. The understanding of the interfacial ion transport would be helpful for developing high-performance SSLBs. Advanced characterization techniques such as NMR, synchrotron radiation-based X-ray techniques (XAS, STXM, X-ray computed tomography), HR-TEM, Rutherford backscattering spectroscopy, etc., are very powerful tools for studying the interfacial engineering mechanism and interfacial ions transport. Especially, in-situ study at the interface shall give fundamental understandings and guidance for interfacial engineering designs [40, 47, 332-335].

## Acknowledgments

This work is supported by China Automotive Battery Research Institute-Western University Joint Laboratory, Natural Sciences and Engineering Research Council of Canada (NSERC), Canada

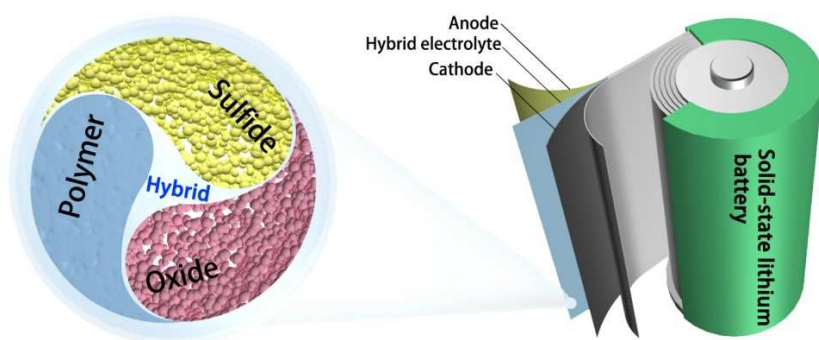


Research Chair Program (CRC), China Scholarship Council (CSC), and University of Western Ontario.

ACCEPTED MANUSCRIPT

**Graphical abstract:**

Hybrid electrolytes combining soft polymer and sulfide-based solid-state electrolyte, or oxide-based solid-state electrolyte enable high ionic conductivity, intimate interface contact and flexible mechanical properties, which are promising candidates for solid-state lithium batteries with high safety.



## Reference

- [1] T. Nagaura, K. Tozawa, *Prog. Batt. Solar Cells*, 9 (1990) 209-217.
- [2] A. Manthiram, B. Song, W. Li, *Energy Storage Mater.*, 6 (2017) 125-139.
- [3] X. Li, J. Liu, M.N. Banis, A. Lushington, R. Li, M. Cai, X. Sun, *Energy Environ. Sci.*, 7 (2014) 768-778.
- [4] B. Xiao, B. Wang, J. Liu, K. Kaliyappan, Q. Sun, Y. Liu, G. Dadheech, M.P. Balogh, L. Yang, T.-K. Sham, R. Li, M. Cai, X. Sun, *Nano Energy*, 34 (2017) 120-130.
- [5] S. Hy, J.-H. Cheng, J.-Y. Liu, C.-J. Pan, J. Rick, J.-F. Lee, J.-M. Chen, B.J. Hwang, *Chem. Mater.*, 26 (2014) 6919-6927.
- [6] C. Chen, J. Liu, M. Stoll, G. Henriksen, D. Vissers, K. Amine, *J. Power Sources*, 128 (2004) 278-285.
- [7] M. Jo, M. Noh, P. Oh, Y. Kim, J. Cho, *Adv. Energy Mater.*, 4 (2014) 1301583.
- [8] X. Ji, K.T. Lee, L.F. Nazar, *Nat. Mater.*, 8 (2009) 500-506.
- [9] X. Li, A. Lushington, Q. Sun, W. Xiao, J. Liu, B. Wang, Y. Ye, K. Nie, Y. Hu, Q. Xiao, R. Li, J. Guo, T.-K. Sham, X. Sun, *Nano Lett.*, 16 (2016) 3545-3549.
- [10] C. Zhao, J. Liang, Q. Sun, J. Luo, Y. Liu, X. Lin, Y. Zhao, H. Yadegari, M.N. Banis, R. Li, H. Huang, L. Zhang, R. Yang, S. Lu, X. Sun, *Small Methods*, 3 (2019) 1800437.
- [11] H.-G. Jung, J. Hassoun, J.-B. Park, Y.-K. Sun, B. Scrosati, *Nat. Chem.*, 4 (2012) 579-585.
- [12] X. Li, M. N. Banis, A. Lushington, X. Yang, Q. Sun, Y. Zhao, C. Liu, Q. Li, B. Wang, W. Xiao, C. Wang, M. Li, J. Liang, R. Li, Y. Hu, L. Goncharova, H. Zhang, T.-K. Sham, X. Sun, *Nat. Commun.*, 9 (2018) 4509.
- [13] S. Hess, M. Wohlfahrt-Mehrens, M. Wachtler, *J. Electrochem. Soc.*, 162 (2015) A3084-A3097.
- [14] Q. Li, J. Chen, L. Fan, X. Kong, Y. Lu, *Green Energy Environ.*, 1 (2016) 18-42.
- [15] D. Di Lecce, L. Carbone, V. Gancitano, J. Hassoun, *J. Power Sources*, 334 (2016) 146-153.
- [16] Q. Wang, L. Jiang, Y. Yu, J. Sun, *Nano Energy*, (2018).
- [17] Y. Sun, Y. Zhao, J. Wang, J. Liang, C. Wang, Q. Sun, X. Lin, K.R. Adair, J. Luo, D. Wang, R. Li, C. Mai, T.-K. Sham, X. Sun, *Adv. Mater.*, 31 (2018) 1806541.
- [18] Y. Zhao, X. Yang, L.Y. Kuo, P. Kaghazchi, Q. Sun, J. Liang, B. Wang, A. Lushington, R. Li, H. Zhang, X. Sun, *Small*, 14 (2018) 1703717.
- [19] J. Liang, X. Li, Y. Zhao, L.V. Goncharova, G. Wang, K.R. Adair, C. Wang, R. Li, Y. Zhu, Y. Qian, L. Zhang, R. Yang, S. Lu, X. Sun, *Adv. Mater.*, 30 (2018) 1804684.
- [20] X. Tang, D. Zhou, P. Li, X. Guo, C. Wang, F. Kang, B. Li, G. Wang, *ACS Cent. Sci.*, 5 (2019) 365-373.
- [21] D. Zhou, A. Tkacheva, X. Tang, B. Sun, D. Shanmukaraj, P. Li, F. Zhang, M. Armand, G. Wang, *Angew. Chem. Int. Ed.*, 58 (2019) 6001-6006.
- [22] H. Morimoto, H. Awano, J. Terashima, Y. Shindo, S. Nakanishi, N. Ito, K. Ishikawa, S.-i. Tobishima, *J. Power Sources*, 240 (2013) 636-643.
- [23] D. Safanama, N. Sharma, R.P. Rao, H.E. Brand, S. Adams, *J. Mater. Chem. A*, 4 (2016) 7718-7726.
- [24] R. Murugan, V. Thangadurai, W. Weppner, *Angew. Chem. Int. Ed.*, 46 (2007) 7778-7781.
- [25] W.J. Kwon, H. Kim, K.-N. Jung, W. Cho, S.H. Kim, J.-W. Lee, M.-S. Park, *J. Mater. Chem. A*, 5

(2017) 6257-6262.

- [26] J. Haruyama, K. Sodeyama, L. Han, K. Takada, Y. Tateyama, *Chem. Mater.*, 26 (2014) 4248-4255.
- [27] X. Tao, Y. Liu, W. Liu, G. Zhou, J. Zhao, D. Lin, C. Zu, O. Sheng, W. Zhang, H.-W. Lee, Y. Cui, *Nano Lett.*, 17 (2017) 2967 - 2972.
- [28] K.K. Fu, Y. Gong, J. Dai, A. Gong, X. Han, Y. Yao, C. Wang, Y. Wang, Y. Chen, C. Yan, Y. Li, E.D. Wachsman, L. Hu, *Proc. Natl. Acad. Sci. USA*, 113 (2016) 7094-7099.
- [29] K.J. Harry, D.T. Hallinan, D.Y. Parkinson, A.A. MacDowell, N.P. Balsara, *Nat. Mater.*, 13 (2014) 69-73.
- [30] M. Keller, A. Varzi, S. Passerini, *J. Power Sources*, 392 (2018) 206-225.
- [31] X. Liu, X. Li, H. Li, H.B. Wu, *Chem. Eur. J.*, 24 (2018) 18293-18306.
- [32] L.Z. Long, S.J. Wang, M. Xiao, Y.Z. Meng, *J. Mater. Chem. A*, 4 (2016) 10038-10069.
- [33] S. Chen, D. Xie, G. Liu, J.P. Mwizerwa, Q. Zhang, Y. Zhao, X. Xu, X. Yao, *Energy Storage Mater.*, 14 (2018) 58-74.
- [34] Z. Gao, H. Sun, L. Fu, F. Ye, Y. Zhang, W. Luo, Y. Huang, *Adv. Mater.*, 30 (2018) 1705702.
- [35] K. Kerman, A. Luntz, V. Viswanathan, Y.-M. Chiang, Z. Chen, *J. Electrochem. Soc.*, 164 (2017) A1731-A1744.
- [36] R. Chen, W. Qu, X. Guo, L. Li, F. Wu, *Mater. Horiz.*, 3 (2016) 487-516.
- [37] Z. Zhang, Y. Shao, B.V. Lotsch, Y.-S. Hu, H. Li, J. Janek, C. Nan, L. Nazar, J. Maier, M. Armand, L. Chen, *Energy Environ. Sci.*, 11 (2018) 1945-1976.
- [38] Y.-Z. Sun, J.-Q. Huang, C.-Z. Zhao, Q. Zhang, *Sci. China Chem.*, 60 (2017) 1508-1526.
- [39] Ö.U. Kudu, T. Famprakis, B. Fleutot, M.-D. Braida, T. Le Mercier, M.S. Islam, C. Masquelier, *J. Power Sources*, 407 (2018) 31-43.
- [40] X. Liu, L. Gu, *Small Methods*, 2 (2018) 1800006.
- [41] L. Yue, J. Ma, J. Zhang, J. Zhao, S. Dong, Z. Liu, G. Cui, L. Chen, *Energy Storage Mater.*, 5 (2016) 139-164.
- [42] A. Varzi, R. Raccichini, S. Passerini, B. Scrosati, *J. Mater. Chem. A*, 4 (2016) 17251-17259.
- [43] A.M. Nolan, Y. Zhu, X. He, Q. Bai, Y. Mo, *Joule*, 2 (2018) 2016-2046.
- [44] X. Yu, A. Manthiram, *Acc. Chem. Res.*, 50 (2017) 2653-2660.
- [45] J.C. Bachman, S. Muy, A. Grimaud, H.-H. Chang, N. Pour, S.F. Lux, O. Paschos, F. Maglia, S. Lupart, P. Lamp, L. Giordano, Y. Shao-Horn, *Chem. Rev.*, 116 (2016) 140-162.
- [46] J. Dai, C. Yang, C. Wang, G. Pastel, L. Hu, *Adv. Mater.*, 30 (2018) 1802068.
- [47] L. Xu, S. Tang, Y. Cheng, K. Wang, J. Liang, C. Liu, Y.-C. Cao, F. Wei, L. Mai, *Joule*, 2 (2018) 1991-2015.
- [48] R. Xu, X. Xia, S. Zhang, D. Xie, X. Wang, J. Tu, *Electrochim. Acta*, 284 (2018) 177-187.
- [49] J. Gao, Y.-S. Zhao, S.-Q. Shi, H. Li, *Chin. Phys. B*, 25 (2016) 018211.
- [50] B. Zhang, R. Tan, L. Yang, J. Zheng, K. Zhang, S. Mo, Z. Lin, F. Pan, *Energy Storage Mater.*, 10 (2018) 139-159.
- [51] G. Ceder, S.P. Ong, Y. Wang, *MRS Bull.*, 43 (2018) 746-751.
- [52] Z. Ma, H.-G. Xue, S.-P. Guo, *J. Mater. Sci.*, 53 (2018) 3927-3938.
- [53] S.-J. Tan, X.-X. Zeng, Q. Ma, X.-W. Wu, Y.-G. Guo, *Electrochem. Energy Rev.*, 1 (2018) 113-138.
- [54] C. Sun, J. Liu, Y. Gong, D.P. Wilkinson, J. Zhang, *Nano Energy*, 33 (2017) 363-386.
- [55] X.-B. Cheng, C.-Z. Zhao, Y.-X. Yao, H. Liu, Q. Zhang, *Chem*, 5 (2019) 74-96.
- [56] M. Shoji, E.J. Cheng, T. Kimura, K. Kanamura, *J. Phys. D: Appl. Phys.*, 52 (2019) 103001.

- [57] L. Fan, S. Wei, S. Li, Q. Li, Y. Lu, *Adv. Energy Mater.*, 8 (2018) 1702657.
- [58] F. Zheng, M. Kotobuki, S. Song, M.O. Lai, L. Lu, *J. Power Sources*, 389 (2018) 198-213.
- [59] J.B. Goodenough, P. Singh, *J. Electrochem. Soc.*, 162 (2015) A2387-A2392.
- [60] H. Zhang, C. Li, M. Piszcz, E. Coya, T. Rojo, L.M. Rodriguez-Martinez, M. Armand, Z. Zhou, *Chem. Soc. Rev.*, 46 (2017) 797-815.
- [61] J. Yi, S. Guo, P. He, H. Zhou, *Energy Environ. Sci.*, 10 (2017) 860-884.
- [62] J. Lau, R.H. DeBlock, D.M. Butts, D.S. Ashby, C.S. Choi, B.S. Dunn, *Adv. Energy Mater.*, 8 (2018) 1800933.
- [63] Y. Shen, Y. Zhang, S. Han, J. Wang, Z. Peng, L. Chen, *Joule*, 2 (2018) 1674-1689.
- [64] K. Liu, Y. Liu, D. Lin, A. Pei, Y. Cui, *Sci. Adv.*, 4 (2018) eaas9820.
- [65] K.K. Fu, Y. Gong, B. Liu, Y. Zhu, S. Xu, Y. Yao, W. Luo, C. Wang, S.D. Lacey, J. Dai, *Sci. Adv.*, 3 (2017) e1601659.
- [66] Y. Zhang, F. Chen, D. Yang, W. Zha, J. Li, Q. Shen, X. Zhang, L. Zhang, *J. Electrochem. Soc.*, 164 (2017) A1695-A1702.
- [67] F. Han, Y. Zhu, X. He, Y. Mo, C. Wang, *Adv. Energy Mater.*, 6 (2016) 1501590.
- [68] A. Hayashi, A. Sakuda, M. Tatsumisago, *Front. Energy Res.*, 4 (2016) 25.
- [69] Y. Xia, T. Fujieda, K. Tatsumi, P.P. Prosini, T. Sakai, *J. Power Sources*, 92 (2001) 234-243.
- [70] Y. Zhu, X. He, Y. Mo, *ACS Appl. Mater. Interfaces*, 7 (2015) 23685-23693.
- [71] L. Chen, Y. Li, S.-P. Li, L.-Z. Fan, C.-W. Nan, J.B. Goodenough, *Nano Energy*, 46 (2018) 176-184.
- [72] Z. Zhang, Y. Zhao, S. Chen, D. Xie, X. Yao, P. Cui, X. Xu, *J. Mater. Chem. A*, 5 (2017) 16984-16993.
- [73] W. Zhou, S. Wang, Y. Li, S. Xin, A. Manthiram, J.B. Goodenough, *J. Am. Chem. Soc.*, 138 (2016) 9385-9388.
- [74] A. Manthiram, X. Yu, S. Wang, *Nat. Rev. Mater.*, 2 (2017) 16103.
- [75] D. Fenton, J. Parker, P. Wright, *Polymer*, 14 (1973) 589.
- [76] F. Croce, G. Appetecchi, L. Persi, B. Scrosati, *Nature*, 394 (1998) 456-458.
- [77] G.S. MacGlashan, Y.G. Andreev, P.G. Bruce, *Nature*, 398 (1999) 792-794.
- [78] Z. Gadjourova, Y.G. Andreev, D.P. Tunstall, P.G. Bruce, *Nature*, 412 (2001) 520-523.
- [79] K. Zaghib, K. Kinoshita, *J. Power Sources*, 125 (2004) 214-220.
- [80] K. Zaghib, Y. Choquette, A. Guerfi, M. Simoneau, A. Belanger, M. Gauthier, *J. Power Sources*, 68 (1997) 368-371.
- [81] K. Zaghib, M. Simoneau, M. Armand, M. Gauthier, *J. Power Sources*, 81 (1999) 300-305.
- [82] H. Marceau, C.-S. Kim, A. Paoletta, S. Ladouceur, M. Lagacé, M. Chaker, A. Vijh, A. Guerfi, C.M. Julien, A. Mauger, M. Armand, P. Hovington, K. Zaghib, *J. Power Sources*, 319 (2016) 247-254.
- [83] J.-C. Daigle, A. Vijh, P. Hovington, C. Gagnon, J. Hamel-Pâquet, S. Verreault, N. Turcotte, D. Clément, A. Guerfi, K. Zaghib, *J. Power Sources*, 279 (2015) 372-383.
- [84] P. Hovington, M. Lagacé, A. Guerfi, P. Bouchard, A. Mauger, C. Julien, M. Armand, K. Zaghib, *Nano Lett.*, 15 (2015) 2671-2678.
- [85] Y. Chen, Y. Chuang, J. Su, H. Yu, Y. Chen-Yang, *J. Power Sources*, 196 (2011) 2802-2809.
- [86] C. Yang, H. Ywi Chen, F. Lin, C. Chen, *Solid State Ion.*, 150 (2002) 327-335.
- [87] H. Choe, B. Carroll, D. Pasquariello, K. Abraham, *Chem. Mater.*, 9 (1997) 369-379.
- [88] H.-W. Chen, T.-P. Lin, F.-C. Chang, *Polymer*, 43 (2002) 5281-5288.
- [89] S. Ahmad, T. Saxena, S. Ahmad, S. Agnihotry, *J. Power Sources*, 159 (2006) 205-209.
- [90] D. Saikia, A. Kumar, *Electrochim. Acta*, 49 (2004) 2581-2589.



- [91] R. Miao, B. Liu, Z. Zhu, Y. Liu, J. Li, X. Wang, Q. Li, *J. Power Sources*, 184 (2008) 420-426.
- [92] D. Zhou, R. Zhou, C. Chen, W.-A. Yee, J. Kong, G. Ding, X. Lu, *J. Phys. Chem. B*, 117 (2013) 7783-7789.
- [93] J. Zhang, X. Zang, H. Wen, T. Dong, J. Chai, Y. Li, B. Chen, J. Zhao, S. Dong, J. Ma, *J. Mater. Chem. A*, 5 (2017) 4940-4948.
- [94] L. Meabe, T.V. Huynh, N. Lago, H. Sardon, C. Li, L.A. O'Dell, M. Armand, M. Forsyth, D. Mecerreyes, *Electrochim. Acta*, 264 (2018) 367-375.
- [95] N.S. Schausier, K.J. Harry, D.Y. Parkinson, H. Watanabe, N.P. Balsara, *J. Electrochem. Soc.*, 162 (2015) A398-A405.
- [96] P. Barai, K. Higa, V. Srinivasan, *Phys. Chem. Chem. Phys.*, 19 (2017) 20493-20505.
- [97] R. Khurana, J.L. Schaefer, L.A. Archer, G.W. Coates, *J. Am. Chem. Soc.*, 136 (2014) 7395-7402.
- [98] A. Mauer, M. Armand, C. Julien, K. Zaghib, *J. Power Sources*, 353 (2017) 333-342.
- [99] C. Monroe, J. Newman, *J. Electrochem. Soc.*, 152 (2005) A396-A404.
- [100] H. Miyashiro, Y. Kobayashi, S. Seki, Y. Mita, A. Usami, M. Nakayama, M. Wakihara, *Chem. Mater.*, 17 (2005) 5603-5605.
- [101] J. Ma, Z. Liu, B. Chen, L. Wang, L. Yue, H. Liu, J. Zhang, Z. Liu, G. Cui, *J. Electrochem. Soc.*, 164 (2017) A3454-A3461.
- [102] S. Seki, Y. Kobayashi, H. Miyashiro, Y. Mita, T. Iwahori, *Chem. Mater.*, 17 (2005) 2041-2045.
- [103] Z. Gadjourova, Y.G. Andreev, D.P. Tunstall, P.G. Bruce, *Nature*, 412 (2001) 520.
- [104] Y. Tominaga, K. Yamazaki, *Chem. Commun.*, 50 (2014) 4448-4450.
- [105] C.R. Mariappan, C. Yada, F. Rosciano, B. Roling, *J. Power Sources*, 196 (2011) 6456-6464.
- [106] B. Kumar, D. Thomas, J. Kumar, *J. Electrochem. Soc.*, 156 (2009) A506-A513.
- [107] V. Thangadurai, S. Narayanan, D. Pinzaru, *Chem. Soc. Rev.*, 43 (2014) 4714-4727.
- [108] M.P. O'Callaghan, D.R. Lynham, E.J. Cussen, G.Z. Chen, *Chem. Mater.*, 18 (2006) 4681-4689.
- [109] V. Thangadurai, H. Kaack, W.J. Weppner, *J. Am. Ceram. Soc.*, 86 (2003) 437-440.
- [110] V. Thangadurai, W. Weppner, *J. Am. Ceram. Soc.*, 88 (2005) 411-418.
- [111] D. Rettenwander, G.n. Redhammer, F. Preishuber-Pflügl, L. Cheng, L. Miara, R. Wagner, A. Welzl, E. Suard, M.M. Doeff, M. Wilkening, J. Fleig, G. Amthauer, *Chem. Mater.*, 28 (2016) 2384-2392.
- [112] R. Jalem, M. Rushton, W. Manalastas Jr, M. Nakayama, T. Kasuga, J.A. Kilner, R.W. Grimes, *Chem. Mater.*, 27 (2015) 2821-2831.
- [113] D. Wang, G. Zhong, W.K. Pang, Z. Guo, Y. Li, M.J. McDonald, R. Fu, J.-X. Mi, Y. Yang, *Chem. Mater.*, 27 (2015) 6650-6659.
- [114] L. Truong, V. Thangadurai, *Chem. Mater.*, 23 (2011) 3970-3977.
- [115] Y. Ren, Y. Shen, Y. Lin, C.-W. Nan, *Electrochem. Commun.*, 57 (2015) 27-30.
- [116] L. Porz, T. Swamy, B.W. Sheldon, D. Rettenwander, T. Frömling, H.L. Thaman, S. Berendts, R. Uecker, W.C. Carter, Y.M. Chiang, *Adv. Energy Mater.*, 7 (2017) 1701003.
- [117] T. Takahashi, H. Iwahara, *Energy Convers.*, 11 (1971) 105-111.
- [118] Y. Inaguma, C. Liqun, M. Itoh, T. Nakamura, T. Uchida, H. Ikuta, M. Wakihara, *Solid State Commun.*, 86 (1993) 689-693.
- [119] S.D. Jackman, R.A. Cutler, *J. Power Sources*, 218 (2012) 65-72.
- [120] S. Yu, R.D. Schmidt, R. Garcia-Mendez, E. Herbert, N.J. Dudney, J.B. Wolfenstine, J. Sakamoto, D.J. Siegel, *Chem. Mater.*, 28 (2016) 197-206.

- [121] K.G. Schell, F. Lemke, E.C. Bucharsky, A. Hintennach, M. Hoffmann, *J. Mater. Sci.*, 52 (2017) 2232-2240.
- [122] W. Luo, Y. Gong, Y. Zhu, Y. Li, Y. Yao, Y. Zhang, K.K. Fu, G. Pastel, C.F. Lin, Y. Mo, E. D. Wachsman, L. Hu, *Adv. Mater.*, 29 (2017) 1606042.
- [123] X. Han, Y. Gong, K.K. Fu, X. He, G.T. Hitz, J. Dai, A. Pearse, B. Liu, H. Wang, G. Rubloff, Y. Mo, V. Thangadurai, E. D. Wachsman, L. Hu, *Nat. Mater.*, 16 (2017) 572-579.
- [124] C. Wang, Y. Gong, B. Liu, K. Fu, Y. Yao, E. Hitz, Y. Li, J. Dai, S. Xu, W. Luo, E. D. Wachsman, L. Hu, *Nano Lett.*, 17 (2016) 565-571.
- [125] S. Ohta, S. Komagata, J. Seki, T. Saeki, S. Morishita, T. Asaoka, *J. Power Sources*, 238 (2013) 53-56.
- [126] F. Han, J. Yue, C. Chen, N. Zhao, X. Fan, Z. Ma, T. Gao, F. Wang, X. Guo, C. Wang, *Joule*, 2 (2018) 497-508.
- [127] J. Van Den Broek, S. Afyon, J.L. Rupp, *Adv. Energy Mater.*, 6 (2016) 1600736.
- [128] S. Ohta, J. Seki, Y. Yagi, Y. Kihira, T. Tani, T. Asaoka, *J. Power Sources*, 265 (2014) 40-44.
- [129] K. Park, B.-C. Yu, J.-W. Jung, Y. Li, W. Zhou, H. Gao, S. Son, J.B. Goodenough, *Chem. Mater.*, 28 (2016) 8051-8059.
- [130] M. Shoji, H. Munakata, K. Kanamura, *Front. Energy Res.*, 4 (2016) 32.
- [131] K.K. Fu, Y. Gong, G.T. Hitz, D.W. McOwen, Y. Li, S. Xu, Y. Wen, L. Zhang, C. Wang, G. Pastel, J. Dai, B. Liu, H. Xie, Y. Yao, E. D. Wachsman, L. Hu, *Energy Environ. Sci.*, 10 (2017) 1568-1575.
- [132] R. Koerver, W. Zhang, L. de Biasi, S. Schweidler, A. Kondrakov, S. Kolling, T. Brezesinski, P. Hartmann, W. Zeier, J. Janek, *Energy Environ. Sci.*, 11 (2018) 2142-2158.
- [133] H. Huo, J. Sun, X. Meng, M. He, N. Zhao, X. Guo, *J. Power Sources*, 383 (2018) 150-156.
- [134] X. Yao, N. Huang, F. Han, Q. Zhang, H. Wan, J.P. Mwizerwa, C. Wang, X. Xu, *Adv. Energy Mater.*, 7 (2017) 1602923.
- [135] K.H. Kim, Y. Iriyama, K. Yamamoto, S. Kumazaki, T. Asaka, K. Tanabe, C.A. Fisher, T. Hirayama, R. Murugan, Z. Ogumi, *J. Power Sources*, 196 (2011) 764-767.
- [136] F. Han, A.S. Westover, J. Yue, X. Fan, F. Wang, M. Chi, D.N. Leonard, N.J. Dudney, H. Wang, C. Wang, *Nat. Energy*, 4 (2019) 187-196.
- [137] Y. Song, L. Yang, W. Zhao, Z. Wang, Y. Zhao, Z. Wang, Q. Zhao, H. Liu, F. Pan, *Adv. Energy Mater.*, 12 (2019) 1900671.
- [138] Y. Liu, Q. Sun, Y. Zhao, B. Wang, P. Kaghazchi, K.R. Adair, R. Li, C. Zhang, J. Liu, L.-Y. Kuo, Y. Hu, T.-K. Sham, L. Zhang, R. Yang, S. Lu, X. Song, X. Sun, *ACS Appl. Mater. Interfaces*, 10 (2018) 31240-31248.
- [139] Y. Liu, P. He, H. Zhou, *Adv. Energy Mater.*, 8 (2018) 1701602.
- [140] N.M. Asl, J. Keith, C. Lim, L. Zhu, Y. Kim, *Electrochim. Acta*, 79 (2012) 8-16.
- [141] A. Hayashi, S. Hama, H. Morimoto, M. Tatsumisago, T. Minami, *J. Am. Ceram. Soc.*, 84 (2001) 477-479.
- [142] S. Kondo, K. Takada, Y. Yamamura, *Solid State Ion.*, 53 (1992) 1183-1186.
- [143] M. Tachez, J.-P. Malugani, R. Mercier, G. Robert, *Solid State Ion.*, 14 (1984) 181-185.
- [144] R. Kanno, T. Hata, Y. Kawamoto, M. Irie, *Solid State Ion.*, 130 (2000) 97-104.
- [145] R. Kanno, M. Murayama, *J. Electrochem. Soc.*, 148 (2001) A742-A746.
- [146] N. Kamaya, K. Homma, Y. Yamakawa, M. Hirayama, R. Kanno, M. Yonemura, T. Kamiyama, Y. Kato, S. Hama, K. Kawamoto, A. Mitsui, *Nat. Mater.*, 10 (2011) 682-686.

- [147] M. Murayama, N. Sonoyama, A. Yamada, R. Kanno, *Solid State Ion.*, 170 (2004) 173-180.
- [148] X. Yao, D. Liu, C. Wang, P. Long, G. Peng, Y.-S. Hu, H. Li, L. Chen, X. Xu, *Nano Lett.*, 16 (2016) 7148-7154.
- [149] Y. Kato, S. Hori, T. Saito, K. Suzuki, M. Hirayama, A. Mitsui, M. Yonemura, H. Iba, R. Kanno, *Nat. Energy*, 1 (2016) 16030.
- [150] A. Kuhn, O. Gerbig, C. Zhu, F. Falkenberg, J. Maier, B.V. Lotsch, *Phys. Chem. Chem. Phys.*, 16 (2014) 14669-14674.
- [151] C. Wang, Y. Zhao, Q. Sun, X. Li, Y. Liu, J. Liang, X. Li, X. Lin, R. Li, K.R. Adair, L. Zhang, R. Yang, S. Lu, X. Sun, *Nano Energy*, 53 (2018) 168-174.
- [152] W.D. Richards, L.J. Miara, Y. Wang, J.C. Kim, G. Ceder, *Chem. Mater.*, 28 (2015) 266-273.
- [153] S. Wenzel, S. Randau, T. Leichtweiß, D.A. Weber, J. Sann, W.G. Zeier, J.r. Janek, *Chem. Mater.*, 28 (2016) 2400-2407.
- [154] Y. Zhu, X. He, Y. Mo, *J. Mater. Chem. A*, 4 (2016) 3253-3266.
- [155] F. Han, T. Gao, Y. Zhu, K.J. Gaskell, C. Wang, *Adv. Mater.*, 27 (2015) 3473-3483.
- [156] M. Nagao, A. Hayashi, M. Tatsumisago, *Electrochemistry*, 80 (2012) 734-736.
- [157] Z. Zhang, S. Chen, J. Yang, J. Wang, L. Yao, X. Yao, P. Cui, X. Xu, *ACS Appl. Mater. Interfaces*, 10 (2018) 2556-2565.
- [158] R. Xu, F. Han, X. Ji, X. Fan, J. Tu, C. Wang, *Nano Energy*, 53 (2018) 958-966.
- [159] F. Han, J. Yue, X. Zhu, C. Wang, *Adv. Energy Mater.*, 8 (2018) 1703644.
- [160] A. Sakuda, A. Hayashi, M. Tatsumisago, *Chem. Mater.*, 22 (2009) 949-956.
- [161] J.H. Woo, J.E. Trevey, A.S. Cavanagh, Y.S. Choi, S.C. Kim, S.M. George, K.H. Oh, S.-H. Lee, *J. Electrochem. Soc.*, 159 (2012) A1120-A1124.
- [162] N. Ohta, K. Takada, L. Zhang, R. Ma, M. Osada, T. Sasaki, *Adv. Mater.*, 18 (2006) 2226-2229.
- [163] R. Koerver, I. Aygün, T. Leichtweiß, C. Dietrich, W. Zhang, J.O. Binder, P. Hartmann, W.G. Zeier, J.r. Janek, *Chem. Mater.*, 29 (2017) 5574-5582.
- [164] Z. Deng, Z. Wang, I.-H. Chu, J. Luo, S.P. Ong, *J. Electrochem. Soc.*, 163 (2016) A67-A74.
- [165] A. Kato, M. Nose, M. Yamamoto, A. Sakuda, A. Hayashi, M. Tatsumisago, *J. Ceram. Soc. Jpn.*, 126 (2018) 719-727.
- [166] G. Bucci, T. Swamy, Y.-M. Chiang, W.C. Carter, *J. Mater. Chem. A*, 5 (2017) 19422-19430.
- [167] G. Bucci, B. Talamini, A.R. Balakrishna, Y.-M. Chiang, W.C. Carter, *Phys. Rev. Mater.*, 2 (2018) 105407.
- [168] A. Sakuda, A. Hayashi, M. Tatsumisago, *Sci. Rep.*, 3 (2013) 2261.
- [169] T. Swamy, R. Park, B.W. Sheldon, D. Rettenwander, L. Porz, S. Berendts, R. Uecker, W.C. Carter, Y.-M. Chiang, *J. Electrochem. Soc.*, 165 (2018) A3648-A3655.
- [170] A. Kato, M. Yamamoto, A. Sakuda, A. Hayashi, M. Tatsumisago, *ACS Appl. Energy Mater.*, 1 (2018) 1002-1007.
- [171] J.E. Ni, E.D. Case, J.S. Sakamoto, E. Rangasamy, J.B. Wolfenstine, *J. Mater. Sci.*, 47 (2012) 7978-7985.
- [172] Y. Kim, H. Jo, J.L. Allen, H. Choe, J. Wolfenstine, J. Sakamoto, *J. Am. Ceram. Soc.*, 99 (2016) 1367-1374.
- [173] J. Wolfenstine, H. Jo, Y.-H. Cho, I.N. David, P. Askeland, E.D. Case, H. Kim, H. Choe, J. Sakamoto, *Mater. Lett.*, 96 (2013) 117-120.
- [174] Y.-H. Cho, J. Wolfenstine, E. Rangasamy, H. Kim, H. Choe, J. Sakamoto, *J. Mater. Sci.*, 47 (2012)

5970-5977.

- [175] C. Cooper, A.C. Sutorik, J. Wright, E.A. Luoto III, G. Gilde, J. Wolfenstine, *Adv. Eng. Mater.*, 16 (2014) 755-759.
- [176] A. Sakuda, A. Hayashi, Y. Takigawa, K. Higashi, M. Tatsumisago, *J. Ceram. Soc. Jpn.*, 121 (2013) 946-949.
- [177] F.P. McGrogan, T. Swamy, S.R. Bishop, E. Eggleton, L. Porz, X. Chen, Y.-M. Chiang, K.J. Van Vliet, *Adv. Energy Mater.*, 7 (2017) 1602011.
- [178] Z. Wang, M. Wu, G. Liu, X. Lei, B. Xu, C. Ouyang, *Int. J. Electrochem. Sci.*, 9 (2014) 562-568.
- [179] E.G. Herbert, W.E. Tenhaeff, N.J. Dudney, G.M. Pharr, *Thin Solid Films*, 520 (2011) 413-418.
- [180] J. Ji, B. Li, W.-H. Zhong, *J. Phys. Chem. B*, 114 (2010) 13637-13643.
- [181] C. Wang, Y. Yang, X. Liu, H. Zhong, H. Xu, Z. Xu, H. Shao, F. Ding, *ACS Appl. Mater. Interfaces*, 9 (2017) 13694-13702.
- [182] J. Xie, R.G. Duan, Y. Han, J.B. Kerr, *Solid State Ion.*, 175 (2004) 755-758.
- [183] S. Ramesh, T. Winie, A.K. Arof, *J. Mater. Sci.*, 45 (2010) 1280-1283.
- [184] P. Raghavan, X. Zhao, J.-K. Kim, J. Manuel, G.S. Chauhan, J.-H. Ahn, C. Nah, *Electrochim. Acta*, 54 (2008) 228-234.
- [185] N. Shubha, R. Prasanth, H.H. Hng, M. Srinivasan, *J. Power Sources*, 267 (2014) 48-57.
- [186] I. Villaluenga, K.H. Wujcik, W. Tong, D. Devaux, D.H. Wong, J.M. DeSimone, N.P. Balsara, *Proc. Natl. Acad. Sci. USA*, 113 (2016) 52-57.
- [187] H. Huo, B. Wu, T. Zhang, X. Zheng, L. Ge, T. Xu, X. Guo, X. Sun, *Energy Storage Mater.*, (2019).
- [188] J. Zhang, L. Yue, Q. Kong, Z. Liu, X. Zhou, C. Zhang, Q. Xu, B. Zhang, G. Ding, B. Qin, Y. Duan, Q. Wang, J. Yao, G. Cui, L. Chen, *Sci. Rep.*, 4 (2014) 3935.
- [189] D. Li, L. Chen, T. Wang, L.-Z. Fan, *ACS Appl. Mater. Interfaces*, 10 (2018) 7069-7078.
- [190] R. Khurana, J.L. Schaefer, L.A. Archer, G.W. Coates, *J. Am. Chem. Soc.*, 136 (2014) 7395-7402.
- [191] W. Zhou, Z. Wang, Y. Pu, Y. Li, S. Xin, X. Li, J. Chen, J.B. Goodenough, *Adv. Mater.*, 31 (2019) 1805574.
- [192] J.-F. Wu, B.-W. Pu, D. Wang, S.-Q. Shi, N. Zhao, X. Guo, X. Guo, *ACS Appl. Mater. Interfaces*, 11 (2019) 898-905.
- [193] D. Wang, Q. Sun, J. Luo, J. Liang, Y. Sun, R. Li, K. Adair, L. Zhang, R. Yang, S. Lu, H. Huang, X. Sun, *ACS Appl. Mater. Interfaces*, 11 (2019) 4954-4961.
- [194] F. Lu, Y. Pang, M. Zhu, F. Han, J. Yang, F. Fang, D. Sun, S. Zheng, C. Wang, *Adv. Funct. Mater.*, 29 (2019) 1809219.
- [195] T. Lapp, S. Skaarup, A. Hooper, *Solid State Ion.*, 11 (1983) 97-103.
- [196] J. Bates, N. Dudney, B. Neudecker, A. Ueda, C. Evans, *Solid State Ion.*, 135 (2000) 33-45.
- [197] D. Lin, W. Liu, Y. Liu, H.R. Lee, P.-C. Hsu, K. Liu, Y. Cui, *Nano Lett.*, 16 (2015) 459-465.
- [198] Y. Liu, J.Y. Lee, L. Hong, *J. Appl. Polym. Sci.*, 89 (2003) 2815-2822.
- [199] C. Galven, J.-L. Fourquet, M.-P. Crosnier-Lopez, F.o. Le Berre, *Chem. Mater.*, 23 (2011) 1892-1900.
- [200] G. Sahu, Z. Lin, J. Li, Z. Liu, N. Dudney, C. Liang, *Energy Environ. Sci.*, 7 (2014) 1053-1058.
- [201] Y.G. Zhang, Y. Zhao, D. Gosselink, P. Chen, *Ionics*, 21 (2015) 381-385.
- [202] M. Keller, G.B. Appetecchi, G.-T. Kim, V. Sharova, M. Schneider, J. Schuhmacher, A. Roters, S. Passerini, *J. Power Sources*, 353 (2017) 287-297.
- [203] D.W. McOwen, S. Xu, Y. Gong, Y. Wen, G.L. Godbey, J.E. Gritton, T.R. Hamann, J. Dai, G.T. Hitz,

L. Hu, *Adv. Mater.*, 30 (2018) 1707132.

[204] A. Hayashi, T. Harayama, F. Mizuno, M. Tatsumisago, *J. Power Sources*, 163 (2006) 289-293.

[205] E. Rangasamy, G. Sahu, J.K. Keum, A.J. Rondinone, N.J. Dudney, C. Liang, *J. Mater. Chem. A*, 2 (2014) 4111-4116.

[206] R.-J. Chen, Y.-B. Zhang, T. Liu, B.-Q. Xu, Y.-H. Lin, C.-W. Nan, Y. Shen, *ACS Appl. Mater. Interfaces*, 9 (2017) 9654-9661.

[207] H. Zhai, P. Xu, M. Ning, Q. Cheng, J. Mandal, Y. Yang, *Nano Lett.*, 17 (2017) 3182-3187.

[208] J. Bae, Y. Li, J. Zhang, X. Zhou, F. Zhao, Y. Shi, J.B. Goodenough, G. Yu, *Angew. Chem. Int. Ed.*, 57 (2018) 2096-2100.

[209] K. Fu, Y. Wang, C. Yan, Y. Yao, Y. Chen, J. Dai, S. Lacey, Y. Wang, J. Wan, T. Li, Z. Wang, Y. Xu, L. Hu, *Adv. Mater.*, 28 (2016) 2587-2594.

[210] J. Li, M.C. Leu, R. Panat, J. Park, *Materials & Design*, 119 (2017) 417-424.

[211] X. Gao, Q. Sun, X. Yang, J. Liang, A. Koo, W. Li, J. Liang, J. Wang, R. Li, F.B. Holness, A. D. Price, S. Yang, T.-K. Sham, X. Sun, *Nano Energy*, 56 (2019) 595-603.

[212] A.J. Blake, R.R. Kohlmeier, J.O. Hardin, E.A. Carmona, B. Maruyama, J.D. Berrigan, H. Huang, M.F. Durstock, *Adv. Energy Mater.*, 7 (2017) 1602920.

[213] M. Cheng, Y. Jiang, W. Yao, Y. Yuan, R. Deivanayagam, T. Foroozan, Z. Huang, B. Song, R. Rojaee, T. Shokuhfar, Y. Pan, J. Lu, R. Shahbazian-Yassar, *Adv. Mater.*, 30 (2018) 1800615.

[214] K. Sun, T.-S. Wei, B. Y. Ahn, J. Y. Seo, S. J. Dillon, J. A. Lewis, *Adv. Mater.*, 25(2013), 4539-4543.

[215] K. Fu, Y. Yao, J. Dai, L. Hu, *Adv. Mater.*, 29(2017)1603486.

[216] X. Tian, J. Jin, S. Yuan, C. K. Chua, S. B. Tor, K. Zhou, *Adv. Energy Mater.*, 7(2017), 1700127.

[217] J.E. Weston, B.C.H. Steele, *Solid State Ion.*, 7 (1982) 75-79.

[218] F. Croce, L. Persi, F. Ronci, B. Scrosati, *Solid State Ion.*, 135 (2000) 47-52.

[219] C.W. Lin, C.L. Hung, M. Venkateswarlu, B.J. Hwang, *Journal of Power Sources*, 146 (2005) 397-401.

[220] S. Jayanthi, K. Kulasekarapandian, A. Arulsankar, K. Sankaranarayanan, B. Sundaresan, *J. Compos. Mater.*, 49 (2015) 1035-1045.

[221] O. Sheng, C. Jin, J. Luo, H. Yuan, C. Fang, H. Huang, Y. Gan, J. Zhang, Y. Xia, C. Liang, W. Zhang, X. Tao, *J. Mater. Chem. A*, 5 (2017) 12934-12942.

[222] K. Liu, F. Ding, Q.W. Lu, J.Q. Liu, Q.Q. Zhang, X.J. Liu, Q. Xu, *Solid State Ion.*, 289 (2016) 1-8.

[223] A.M. Stephan, T.P. Kumar, M.A. Kulandainathan, N.A. Laksh, *J. Phys. Chem. B*, 113 (2009) 1963-1971.

[224] J.L. Schaefer, D.A. Yanga, L.A. Archer, *Chem. Mater.*, 25 (2013) 834-839.

[225] Z. Wang, S. Wang, A. Wang, X. Liu, J. Chen, Q. Zeng, L. Zhang, W. Liu, L. Zhang, *J. Mater. Chem. A*, 6 (2018) 17227-17234.

[226] C. Yuan, J. Li, P. Han, Y. Lai, Z. Zhang, J. Liu, *J. Power Sources* 240 (2013) 653-658.

[227] C. Gerbaldi, J.R. Nair, M.A. Kulandainathan, R.S. Kumar, C. Ferrara, P. Mustarell, A.M. Stephan, *J. Mater. Chem. A*, 2 (2014) 9948-9954.

[228] K. Zhu, Y. Liu, J. Liu, *RSC Adv.*, 4 (2014) 42278-42284.

[229] Y.J. Wang, Y. Pan, L. Wang, M.J. Pang, L. Chen, *J. Appl. Polym. Sci.*, 102 (2006) 4269-4275.

[230] Y.J. Wang, Y. Pan, D. Kim, *J. Power Sources*, 159 (2006) 690-701.

[231] S.-K. Kim, Y.-C. Jung, D.-H. Kim, W.-C. Shin, M. Ue, D.-W. Kim, *J. Electrochem. Soc.*, 163 (2016) A974-A980.



- [232] Y.-C. Jung, M.-S. Park, C.-H. Doh, D.-W. Kim, *Electrochim. Acta*, 218 (2016) 271-277.
- [233] Y. Zhao, Z. Huang, S. Chen, B. Chen, J. Yang, Q. Zhang, F. Ding, Y. Chen, X. Xu, *Solid State Ion.*, 295 (2016) 65-71.
- [234] W. Liu, N. Liu, J. Sun, P.-C. Hsu, Y. Li, H.-W. Lee, Y. Cui, *Nano Lett.*, 15 (2015) 2740-2745.
- [235] S. Ohta, T. Kobayashi, T. Asaoka, *J. Power Sources*, 196 (2011) 3342-3345.
- [236] J.H. Choi, C.H. Lee, J.H. Yu, C.H. Doh, S.M. Lee, *J. Power Sources*, 274 (2015) 458-463.
- [237] J. Zhang, N. Zhao, M. Zhang, Y. Li, P.K. Chu, X. Guo, Z. Di, X. Wang, H. Li, *Nano Energy*, 28 (2016) 447-454.
- [238] Z. He, L. Chen, B. Zhang, Y. Liu, L.-Z. Fan, *J. Power Sources*, 392 (2018) 232-238.
- [239] X. Zhang, T. Liu, S. Zhang, X. Huang, B. Xu, Y. Lin, B. Xu, L. Li, C.-W. Nan, Y. Shen, *J. Am. Chem. Soc.*, 139 (2017) 13779-13785.
- [240] J. Yu, S.C.T. Kwok, Z. Lu, M.B. Effat, Y.-Q. Lyu, M.M.F. Yuen, F. Ciucci, *Chemelectrochem*, 5 (2018) 2873-2881.
- [241] K. Kimura, H. Matsumoto, J. Hassoun, S. Panero, B. Scrosati, Y. Tominaga, *Electrochimica Acta*, 175 (2015) 134-140.
- [242] W. Zhang, J. Nie, F. Li, Z.L. Wang, C. Sun, *Nano Energy*, 45 (2018) 413-419.
- [243] H. Huo, Y. Chen, J. Luo, X. Yang, X. Guo, X. Sun, *Adv. Energy Mater.*, 9 (2019) 1804004.
- [244] Y. Zhao, C. Wu, G. Peng, X. Chen, X. Yao, Y. Bai, F. Wu, S. Chen, X. Xu, *J. Power Sources*, 301 (2016) 47-53.
- [245] S. Chen, J. Wang, Z. Zhang, L. Wu, L. Yao, Z. Wei, Y. Deng, D. Xie, X. Yao, X. Xu, *J. Power Sources*, 387 (2018) 72-80.
- [246] J. Wolfenstine, J.L. Allen, J. Sakamoto, D.J. Siegel, H. Choe, *Ionics*, 24 (2018) 1271-1276.
- [247] S. Bi, C.N. Sun, T.A. Zawodzinski, F. Ren, J.K. Keum, S.K. Ahn, D. Li, J. Chen, *J. Polym. Sci. Part B: Polym. Phys.*, 53 (2015) 1450-1457.
- [248] S. Kohjiya, T. Kitade, Y. Ikeda, A. Hayashi, A. Matsuda, M. Tatsumisago, T. Minami, *Solid State Ion.*, 154 (2002) 1-6.
- [249] D.H. Wong, J.L. Thelen, Y. Fu, D. Devaux, A.A. Pandya, V.S. Battaglia, N.P. Balsara, J.M. DeSimone, *Proc. Natl. Acad. Sci. USA*, 111 (2014) 3327-3331.
- [250] H. Aono, E. Sugimoto, Y. Sadaaka, N. Imanaka, G. Adachi, *J. Electrochem. Soc.*, 136 (1989) 590-591.
- [251] X. Xu, Z. Wen, X. Yang, J. Zhang, Z. Gu, *Solid State Ion.*, 177 (2006) 2611-2615.
- [252] P. Knauth, *Solid State Ion.*, 180 (2009) 911-916.
- [253] K. Takada, M. Tansho, I. Yanase, T. Inada, A. Kajiyama, M. Kouguchi, S. Kondo, M. Watanabe, *Solid State Ion.*, 139 (2001) 241-247.
- [254] K. Arbi, S. Mandal, J. Rojo, J. Sanz, *Chem. Mater.*, 14 (2002) 1091-1097.
- [255] M. Kotobuki, M. Koishi, *Ceram. Int.*, 39 (2013) 4645-4649.
- [256] H. Chung, B. Kang, *Solid State Ion.*, 263 (2014) 125-130.
- [257] V. Thangadurai, W. Weppner, *J. Solid State Chem.*, 179 (2006) 974-984.
- [258] Y. Gao, X. Wang, W. Wang, Z. Zhuang, D. Zhang, Q. Fang, *Solid State Ion.*, 181 (2010) 1415-1419.
- [259] H. Xie, Y. Li, J. Han, Y. Dong, M.P. Paranthaman, L. Wang, M. Xu, A. Gupta, Z. Bi, C.A. Bridges, M. Nakanishui, A. P. Sokolov, J. B. Goodenough, *J. Electrochem. Soc.*, 159 (2012) A1148-A1151.
- [260] Y. Li, J.-T. Han, C.-A. Wang, H. Xie, J.B. Goodenough, *J. Mater. Chem.*, 22 (2012) 15357-15361.

- [261] V. Thangadurai, W. Weppner, *J. Electrochem. Soc.*, 151 (2004) H1-H6.
- [262] M. Itoh, Y. Inaguma, W.-H. Jung, L. Chen, T. Nakamura, *Solid State Ion.*, 70 (1994) 203-207.
- [263] V. Thangadurai, W. Weppner, *Ionics*, 6 (2000) 70-77.
- [264] K. Mizumoto, S. Hayashi, *Solid State Ion.*, 116 (1999) 263-269.
- [265] S. Garcia-Martín, J. Rojo, H. Tsukamoto, E. Morán, M. Alario-Franco, *Solid State Ion.*, 116 (1999) 11-18.
- [266] S. Stramare, V. Thangadurai, W. Weppner, *Chem. Mater.*, 15 (2003) 3974-3990.
- [267] P. Bron, S. Johansson, K. Zick, J.r. Schmedt auf der Günne, S. Dehnen, B. Roling, *J. Am. Chem. Soc.*, 135 (2013) 15694-15697.
- [268] Y. Seino, T. Ota, K. Takada, A. Hayashi, M. Tatsumisago, *Energy Environ. Sci.*, 7 (2014) 627-631.
- [269] H. Yamane, M. Shibata, Y. Shimane, T. Junke, Y. Seino, S. Adams, K. Minami, A. Hayashi, M. Tatsumisago, *Solid State Ion.*, 178 (2007) 1163-1167.
- [270] Z. Liu, W. Fu, E.A. Payzant, X. Yu, Z. Wu, N.J. Dudney, J. Kiggans, K. Hong, A.J. Rondinone, C. Liang, *J. Am. Chem. Soc.*, 135 (2013) 975-978.
- [271] M. Tatsumisago, *Solid State Ion.*, 175 (2004) 13-18.
- [272] E. Rietman, M. Kaplan, R. Cava, *Solid State Ion.*, 25 (1987) 41-44.
- [273] S.K. Fullerton-Shirey, J.K. Maranas, *J. Phys. Chem. C*, 114 (2010) 9196-9206.
- [274] S.H.-S. Cheng, K.-Q. He, Y. Liu, J.-W. Zha, M. Kamruzzaman, R.L.-W. Ma, Z.-M. Dang, R.K. Li, C. Chung, *Electrochim. Acta*, 253 (2017) 430-438.
- [275] C.-Z. Zhao, X.-Q. Zhang, X.-B. Cheng, R. Zhang, R. Xu, P.-Y. Chen, H.-J. Peng, J.-Q. Huang, Q. Zhang, *Proc. Natl. Acad. Sci. USA*, 114 (2017) 11069-11074.
- [276] M. Dissanayake, P. Jayathilaka, R. Bokalawala, I. Albinsson, B.-E. Mellander, *J. Power Sources*, 119 (2003) 409-414.
- [277] F. Croce, L. Persi, B. Scrosati, F. Serraino-Fiory, E. Plichta, M. Hendrickson, *Electrochim. Acta*, 46 (2001) 2457-2461.
- [278] Z. Wang, X. Huang, L. Chen, *Electrochem. Solid-State Lett.*, 6 (2003) E40-E44.
- [279] J. Shin, S. Passerini, *J. Electrochem. Soc.*, 151 (2004) A238-A245.
- [280] G. Appetecchi, F. Croce, L. Persi, F. Ronci, B. Scrosati, *Electrochim. Acta*, 45 (2000) 1481-1490.
- [281] J. Zheng, M. Tang, Y.Y. Hu, *Angew. Chem.*, 128 (2016) 12726-12730.
- [282] W. Gang, J. Roos, D. Brinkmann, F. Capuano, F. Croce, B. Scrosati, *Solid State Ion.*, 53 (1992) 1102-1105.
- [283] E.M. Masoud, A.A. El-Bellihi, W.A. Bayoumy, M.A. Mousa, *J. Alloy Compd.*, 575 (2013) 223-228.
- [284] P. Sun, Y.H. Liao, X.Y. Luo, Z.H. Li, T.T. Chen, L.D. Xing, W.S. Li, *RSC Adv.*, 5 (2015) 64368-64377.
- [285] H. Xie, C. Yang, K. Fu, Y. Yao, F. Jiang, E. Hitz, B. Liu, S. Wang, L. Hu, *Adv. Energy Mater.*, 8 (2018) 1703474.
- [286] Y.-T. Kim, E.S. Smotkin, *Solid State Ion.*, 149 (2002) 29-37.
- [287] S. Ibrahim, M.R. Johan, *Int. J. Electrochem. Sci*, 6 (2011) 5565-5587.
- [288] H. Huo, N. Zhao, J. Sun, F. Du, Y. Li, X. Guo, *J. Power Sources*, 372 (2017) 1-7.
- [289] P.-J. Alarco, Y. Abu-Lebdeh, A. Abouimrane, M. Armand, *Nat. Mater.*, 3 (2004) 476-481.
- [290] H.T. Le, D.T. Ngo, R.S. Kalubarme, G. Cao, C.-N. Park, C.-J. Park, *ACS Appl. Mater. Interfaces*, 8 (2016) 20710-20719.
- [291] J. Zheng, H. Dang, X. Feng, P.-H. Chien, Y.-Y. Hu, *J. Mater. Chem. A*, 5 (2017) 18457-18463.

- [292] W.A. Henderson, N.R. Brooks, V.G. Young, *J. Am. Chem. Soc.*, 125 (2003) 12098-12099.
- [293] Y. Noda, K. Nakano, H. Takeda, M. Kotobuki, L. Lu, M. Nakayama, *Chem. Mater.*, 29 (2017) 8983-8991.
- [294] B. Lang, B. Ziebarth, C. Elsässer, *Chem. Mater.*, 27 (2015) 5040-5048.
- [295] E. Quartarone, P. Mustarelli, *Chem. Soc. Rev.*, 40 (2011) 2525-2540.
- [296] Q. Ma, X.X. Zeng, J. Yue, Y.X. Yin, T.T. Zuo, J.Y. Liang, Q. Deng, X.W. Wu, Y.G. Guo, *Adv. Energy Mater.*, 9 (2019) 1803854.
- [297] Z. Wan, D. Lei, W. Yang, C. Liu, K. Shi, X. Hao, L. Shen, W. Lv, B. Li, Q.-H. Yang, F. Kang, Y.-B. He, *Adv. Funct. Mater.*, 29 (2019) 1805301.
- [298] X. Chen, W. He, L.-X. Ding, S. Wang, H. Wang, *Energy Environ. Sci.*, 12 (2019) 938-944.
- [299] M. Jo, Y.-S. Hong, J. Choo, J. Cho, *J. Electrochem. Soc.*, 156 (2009) A430-A434.
- [300] D.W. Dees, K.G. Gallagher, D.P. Abraham, A.N. Jansen, *J. Electrochem. Soc.*, 160 (2013) A478-A486.
- [301] L. Wang, Y. Wang, Y. Xia, *Energy Environ. Sci.*, 8 (2015) 1551-1558.
- [302] S. Wang, Y. Ding, G. Zhou, G. Yu, A. Manthiram, *ACS Energy Lett.*, 1 (2016) 1080-1085.
- [303] C. Wang, Q. Sun, Y. Liu, Y. Zhao, X. Li, X. Lin, M.N. Banis, M. Li, W. Li, K.R. Adair, D. Wang, J. Liang, R. Li, L. Zhang, R. Yang, S. Lu, X. Sun, *Nano Energy*, 48 (2018) 35-43.
- [304] A. Hayashi, T. Ohtomo, F. Mizuno, K. Tadanaga, M. Tatsumisago, *Electrochem. Commun.*, 5 (2003) 701-705.
- [305] J. Hassoun, B. Scrosati, *Adv. Mater.*, 22 (2010) 5198-5201.
- [306] A. Hayashi, R. Ohtsubo, T. Ohtomo, F. Mizuno, M. Tatsumisago, *J. Power Sources*, 183 (2008) 422-426.
- [307] M. Nagao, A. Hayashi, M. Tatsumisago, *J. Mater. Chem.*, 22 (2012) 10015-10020.
- [308] D. Zhou, Y. Chen, B. Li, H. Fan, F. Cheng, D. Shanmukaraj, T. Rojo, M. Armand, G. Wang, *Angew. Chem. Int. Ed.*, 57 (2018) 10168-10172.
- [309] X. Yu, Z. Bi, F. Zhao, A. Manthiram, *ACS Appl. Mater. Interfaces*, 7 (2015) 16625-16631.
- [310] N. Li, Z. Weng, Y. Wang, F. Li, H.-M. Cheng, H. Zhou, *Energy Environ. Sci.*, 7 (2014) 3307-3312.
- [311] X. Yu, Z. Bi, F. Zhao, A. Manthiram, *Adv. Energy Mater.*, 6 (2016) 1601392.
- [312] Q. Wang, J. Jin, X. Wu, G. Ma, J. Yang, Z. Wen, *Phys. Chem. Chem. Phys.*, 16 (2014) 21225-21229.
- [313] H. Zhou, Y. Wang, H. Li, P. He, *ChemSuschem*, 3 (2010) 1009-1019.
- [314] M.R. Busche, T. Drossel, T. Leichtweiss, D.A. Weber, M. Falk, M. Schneider, M.-L. Reich, H. Sommer, P. Adelhelm, J. Janek, *Nat. Chem.*, 8 (2016) 426-434.
- [315] Y.T. Li, B.Y. Xu, H.H. Xu, H.N. Duan, X.J. Lu, S. Xin, W.D. Zhou, L.G. Xue, G.T. Fu, A. Manthiram, J.B. Goodenough, *Angew. Chem. Int. Ed.*, 56 (2017) 753-756.
- [316] B. Liu, Y. Gong, K. Fu, X. Han, Y. Yao, G. Pastel, C. Yang, H. Xie, E.D. Wachsman, L. Hu, *ACS Appl. Mater. Interfaces*, (2017).
- [317] Q. Wang, Z. Wen, J. Jin, J. Guo, X. Huang, J. Yang, C. Chen, *Chem. Commun.*, 52 (2016) 1637-1640.
- [318] J. Liang, Q. Sun, Y. Zhao, Y. Sun, C. Wang, W. Li, M. Li, D. Wang, X. Li, Y. Liu, *J. Mater. Chem. A*, 6 (2018) 23712-23719.
- [319] S.-S. Chi, Y. Liu, N. Zhao, X. Guo, C.-W. Nan, L.-Z. Fan, *Energy Storage Mater.*, 17 (2019) 309-316.

- [320] C. Wang, K.R. Adair, J. Liang, X. Li, Y. Sun, X. Li, J. Wang, Q. Sun, F. Zhao, X. Lin, R. Li, H. Huang, L. Zhang, R. Yang, S. Lu, X. Sun, *Adv. Funct. Mater.*, (2019) 1900392.
- [321] Y. Li, B. Xu, H. Xu, H. Duan, X. Lü, S. Xin, W. Zhou, L. Xue, G. Fu, A. Manthiram, *Angew. Chem. Int. Ed.*, 56 (2017) 753-756.
- [322] T. Abe, M. Ohtsuka, F. Sagane, Y. Iriyama, Z. Ogumi, *J. Electrochem. Soc.*, 151 (2004) A1950-A1953.
- [323] W.E. Tenhaeff, K.A. Perry, N.J. Dudney, *J. Electrochem. Soc.*, 159 (2012) A2118-A2123.
- [324] W.C. Chueh, F. El Gabaly, J.D. Sugar, N.C. Bartelt, A.H. McDaniel, K.R. Fenton, K.R. Zavadil, T. Tyliszczak, W. Lai, K.F. McCarty, *Nano Lett.*, 13 (2013) 866-872.
- [325] M. Yashima, M. Itoh, Y. Inaguma, Y. Morii, *J. Am. Chem. Soc.*, 127 (2005) 3491-3495.
- [326] C. Li, H. Zhang, L. Otaegui, G. Singh, M. Armand, L.M. Rodriguez-Martinez, *J. Power Sources*, 326 (2016) 1-5.
- [327] Y. Hamon, A. Douard, F. Sabary, C. Marcel, P. Vinatier, B. Pecquenard, A. Levasseur, *Solid State Ion.*, 177 (2006) 257-261.
- [328] R.A. Jonson, P.J. McGinn, *Solid State Ion.*, 323 (2018) 49-55.
- [329] N. Ohta, K. Takada, I. Sakaguchi, L. Zhang, R. Ma, K. Fukuda, M. Osada, T. Sasaki, *Electrochem. Commun.*, 9 (2007) 1486-1490.
- [330] Y. Zhao, X. Sun, *ACS Energy Lett.*, 3 (2018) 899-914.
- [331] Y. Zhao, K. Zheng, X. Sun, *Joule*, 2 (2018) 1-22.
- [332] F. Lin, Y. Liu, X. Yu, L. Cheng, A. Singer, O.G. Shpyrko, H.L. Xin, N. Tamura, C. Tian, T.-C. Weng, X.-Q. Yang, Y. S. Meng, D. Nordlund, W. Yang, M.M. Doeff, *Chem. Rev.*, 117 (2017) 13123-13186.
- [333] J. Lu, T. Wu, K. Amine, *Nat. Energy*, 2 (2017) 17011.
- [334] Y. Yang, X. Liu, Z. Dai, F. Yuan, Y. Bando, D. Golberg, X. Wang, *Adv. Mater.*, 29 (2017) 1606922.
- [335] X. Li, H.Y. Wang, H. Yang, W. Cai, S. Liu, B. Liu, *Small Methods*, 2 (2018) 1700395.